Volume 6 No. 6, December 2018

Transactions on Networks and Communications

ISSN: 2054-7420

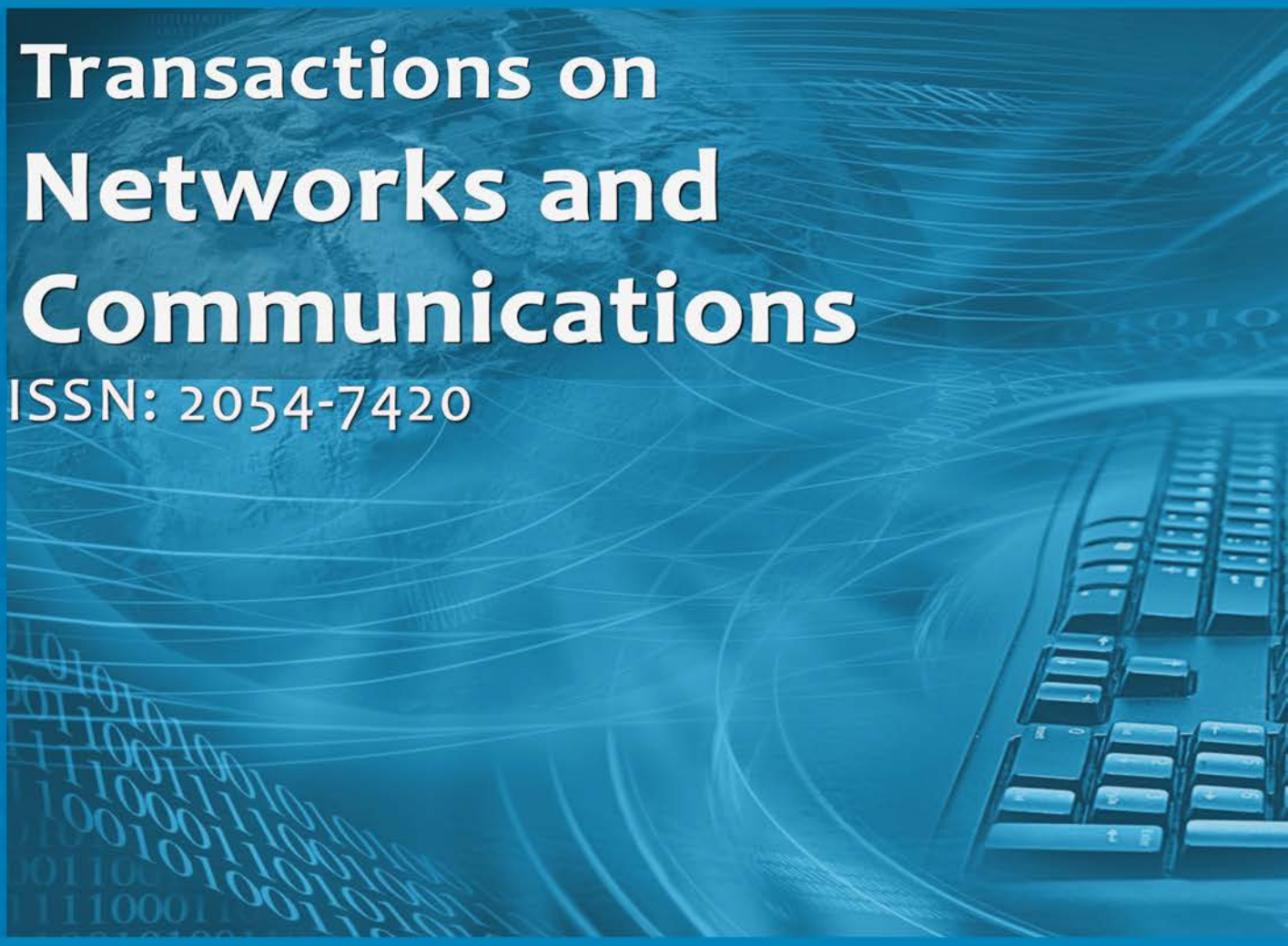

Society for Sciences and Education - United Kingdom

TABLE OF CONTENTS

EDITORIAL ADVISORY BOARD	I
DISCLAIMER	II
Quality Analysis of Streaming Audio over Mobile Networks Sikha Bagui, Amitabh Mishra, John Compo, Debarghya Nandi and Subhash Bagui	1
Mitigation of Terrain Effects using Beamforming Antennas in Ad Hoc Networks Vinay B. Ramakrishnaiah, Robert F. Kubichek, and Suresh S. Muknahallipatna	15
Forwarding with Prediction over Machine Learning based Nodes in Wireless Mesh Networks Jianjun Yang, Ju Shen, Mengyi Ying	33
SDN/NFV Based Internet of Things for Multi-Tenant Networks Do Sinh, Luong-Vy Le, Bao-Shuh Paul Lin, Li-Ping Tung	40
Simulation on Collective Panic Behavior Based on PI Wen ZHENG, Da ZHU	57
Research and Implementation of Bluetooth Indoor Auto-Tracking System Yen-Jen Chen, Kai-Wen Zheng	76
Data Fusion in Wireless Communication Network Node Positioning Ya Luo, Xiaoyang Liu, Chao Liu	87

DISCLAIMER

All the contributions are published in good faith and intentions to promote and encourage research activities around the globe. The contributions are property of their respective authors/owners and the journal is not responsible for any content that hurts someone's views or feelings etc.

SOCIETY FOR SCIENCE AND EDUCATION
UNITED KINGDOM

TNC TRANSACTIONS ON NETWORKS AND COMMUNICATIONS

VOLUME 6, NO. 6
ISSN: 2054 -7420

Quality Analysis of Streaming Audio over Mobile Networks

Sikha Bagui[1], Amitabh Mishra[1], John Compo[1], Debarghya Nandi[1] and Subhash Bagui[2]
[1]*Department of Computer Science,*
[2]*Department of Mathematics and Statistics, The University of West Florida, Pensacola, FL 32514*
bagui@uwf.edu; amishra@uwf.edu; johncompo@gmail.com, dnandi4@uic.edu

ABSTRACT

This paper utilizes open source software to analyze the quality of audio streamed over mobile cellular networks. Industry conventions have been developed to assess audio quality such as the Mean Opinion Score or MOS scale described in the International Telecommunications Union ITU P.800.1 document. The MOS scale is a subjective assessment based on the listener's experience. To eliminate the use of a trained audio listener we automate an estimated MOS calculation by measuring the packet loss, average latency and jitter over the network transport path. The network under test is a pilot network to replace the dedicated analog circuit from the broadcast center to a radio transmitter. We intend to automate the logging of an objective quality assessment using MOS, cellular router and decoder measurements with confirmation using automatically generated visual representations of sample audio received. These visual representations will aid in manual confirmation of poor MOS scores with audio samples available for more in-depth review.

Keywords: Audio Quality, Mean Opinion Score, Streaming Audio, Mobile Networks, Outages

1 Introduction

The production broadcast system text database stores safety and public information messages derived from weather forecast products. The broadcast center creates a broadcast script from these messages and sets up a play schedule. Text to speech software is used to convert these messages into a synthetic, digital voice message. The voice message is converted to an analog signal by a digital to analog audio converter that supplies radio transmitters via a dedicated analog circuit from the broadcast center. In addition to the broadcast voice, various frequency tones can be inserted into the message. Specific Area Message Encoding (SAME) tones are used to send an alert to receivers in a specific geographical location such as a county. Additional tones are used to remotely switch the transmitter from the primary to the secondary transmitter. The dedicated circuit is analogous to an audio cable from a personal computer to a set of speakers. The audio remains an analog signal from the broadcast center to the transmitter. Figure 1 presents a legacy broadcast center to transmitter configuration. In figure 1 we see the text to speech engine pulling text products from the text product database. Once the text is converted to an audio signal, it is transmitting over the analog circuit to the radio transmitter for broadcast.

DOI: 10.14738/tnc.66.5526
Publication Date: 25th November 2018
URL: http://dx.doi.org/10.14738/tnc.66.5526

Figure 1. Legacy broadcast center to transmitter configuration - dedicated circuit (Analog).

Telephone communications continue to evolve from analog copper-wire circuits carrying analog signals between fixed geographical points to newer digital circuits using signals that can reach multiple geographical areas and locations through the Internet or private networks. This evolution is continuing, and analog circuits are becoming rarer and more expensive than digital circuits. In some markets these legacy analog circuits are no longer available.

The pilot system being tested uses cellular network technology commonly used with smart phones and smart devices. Within this cellular network, a Virtual Private Network (VPN) is created between the broadcast center and the radio transmitter to isolate the broadcast stream from the public internet. In Figure 2 the setup is like the previous analog circuit with the exception of the transport method between the broadcast center and transmitter boundaries. The analog audio is now encoded into a digital signal by an audio encoder once the signal is digital, the encoding router sends the Real Time Protocol (RTP) packets via 4G networks to the decoding router. Once received, the audio decoder converts the RTP packets back to an audio signal to supply the radio transmitter.

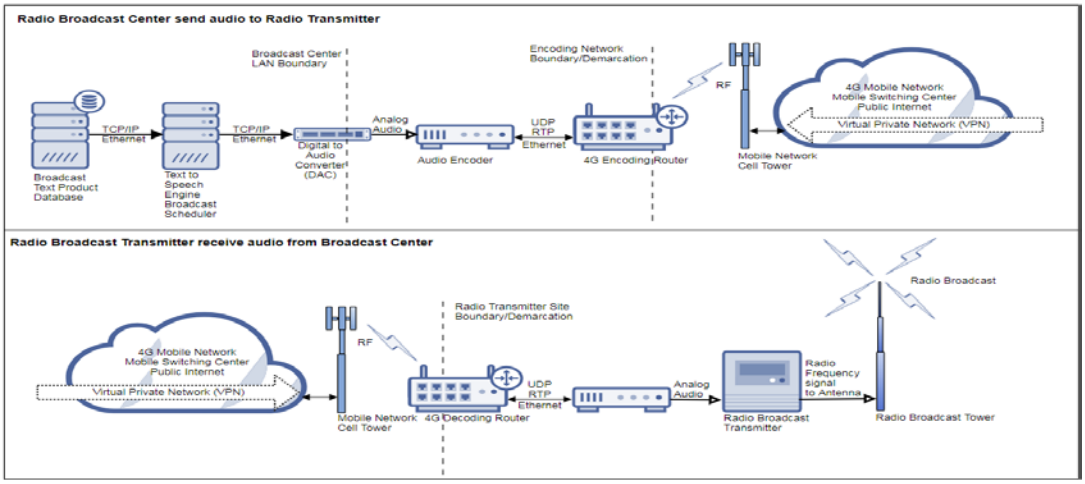

Figure 2. Pilot broadcast center to transmitter configuration - 4G mobile network with VPN (Digital).

The broadcast is a one-way audio stream and is transmitted over the VPN using the Real Time Protocol (RTP) G.711 codec as expressed in the document ITU [4] G.711. One distinct challenge with dedicated analog circuits and RTP is automating the objective assessment of audio quality. Transmitters that are close to the broadcast center can be monitored on a weather radio. Transmitters further away cannot be monitored for audio quality without dialing in to the transmitter and listening to a short sample. The broadcast center relies upon members of the public to report audio problems or outages. Their audio assessment may be subjective based on their experience, receiver setup, terrain blockage and the distance from the transmitter. Any prolonged interruption to streaming audio is noticed immediately by

the intended listener as silence or distortion. Silence could be caused by many factors, most likely an audio or network outage along the transmission path. Poor audio or strange noises such as echoes, or warbling tones would most likely be attributed to network jitter. In this paper we propose a setup using open source software to both automate the calculation of an estimated MOS along with detailed analysis about the audio quality. Our setup also provides automated visual references and sample audio for manual confirmation of poor MOS scores.

The information from the broadcast center to the radio transmitter includes current weather forecasts, watches, warnings, public information statements and emergency messages. Due to the critical nature of such information, a high level of service availability is required. These broadcasts don't have the dynamic range or fidelity requirements of an FM radio station; however, these transmissions should be clear, with limited noise and minimal outages. The transmitters broadcast on narrow band Frequency Modulation (FM). The designed area of coverage is 40 miles from the transmitter. This range should allow a received signal more than -89dBm which is more than adequate for the voice broadcast and more importantly high enough to trigger the receiver when SAME tones are sent.

In this work, we intend to automate the initial analysis of received audio. By using network statistics and software and tools at the radio transmitter received audio. We attempt to automate quality analysis and capture outages. The automated methods should correlate to waveform and spectrograph analysis to assure they are accurate. These visual representations will aid in manual confirmation of poor MOS scores with audio samples available for more in-depth review.

The rest of the paper is organized as follows. Section 2 presents the related works; section 3 presents the pilot setup; section 4 presents the methods used to assess audio quality; section 5 presents the data analysis; section 6 presents the predictions that can be made and finally section 7 presents the conclusions and findings.

2 Related works

[2] used structural similarity index to compare transmitted and received frequency structures. From this they derived a correlation coefficient. Their work was mainly with musical instruments sources and the dynamic range of their signals is much greater than our vocal and tone requirements.

To measure the quality of video streaming, [7] used correlation as well. While the title of their article was video streaming, portions of their setup are applicable to audio streaming as a component of that video. Their work is impacted by round trip time (RTT) and other elements prone to limitations of the TCP/IP protocol suite. One of the major impacts to their results was due to the TCP/IP retransmission or sliding windows flow where the transmit side delays the transmission to assure that the packets are in order. This would cause a serious effect on the quality of streaming audio. In our setup, the encoders and decoders communicate with each other using User Datagram Protocol over IP (UDP) which does not involve the complex handshaking used in TCP. In our application we continuously send audio regardless of packet losses, and there is no re-transmission.

The approach [10] used jitter distortion as a method for assessing audio quality. The focus of their paper was the delivery via cell phone, but they used a listener to provide a subjective assessment of the quality. Moreover, their application focused on sporadic burst transmission. On the contrary, our broadcast stream is continuous and employing a listener over extended periods of time is not feasible.

Authors for [6] specifically identified issues related to audio transmission over "lossy" networks such as the Internet. Their work focused on the comparison of quality to packet loss rates of the decoded signal. They encoded and decoded the audio with different rates to evaluate the quality. However, our system is a live system and our goal is to assess and improve the audio.

3 Setup

The pilot test setup consists of two live broadcast links and a test broadcast link. The live links can revert to their coexisting dedicated analog paths during intrusive testing. Intrusive testing involves transmitting one of the two known audio files over the link. Without switching the site back to the legacy dedicated circuit, the radio transmitter broadcasts the test message. Since tones are included in the test messages, there is an additional risk of causing false alerts on the receivers.

The first pilot 4G link is from a broadcast center in Texas to a simulated transmitter in Vermont, this link is approximately 1,800 miles. This simulated transmitter is the logging PC which also records the audio. The second pilot link is a broadcast from the Vermont broadcast center to a transmitter in Vermont approximately 16 miles away. A third local test setup 4G pilot link for comparison uses collocated routers. This local setup has the two routers separated by a short distance of 25 feet. All three links use mobile network 4G LTE as the primary network technology. The links are named T1800V, V16V and V0V to denote the origin, distance and destination. All three links use commercially available audio encoders and audio decoders in pairs. In addition to the encoders and decoders, single board computers (SBCs) are used at the origin and destination. The originating SBC is used to inject a known audio signal into the encoder during intrusive testing. This audio is either a 30 second loop of a 440 hertz concert A (A4) sine wave tone or a known one-minute loop of synthetic voice reciting the Harvard Sentences [3] List # 11 with some 400Hz and 1 kHz tones. Examples of the transmitted waveform and spectrographs viewed in Audacity [1] are presented in figures 3 to 5.

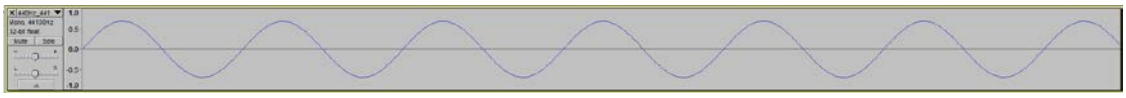

Figure 3. Waveform 440 Hz

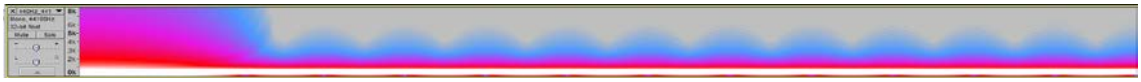

Figure 4. Spectrograph 440 Hz

Figure 5. Harvard Sentences List 11 and tones.

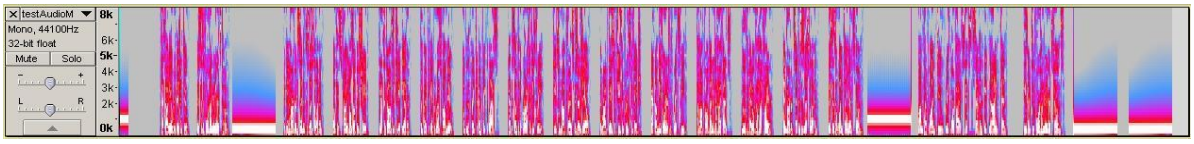

Figure 6. Spectrograph - Harvard Sentences List 11 and tones.

In Figure 6 we see a spectrograph representation of the test audio file. The test audio file was constructed using the Harvard Sentences [3] #11 and a 440Hz at specific locations as marker. This file is of a fixed duration and content will aid in the quality analysis of the received signal. The voice and tone loop or constant tone provide a reference waveform to compare against the received audio. These known audio signals help in detailed manual analysis of the received audio if necessary. The live broadcast varies greatly and is difficult to discern the quality visually. At the receive end an SBC is used to record the audio from the decoder as well as perform the network tests to estimate a MOS Score.

The system setup we designed produces this estimated MOS score based on the network packet loss, average latency and jitter from the decoder to the encoder. A poor estimated MOS provides a timestamp to check in cases where further analysis is required. Our system also logs the encoding and decoding router and decoder data. It records 15 second samples of audio 2-3 times per minute. From this audio, our system automatically logs the audio sample's statistics and automatically generates the waveform, FFT and spectrograph plots using the Matlibplot [5] library in Python [8].

4 Methods

To assess the audio quality one can simply listen to the audio stream and determine if it can be clearly heard and with ease. To establish a scale of that quality, the Mean Opinion Score (MOS) was developed by the International Telecommunication Union (ITU) [4]. The MOS scale is subjective; the listener should be a trained audio professional. Employing a human listener for a continuous MOS scale assessment is not always practical. Table 1 presents the scales used by the ITU [4] and G.711. Table 1 shows the MOS scale ranging from a listener's estimated experience ranging from bad to excellent.

Table 1: MOS scale published by International Telecommunication Union (ITU) for G.711 CODEC.

MOS	ITU-T P.800.2
5.0	Excellent
4.0	Good
3.0	Fair
2.0	Poor
1.0	Bad

Source: ITU-T P.800.2 07/2016

The codec used for our testing is the G.711 Real Time Protocol (RTP) codec defined in ITU-T [4] Recommendation [2, 3] G.711. It is a commonly used codec for Audio over IP (AoIP) applications, available for free. The audio encoding for the encoder and decoder uses μ-law 8-bit Pulse Code Modulation (PCM). One of the benefits of the μ-law is the dynamic range available and reduced bandwidth. It should be noted that a maximum MOS score for the G.711 codec is expressed as 4.4 in the MOS scale table. This maximum theoretical MOS score varies from 4.1 - 4.5 depending on the reference source. Any value above 4.0 is acceptable as the signal is in the good range or satisfied level of quality depending on the chart selection. A subjective good or satisfied MOS threshold can be identified by listening to the received audio and cross referencing against the estimated MOS to establish an acceptable baseline for audio quality if necessary. MOS subsets are defined as MOS-LQE, MOS-LQO and MOS-LQS, where L=listening, Q=quality and E=estimated. O=Objective and S=Subjective were not used.

To test the three AoIP links, we have used a passive approach for the live broadcasts including the estimated MOS, detailed logging as previously mentioned and audio recording. For the intrusive test we inject one of our known audio files into the broadcast stream. For the pure tone injection, we additionally have an automated audio metric log which logs amplitude, norms and deltas of that audio signal.

The broadcast center to radio transmitter sites and distances are identified in table 2.

Table 2: Site to site locations and payload type.

#	Transmit	Receive	Distance (mi)	Type	Payload	MOS Type
1	Texas	Vermont	1,800	Encoder to Decoder	Audio and/or Tones	MOS-LQS/LQO
2	Vermont	Vermont	16	Encoder to Decoder	Audio and/or Tones	MOS-LQS/LQO
3	Vermont	Vermont	0	Encoder to Decoder	Audio and/or Tones	MOS-LQS/LQO

There are many factors that contribute to the audio quality of the broadcast. The audio encoding quality was assumed to be good and constant since we injected a known reference audio signal into all three encoders. We compared this audio file directly against the received audio samples.

There are several possible causes for audio degradation during transmission. The encoder, encoding router (transmit), decoding router (receive), decoder could be suspect. The routers could suffer from poor signal strength or signal to noise ratio. If the routers do not have a strong signal, the attachment to the mobile network will be prone to errors. The audio encoder and decoder pair could have problem exasperated by the network connection/conditions between them. These could cause problems with RTP latency, drops, duplicates and errors. In addition, the audio encoder decoder pair has to sync with each other, this takes approximately 2-3 seconds. Any network disconnects are amplified by this additional time to come back online and sync.

Network transport is another common cause of audio degradation. The situation with network transport is analogous to two tin cans and a string where the string is slack or over-tight or is struck with an object during transmission. Two of the important measurements that should be logged for judging the mobile network connection quality are Received Signal Strength Indicator (RSSI) and the Signal to Interference Noise Ratio (SINR). In our setup, whenever SINR on the router was not available for logging, we logged the Received Signal Received Quality (RSRQ) values.

There are additional parameters related to the decoders that we logged - the most informative of these are the Real Time Protocol attributes for latency, loss, drops duplicates. The decoder buffer, soft errors and reconnects are also logged.

In addition to recording the above data, we used a raw socket Python [8] ping to determine decoder to encoder packet loss, average latency and jitter to calculate an estimated MOS for the transmissions. We also captured 15 second audio samples approximately two to three times per minute. From these samples we plotted the first few cycles of the 440 Hz tone to analyze the sine wave. We also plotted the spectrum of the broadcast a constant tone can be analyzed quickly with a Fast Fourier Transform (FFT). Any frequency deviation of the constant tone can be easily identified. In the image below, the transmitted or reference audio signal is plotted together with the received audio signal. It may be noted that the waveform plot and FFT are plotted for a small fraction of the 15 second sample in figure 7.

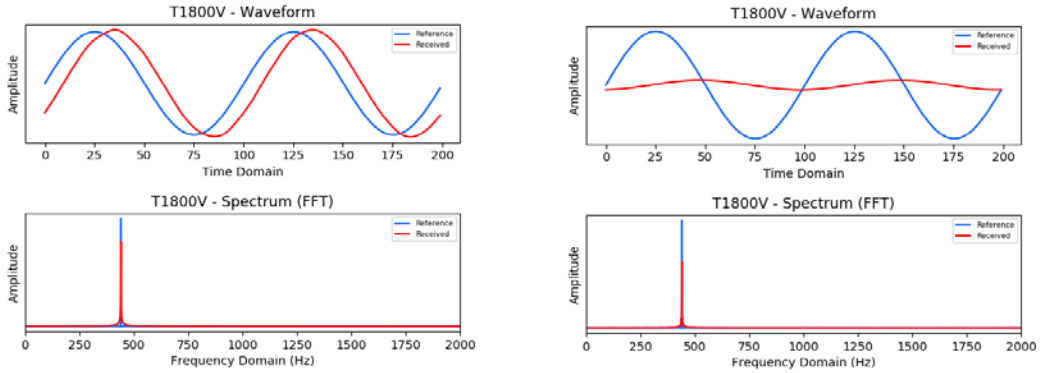

Figure 7: Waveform and FFT plot.

In the above waveform diagram, we analyze the sine wave characteristics of a sample; the phase difference varies based on the transmission delay. The FFT plot shows if the reference and received signals are on same frequency, or if there is a drift. The amplitudes of the transmitted and the received signals are plotted to check just for deviation and may not necessarily be relative to each other. Volume adjustments on the encoder, decoder and SBC can also be the reasons for changes in the amplitude. In the two waveform samples, it is evident that there was signal loss or fade. The entire 15-second sample can be opened in Audacity [1] for detailed information on the complete waveform or to listen to the sample.

The complete 15 second sample is plotted below with a spectrograph. The outages and deviations from the primary frequency are more easily discerned in the spectrograph output as shown in Figure 8.

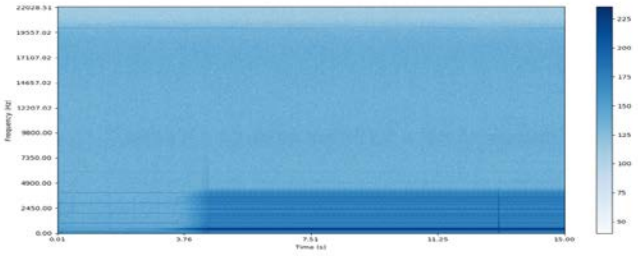

Figure 8: Spectrograph of constant frequency tone.

From figure 8, we can see that, in the first quarter there appears to be no signal in the spectrograph output. The dark blue, highest amplitude component in the plot is the received 440 Hz signal. The signal returns to 440 Hz just before the 3.76 second mark. Once again, we can view the entire 15 second waveform with a tool like Audacity and listen to the audio.

The estimated MOS score and the decoder RTP attributes are the main indices to research further into the spectrographs and recorded audio samples.

5 Data Analysis

Our setup and the experimental process to find bad or missing audio were used at all three sites T1800V, V16V and V0V. The MOS, encoding router, decoding router and decoder log values were plotted to look for trends. Of interest were the MOS scores, routers' signal levels and the decoder buffer, and RTP latency, drops, loss and duplicates.

In all three sites, the encoding and decoding router had a strong received signal and good signal to noise values. The 15 second audio sample log was also plotted to look for trends. From the experiment results, we found that of importance in this log are the root mean squared amplitude and the amplitude mean norm values. The spectrograph and waveform plots were compared against low MOS scores and low values in the root mean squared amplitude and the amplitude mean norm.

The MOS score below is of a live broadcast voice from the Texas site to Vermont T1800V. The MOS score is estimated continuously for all the broadcasts. The MOS score below is 1.93 which is in the 'Poor' category on the ITU [4] MOS scale. In Figure 9 we can see the variance ranging from Poor to Good MOS scores.

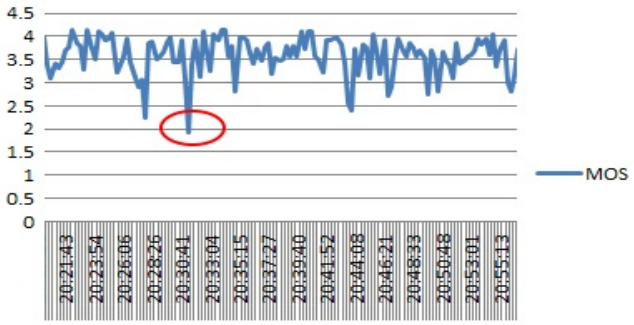

Figure 9: Automated MOS score example Texas to Vermont T1800V link.

Using this low MOS score as the date time reference we selected the correct spectrograph for this audio sample. It may be noted that the darker the shade of blue the higher the amplitude of the signal. Figure 10 is small sample spectrograph of the audio associated with the Poor MOS score in Figure 9.

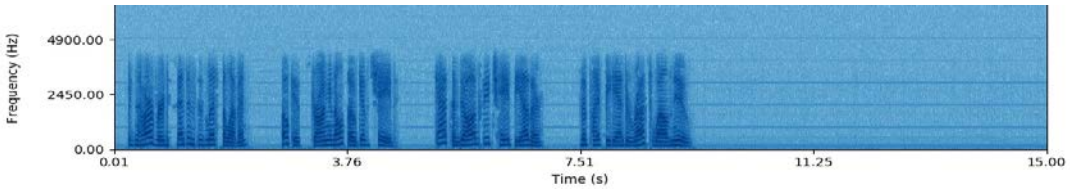

Figure 10: Spectrograph of 15 second sample correlating to MOS score in Figure 9.

The complete 15 second sample of the audio was viewed and listened to in Audacity [1] (figure 10). When we loaded the waveform, the wave signature matched the spectrograph. When we listened to the sample audio, it was confirmed that the audio was missing.

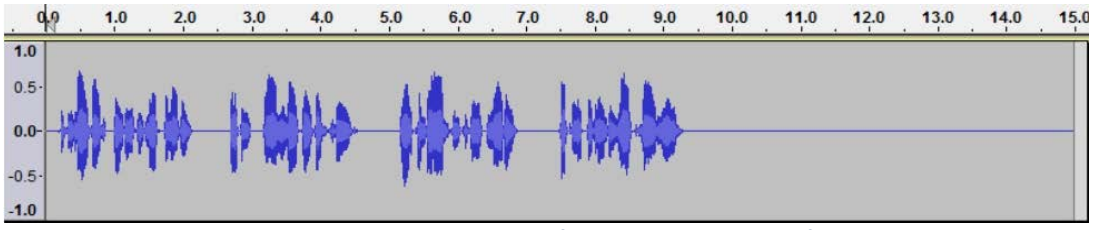

Figure 11: Suspect audio waveform, same sample as figure 10.

The sample below is the voice tone loop injected into the encoder at the Vermont to Vermont site V16V. This site MOS scores ranged from 3.2 "Fair" to 4.29 "Good" on the ITU [4] MOS scale for the total sample

period. The MOS score for this sample was 3.5 which is between “Fair” and “Good” on the ITU [4] MOS scale. We can infer from the plot below that the MOS score was dropping prior to this low value. The score in question is circled in red on figure 12.

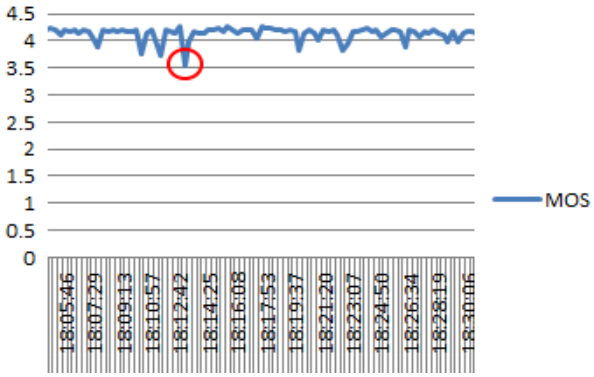

Figure12: Automated MOS score example Vermont to Vermont V16V link.

When we referenced the spectrograph using the time and date from the log we found that the signal was missing and then faded back in. One of the embedded test tones can be seen to the right of the spectrograph represented by the dark horizontal line.

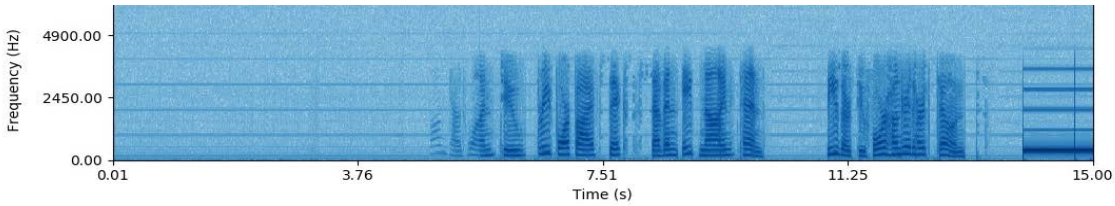

Figure 13: Spectrograph of 15 second sample correlating to MOS score in Figure 12.

From the spectrograph above in Figure 13 it appeared the signal was missing and then faded in. We confirmed this with the aid of waveform representation of the audio in Figure 14 and by listening to the sample.

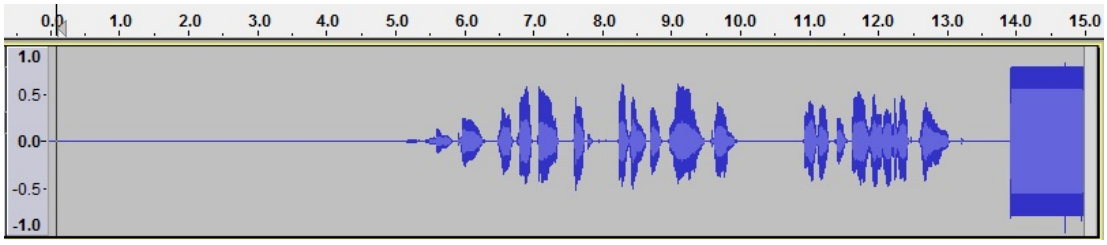

Figure 14: Suspect audio waveform, same sample as figure 13.

The previous samples were from a live broadcast or the test voice and tone loop. Another technique we used to test for audio quality was to inject a constant 440 Hz tone loop into the encoder. The following are examples of audio problems discovered using the MOS method referenced above. In addition, since we are using a constant tone, we can now use audio statistics of the recorded 15 second audio as a reference as well. The reference audio file was tested with the same SoX [9] utility used to generate the logged values as a baseline. The statistics for the test 440 Hz file are below. We expected the log audio

statistics to be different based on audio volume adjustments throughout the audio link; however, the relationships should be similar. In Table 3, we can see the statistics of the 440Hz tone.

Table 3: Sound Exchange Utility (SoX) audio statistics.

Maximum amplitude:	0.692017
Minimum amplitude:	-0.691986
Midline amplitude:	0.000015
Mean norm:	0.44042
Mean amplitude:	0
RMS amplitude:	0.489183
Maximum delta:	0.043854
Minimum delta:	0
Mean delta:	0.027605
RMS delta:	0.030662

Shown below in Figure 15 is a plot of the MOS scores from the T1800V site with an injected tone. Of interest is the negative spike well below 2.5 circled in red (as shown in figure 15).

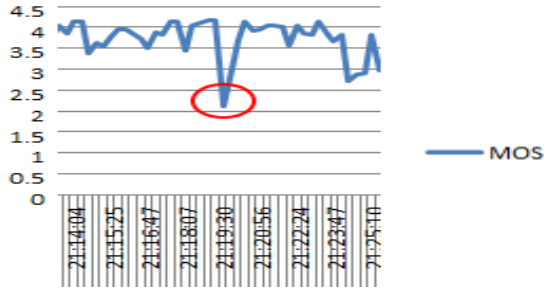

Figure 15: Automated MOS score example Texas to Vermont T1800V link, constant 440Hz tone.

Figure 16 is an example of how the audio statistics can now be used to indicate an outage. The negative spikes seen in the plot below are of special interest. We had high success in correlating these negative spikes to audio problems. For example, the spike circled in red matches the date time of the MOS score negative spike above.

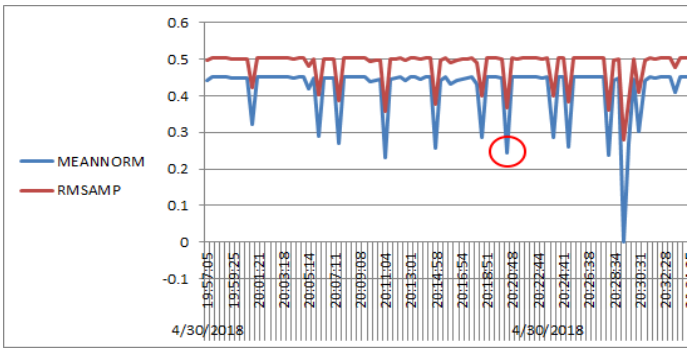

Figure 16: SoX audio statistics correlate with MOS score to indicate an outage.

The outage is clearly seen in the spectrograph below (figure 17) as well as in the waveform image that follows (figure 18).

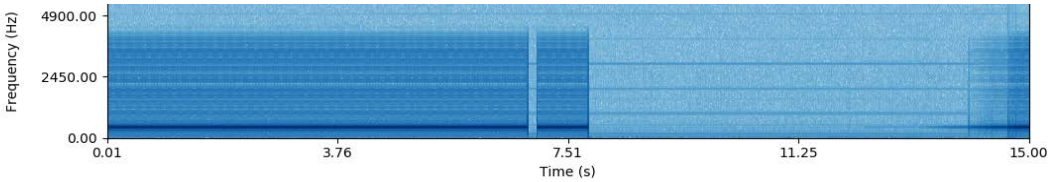

Figure 17: Spectrograph of 15 second sample correlating to MOS score in Figure 15 and SoX audio statistics in Figure 16.

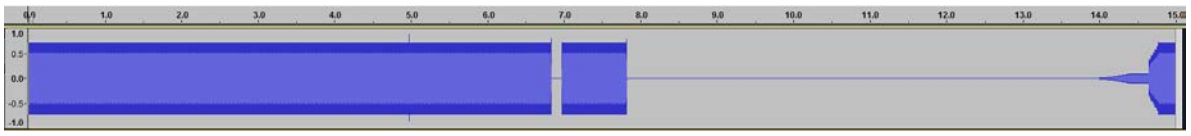

Figure 18: Waveform of 15 second sample correlating to MOS score in Figure 15 and SoX audio statistics in Figure 16.

In the next example, we bypass the MOS score as a reference and utilize the audio statistics alone to find bad audio. Note how defined the audio statistics plot is, each negative spike was correlated to an audio problem. While the MOS score is a useful parameter in rating audio quality, it doesn't always catch all the problems due to the decoder's' buffer. This buffer helps smoothen out network variances in latency and jitter, but the smoothing is not always successful as we observed that bad audio correlated to a low MOS score as well. The buffers effectiveness degrades with lower MOS scores. The audio statistic plot below shows an audio outage which is further represented by the spectrograph, waveform and confirmed by listening to the sample.

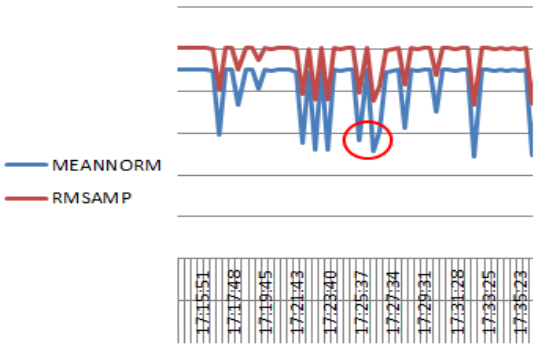

Figure 19: SoX audio statistics as a stand-alone indicator of audio quality problems (constant tone).

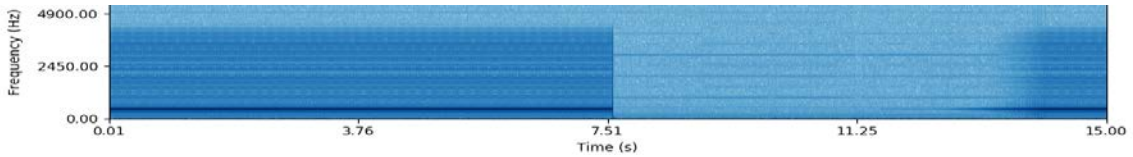

Figure 20: Spectrograph of 15 second audio sample from Figure 19.

Figure 21: Waveform of 15 second audio sample from Figure 19

6 Data Prediction

Using the data collected, we were able to rate audio quality. The MOS score remains the best indicator in our configuration, and we could safely rely upon it to forecast future performance. The audio quality statistics worked well for a constant tone but not for the variable frequency voice of the live broadcast of the voice and tone test loop. We counted the number of MOS scores over a 24-hour period to establish how many were "Good", "Fair", "Poor", "Bad" or "Unusable". The data was compared using the ITU-T rating scale [4] for MOS, and tables 4 to 6 present the results.

Table 4: T1800V

Total Events	5279	100%	
4.0-4.5	2935	56%	Good
3.0-3.9	2215	42%	Fair
2.0-2.9	128	2%	Poor
1.0-1.9	1	0%	Bad
<1.0	0	0%	Unusable

Table 5: V16V

Total Events	5012	100%	
4.0-4.5	4664	93%	Good
3.0-3.9	342	7%	Fair
2.0-2.9	0	0%	Poor
1.0-1.9	0	0%	Bad
<1.0	0	0%	Unusable

Table 6: V0V

Total Events	5402	100%	
4.0-4.5	5238	97%	Good
3.0-3.9	149	3%	Fair
2.0-2.9	0	0%	Poor
1.0-1.9	0	0%	Bad
<1.0	0	0%	Unusable

The T1800V audio link was found to be the link with the poorest quality. Only 56% of the time did it provide "Good" audio. Nearly half the time, 44% it provided "Fair" to "Poor" audio. The V16V and V0V audio links met our goal of "Good" audio 93% and 97% respectively. As the other data received and analyzed by us showed similar, corroborating characteristics, there is no reason to assume the T1800V audio link will improve or the V16V and V0V will degrade below their current levels.

7 Conclusion and Findings

The MOS scores provided the expected date time indicator with variances to research further into the audio outages. The network latency and jitter were negated to some degree by the buffer in the decoder. The buffer helped reduce the impact of a poor MOS score on audio quality to a degree. The T1800V audio link was "Fair" for nearly half the time. As a listener, we found it unacceptable and difficult to listen to. The link had frequent drops of varying durations evident in the spectrographs. This was true for the live

broadcast audio as well as the voice and tone and constant tone loop files. The V16V and V0V links were "Good" most of the time confirmed by the spectrographs and listening to samples.

In our tests it was easiest to locate an audio problem using the audio statistics log for the 440 Hz tone signal. With the constant signal and constant frequency, we were able to use the audio statistics as a further indicator of where to look at the audio. The root mean squared amplitude and mean norm amplitude provided excellent results most of the time. The audio statistics logging was only useful for the tone loop, it didn't perform well with the live broadcast or voice and tone loop. The MOS scores however applied to all audio sources.

To improve on our technique, the SoX [9] statistics could be set up to monitor the live broadcast audio. This may help to provide a baseline for the live broadcast or test voice and tone audio. We could compare this baseline to the live broadcast audio stream. If successful, this would provide a high frequency of audio problem detection, like the results we achieved with the constant tone loop. The logging for the MOS, encoding router, decoding router and decoder could be combined with the audio statistics so that the date times are more in sync. These methods could be refined and applied to live broadcast audio to further automate the process for continuous monitoring of streamed audio to radio broadcast transmitters.

ACKNOWLEDGEMENT

This work was partially supported by Askew Institute at The University of West Florida.

REFERENCES

[1] Audacity Team (2017). Audacity(R): Free Audio Editor and Recorder [Computer application]. Version 2.2.0 retrieved February 5th 2018 from https://audacityteam.org/

[2] Gan, C., Wang, X., Zhu, M., & Yu, X. (2011). Audio quality evaluation using frequency structural similarity measure. IET International Communication Conference on Wireless Mobile and Computing (CCWMC 2011). doi:10.1049/cp.2011.0896

[3] IEEE recommended practice for speech quality measurements (No. 297). (1969). New York, NY: Institute of Electrical and Electronics Engineers.

[4] ITU-T. (1993). G.711 : Pulse code modulation (PCM) of voice frequencies. Retrieved from https://www.itu.int/rec/T-REC-G.711

[5] J. D. Hunter, "Matplotlib: A 2D Graphics Environment," in Computing in Science & Engineering, vol. 9, no. 3,pp. 90-95, May-June 2007. doi: 10.1109/MCSE.2007.55

[6] Khalifeh, A. F., Al-Tamimi, A., & Darabkh, K. A. (2017). Perceptual evaluation of audio quality under lossy networks. 2017 International Conference on Wireless Communications, Signal Processing and Networking (WiSPNET). doi:10.1109/wispnet.2017.8299900

[7] Mok, R. K., Chan, E. W., & Chang, R. K. (2011). Measuring the quality of experience of HTTP video streaming. 12th IFIP/IEEE International Symposium on Integrated Network Management (IM 2011) and Workshops. doi:10.1109/inm.2011.5990550

[8] Python Software Foundation. Python Language Reference, version 2.7. Available at <http://www.python.org/>

[9] SoX (2018). SoX - Sound eXchange: Free Audio Converter and Processor [Computer application]. Version 14.4.2 retrieved February 5th 2018 from http://sox.sourceforge.net/

[10] Yuhong, Y., Hongjiang, Y., Ruimin, H., Song, W., & Songbo, X. (2013). A new mobile audio quality assessment using Jitter Distortion Measure approach. 2013 Fifth International Workshop on Quality of Multimedia Experience (QoMEX). doi:10.1109/qomex.2013.6603234

SOCIETY FOR SCIENCE AND EDUCATION
UNITED KINGDOM

TNC TRANSACTIONS ON NETWORKS AND COMMUNICATIONS

VOLUME 6, NO. 6
ISSN: 2054 -7420

Mitigation of Terrain Effects using Beamforming Antennas in Ad Hoc Networks

Vinay B. Ramakrishnaiah, Robert F. Kubichek, and Suresh S. Muknahallipatna
Department of Electrical and Computer Engineering, University of Wyoming, United States;
vramakr1@uwyo.edu; kubichek@uwyo.edu; sureshm@uwyo.edu

ABSTRACT

Wireless communication is sensitive to ambient noise as well as interference due to the use of a shared medium. The link quality is significantly affected by the surrounding terrain including buildings, hills, foliage, etc. Terrain changes also pose a problem for communication and localization in mobile ad-hoc networks and in the deployment of Internet of Things (IoT). Many of these problems can be addressed through careful antenna design, but these can be challenging as they require complex hardware and software. We propose a new approach called virtual terrain leveling (VTL), which acts as a trade-off between the complex antenna design approaches and the simple omni-directional antennas. VTL virtually nullifies the effects of the terrain using phased array antennas to compensate for the path losses. Convex optimization and the Nelder-Mead simplex method are used to compute the antenna array weights that minimize the error between the ideal and achieved beam patterns. Simulations are performed in the presence of different terrains and the received power at varying distances from the transmitter is analyzed. The results show improved received power up to a specified distance from the transmitter and then power decays rapidly with increasing distance, indicating interference reduction.

Keywords: Terrain nullification, Phased arrays, Convex optimization, Nelder-Mead optimization.

1 Introduction

Unlike wired communication, wireless communication is sensitive to ambient noise as well as interference due to the use of a shared medium. Wireless spectrum is a scarce resource, which makes it impractical for large wireless ad hoc networks to carry out simultaneous transmissions using only frequency division techniques. Therefore, the signal transmissions are separated in space, time, and encoding to facilitate increased simultaneous transmissions. These interference avoidance techniques usually require a-priori planning and centralized control. Increase in the number of nodes exacerbates the interference issue and makes the design of centralized control more difficult.

Signal quality in wireless networks is significantly affected by the surrounding terrain including buildings, hills, foliage, etc. Terrain features pose difficult challenges to implementation of mobile ad hoc networks (MANETs). The performance of MANETs and how they are influenced by their ability to cope with topology changes arising from node mobility under the influence of terrain is analyzed in [1]. They find that the probability of two connected nodes remaining connected falls rapidly as the line-of-sight (LOS) probability

DOI: 10.14738/tnc.66.5481
Publication Date: 12nd December 2018
URL: http://dx.doi.org/10.14738/tnc.66.5481

decreases. Also, most of the routing protocols are designed based on the assumption of omni-directional transmissions, which is unlikely to hold for terrain encountered in most practical applications.

Beamforming antennas can effectively address the interference issue, even without a central control, acting as a spatial filter by directing the beam in certain directions. They create radiation patterns by adding the signals constructively in desired directions and destructively in others. The antenna beam synthesis techniques are marginally addressed for fixed infrastructure networks in previous literature. [2] uses a simplified sector model for antenna beams to approximate azimuth beams. [2] [3] use a simplified cellular model by neglecting the topography. In [4] a coverage goal is defined, and the amount of power radiated outside the cell is compared with the amount of power radiated within the cell. But they use the same approximation as in [2], which does not consider the topography. Smart antenna solutions including switched beam antennas, adaptive beam arrays, and Multiple-Input Multiple-Output (MIMO) systems [5] usually require a separate transceiver behind every antenna element. This is problematic for large antenna array systems as they are expensive and also because of the requirement of high speed Analog-to-Digital / Digital-to-Analog converters to accommodate the necessary bandwidth. Several signal processing techniques like randomization and cancellation are used to reduce inter-cell interference. These techniques try to average the interference across the system bandwidth and null out certain directions. The required processing power and complexity of these advanced techniques limit their use in wireless ad hoc networks.

[6] [7] [8] describe phase-only antenna arrays that achieve optimal beam patterns with maximum average network signal-to-noise ratio (SNR). They use a hybrid analog/digital beamformer to steer the antenna beams using a single transceiver, power splitter/combiner, and electronically controlled analog phase shifters. These solutions are independent of the path loss models, therefore, making it easy to incorporate any terrain or traffic information. However, they are computationally complex requiring a centralized computer to pre-compute the antenna weights. A second order cone programming and semi-definite programming based approach to solve the array synthesis problem in non-uniform array with constraints on the magnitude is presented in [9]. They also address the robust array pattern synthesis in the presence of gain and phase uncertainties.

In [10], we presented a preliminary analysis of Virtual Terrain Leveling (VTL) that acts as a trade-off between the complex antenna design approaches and the simple omni-directional antennas. VTL uses the hybrid analog/digital beam forming technique to limit the radiated power and validates the free space assumption by nullifying the effects of terrain up to a specified range from the transmitter. In other words, phased array antennas are used that provide gain inversely proportional to the path loss. In this paper, we extend our analysis to include active array antennas, and also study different array sizes and geometries. The antenna beams are synthesized using two different approaches, i.e., convex optimization [11] and the Nelder-Mead simplex method [12]. The idea behind VTL relies on efficiently pre-computing the radio propagation maps using a suitable path loss model and using this information to find the antenna array weights at the transmitter. Approximation methods such as the ones presented in [13] [14] can be used to get a low complexity representation of radio propagation maps for VTL implementation. We show that VTL can mitigate issues by providing near omni-directional propagation in the presence of terrain with the use of directional antennas and limiting the range of the radiated signal to reduce interference

and to increase frequency reuse. With the use of pre-computed radio propagation maps, VTL can avoid deafness in MANETs as they will be able to hear their neighboring nodes from all directions.

This paper is organized as follows: Section 2 explains the VTL methodology and the goals of this research. In Section 3, background theory on phased array antennas, the array gain, and the optimization methods used to obtain array gain patterns is discussed. The simulations and analysis of results of the proposed VTL approach is presented in Section 4. Section 5 provides a summary of this research work and concludes the paper.

2 VTL Methodology

In many antenna applications, the problem of antenna pattern synthesis is of extreme importance and therefore it has been studied for decades. However, most of the existing literature assumes the knowledge of the optimal beam pattern and uses some kind of optimization algorithm to solve for system parameters. For example, the authors of [15] assume a desired, synthetic complex array amplitude vector, comprised of ones and zeros, where 1s correspond to the directions of interest, and compute the amplitude weights that minimize the error between the realized beam pattern and the synthetic complex array amplitude vector. Similarly, [16] uses genetic algorithm to search for complex roots that provide nulls in the desired directions. Particle-swarm optimization is used in [17] to search for the optimal array geometry that can realize the main beam with the desired beam width, providing unity gain in the directions of interest. Through VTL, we provide an analytical approach for computing the antenna gain patterns that minimizes the effects of path loss. The analytical approach eliminates the need for speculative beam patterns based on the synthetic complex array amplitude vectors.

VTL virtually nullifies the effects of terrain at a desired distance from the transmitter by increasing the gain in the directions of increased path loss. Typically, the transmitter power is set to provide radio coverage up to a certain virtual radius (VR) based on receiver sensitivity. The idea is to reduce the transmitter power and use an antenna array with a gain distributed in such a way that it compensates for the lower received power. To illustrate the concept, consider a simple wireless network without adaptive power control, whose network protocol assumes homogeneous terrain with equal propagation in all directions. Unfortunately, real-world terrain causes significant variation in propagation distance depending on direction, which impairs network efficiency. In this example, assume the desired "cell radius" is 1 km and that transmitter power P_t has been adjusted so that all locations in the cell are within range of the base station as shown in the cartoon of Figure. 1 (a). By satisfying the worst-case direction of 200°, we see excessive range of over 2 km in other directions, likely causing interference in adjacent cells. VTL uses a passive antenna beam pattern that is inversely related to range, using less gain in some directions in order to provide higher gain in others, as shown in Figure. 1 (b). Figure. 1 (c) shows the range map after VTL is applied. The reason the corrected range map is not an ideal flat line is because a practical antenna array cannot perfectly remove all effects of loss-vs-direction. After VTL is applied, it is clear that the resulting system has excess range, and transmitter power can be reduced while maintaining the desired 1 km cell radius, as shown in Figure. 1 (d). VTL thus gives better power efficiency, reduced adjacent cell interference, and improved frequency reuse.

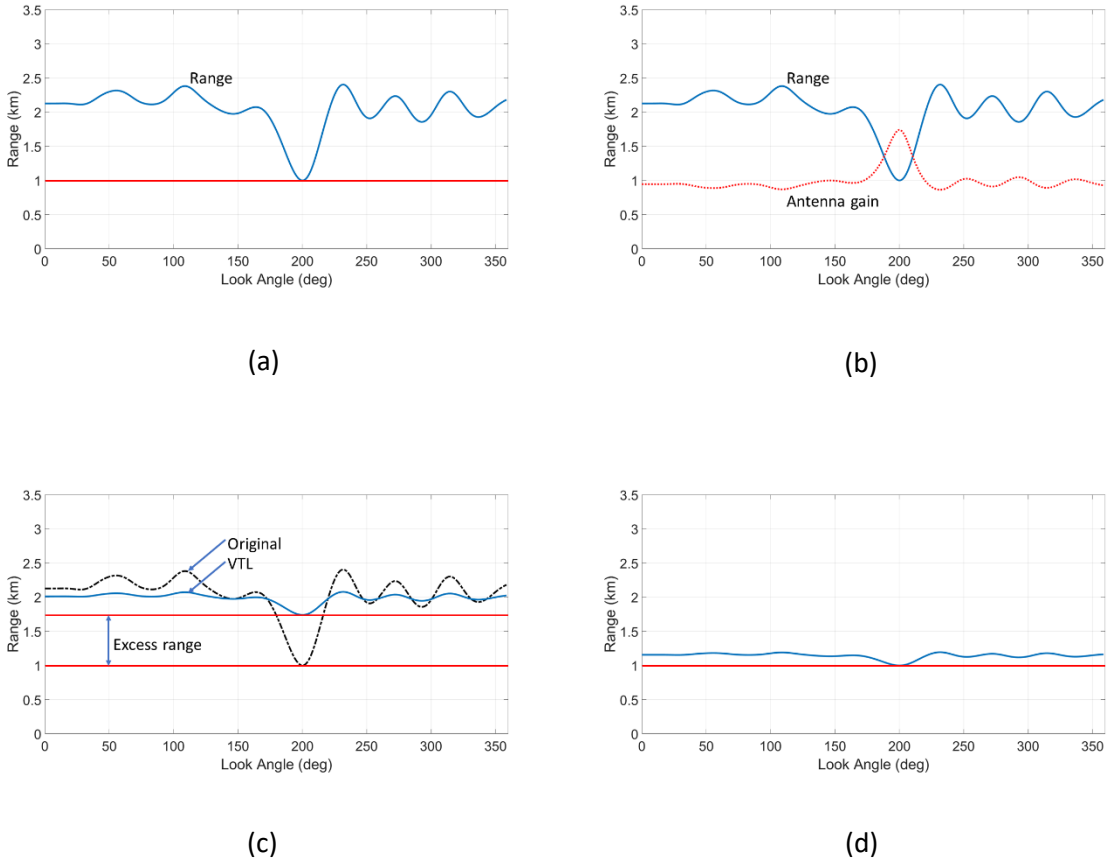

Figure. 1: VTL cartoon showing (a) Range vs. angle, minimum range = 1 km. (b) Antenna gain pattern (not to scale). (c) Range with VTL. (d) Range after VTL, reduced transmitter power.

We make use of the Cost 231 Walfisch-Ikegami model (WIM) [18] [19] to demonstrate the concept of VTL. The WIM provides a theoretical model for urban communication systems. In this model, the rows or blocks of buildings are viewed as diffracting cylinders. Buildings are treated as absorbing screens, which reduces the propagation process to multiple forward diffractions past a series of screens. Diffraction is contemplated right from rooftops down to street level, which provides path loss predictions close to average measurement path loss.

For an omnidirectional antenna, if a free line-of-sight (LOS) exists in an urban canyon, the path loss in decibels is given by

$$L_{\text{WIM}} = 42.6 + 20 \log f + 26 \log R,$$

where the frequency f is given in MHz and R is the range in km. If there is no LOS path between the transmitter and receiver, the path loss is defined as

$$L_{WIM} = \begin{cases} L_{FS} + L_{rts} + L_{msd} \\ L_{FS}, \end{cases} \qquad if\ L_{rts} + L_{msd} < 0,$$

where L_{FS} is the free-space path loss. The coupling of the wave propagating along the multi-screen path into the receiver located in the street is defined as the rooftop-to-street diffraction and scatter loss, L_{rts} given by

$$L_{rts} = \begin{cases} -16.9 - 10\log w + 10\log f + 20\log \Delta h_{receiver} + L_{ori}, & if\ h_{roof} > h_{receiver} \\ 0, & if\ L_{rts} < 0 \end{cases}$$

where L_{ori} is the street orientation loss defined as

$$L_{ori} = \begin{cases} -10 + 0.354\psi & for\ 0 \le \psi < 35 \\ 2.5 + 0.075(\psi - 35) & for\ 35 \le \psi < 55. \\ 4 - 0.114(\psi - 55) & for\ 55 \le \psi \le 90 \end{cases}$$

Here, ψ is the angle in degrees between the base station and the road. The multiscreen diffraction loss L_{msd} is given by

$$L_{msd} = L_{bsh} + k_a + k_d \log R + k_f \log f - 9\log b,$$

where

$$L_{bsh} = \begin{cases} -18\log(1 + \Delta h_{base}) & for\ h_{base} > h_{roof} \\ 0 & for\ h_{base} \le h_{roof} \end{cases},$$

$$k_d = \begin{cases} 18 & for\ h_{base} > h_{roof} \\ 18 - 15\dfrac{\Delta h_{base}}{h_{roof}} & for\ h_{base} \le h_{roof} \end{cases},$$

$$k_a = \begin{cases} 54 & for\ h_{base} > h_{roof} \\ 54 - 0.8\Delta h_{base} & for\ R \ge 0.5\ km\ and\ h_{base} \le h_{roof} \\ 54 - 1.6\Delta h_{base} R & for\ R < 0.5\ km\ and\ h_{base} \le h_{roof} \end{cases},$$

and

$$k_f = -4 + \begin{cases} 0.7\left(\dfrac{f}{925} - 1\right) & suburban\ areas \\ 1.5\left(\dfrac{f}{925} - 1\right) & urban\ areas \end{cases}.$$

The predicted power received at a receiver can be computed using the WIM as

$$P_{rWIM}(\theta) = \frac{P_t G_t(\theta) G_r(\theta)}{L_{WIM}(\theta)},$$

where P is the power, $G(\theta)$ is the antenna gain, $L_{WIM}(\theta)$ is the path loss, and the subscripts indicate the association of the quantities with either the transmitter or the receiver. This compares with the predicted loss in a free-space environment

$$P_{rFSM}(\theta) = \frac{P_t G_t(\theta) G_r(\theta)}{L_{FSM}},$$

where $L_{FSM} = \left(\frac{4\pi R}{\lambda}\right)^2$. Here, λ is the wavelength, and R is the distance from the transmitter in meters. Using omni-directional antennas for both the transmitter and receiver, the power received can be written as $P_{rWIM}(\theta) = \frac{P_t}{L_{WIM}(\theta)}$, and $P_{rFSM} = \frac{P_t}{L_{FSM}}$.

VTL tries to find the transmitter antenna gain such that $P_{rWIM}(\theta) = P_{rFSM}$, i.e.,

$$\frac{P_t G_t(\theta)}{L_{WIM}(\theta)} = \frac{P_t}{L_{FSM}}$$

or

$$G_t(\theta) = \frac{L_{WIM}(\theta)}{L_{FSM}}, \quad (1)$$

where L_{FSM} is the free space path loss. Equation (1) provides an analytical solution for finding the gain pattern that compensates for the propagation path losses. The solution works regardless of the path loss model used. Also, it is important to notice that the antenna gain obtained using equation (1) is the power gain of the antenna. Therefore, the antennas/antenna arrays have to be designed such that they closely match this desired power pattern subject to the design constraints like system power, degrees of freedom, etc. In case of very high path losses, it is beneficial to include the condition $L_{WIM} = \min(L_{WIM}, Maximum\_Loss\_Threshold)$ to prevent futile gain in the directions of very high path loss.

3 Background Theory

3.1 Antenna Arrays

Antenna arrays are effective in providing a flexible and efficient way to synthesize antenna gain patterns. The power radiated or received by the antenna is enhanced in certain directions and diminished in others by addition and cancellation of power. For VTL, a low complexity hybrid analog/digital beamforming antenna described in [6] is used. This system uses a single transceiver along with digitally controlled phase shifters and step attenuators/amplifiers as shown in Figure. 2.

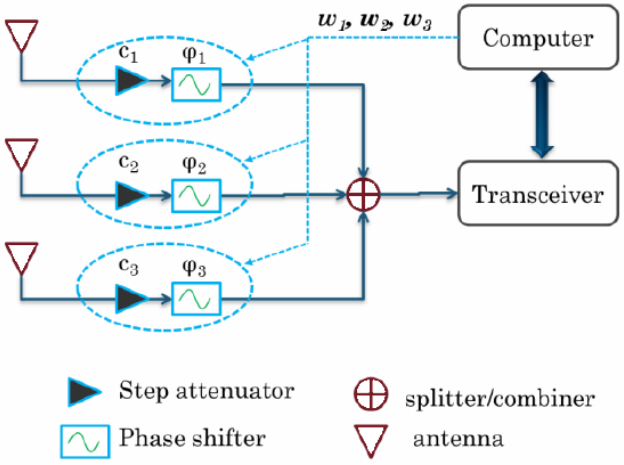

Figure. 2: Low complexity hybrid analog/digital beamformer.

In the hybrid system, the complex antenna weights, w_k are applied by a computer to the receiver outputs to form the desired antenna beams. For a generic system, the antenna weights $w_k = c_k e^{j\phi_k}$, have both magnitude and phase. The complexity of the antenna system can be further reduced by eliminating the step attenuator/amplifier, which will constrain the weights to be phase-only ($w_k = e^{j\phi_k}$).

The transmitted signal can be represented as $r(t) = 2s(t)\cos(\omega_0 t) = s(t)e^{j\omega_0 t} + s(t)e^{-j\omega_0 t}$, where $\omega_0 = 2\pi f_0$ is the angular frequency. The block diagram of the receiver is shown in Figure. 3.

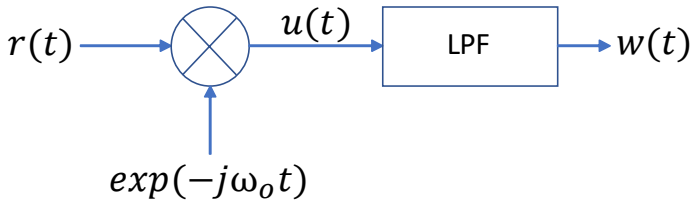

Figure. 3: Block diagram of the receiver.

The mixer output signal $u(t) = s(t)e^{-2j\omega_0 t} + s(t)e^{0}$, but the high frequency component is removed by the low pass filter giving $w(t) = s(t)$. Therefore, we can safely assume the transmitter signal to be $r(t) = s(t)e^{j\omega_0 t}$ to avoid unnecessary calculations.

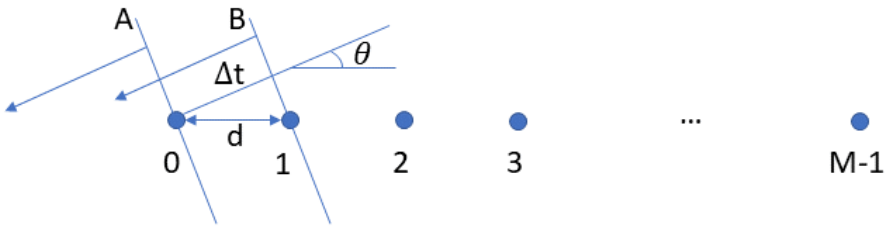

Figure. 4: M-element uniform linear array.

A uniform linear array consisting of M antenna elements is shown in Figure. 4. Consider a single instant of time t, giving a snapshot of the wavefront for a signal arriving from direction θ. By looking at Figure. 4, it is evident that wave B touches antenna #1 before it touches antenna #0. Let the wavefront at antenna #0 be $s_0(t) = s(t)e^{j\omega_0 t}$, then the wavefront at antenna #1 is $s_1(t) = s_0(t + \Delta t)$. We assume a "low-pass narrow-band" signal $s(t)$ with bandwidth << f_0. Therefore, $s(t + \Delta t) \approx s(t)$, where $\Delta t = \frac{dcos\theta}{c}$ and $c = \lambda f_0$. Therefore $\Delta t = \frac{2\pi dcos\theta}{\omega_0 \lambda}$. The signal received at the receiver for antenna m is given as $r_m \simeq s(t)e^{j\omega_0(t+m\Delta t)} = s(t)e^{j\omega_0\left(t+\frac{2\pi mdcos\theta}{\omega_0\lambda}\right)}$. For the entire array, the received signal will be $\boldsymbol{r}(t) = s(t)e^{j\omega_0 t}\left[1, e^{jkdcos\theta}, e^{j2kdcos\theta}, \ldots\right]^T$, where $k = \frac{2\pi}{\lambda}$ is the wavenumber.

The received signal is represented as $r(t) = s(t)\cos(\omega_0 t) + v(t)$, where $s(t)$ is a narrow band message signal and $v(t)$ is the white noise. The receiver down-converts the signal resulting in a complex base-band signal $\boldsymbol{y}(t)$. For example, the result for a uniform linear array is

$$\boldsymbol{y}(t) = \begin{bmatrix} 1 \\ e^{jkdcos\theta} \\ \vdots \\ e^{j(M-1)kdcos\theta} \end{bmatrix} s(t) + \begin{bmatrix} v_0(t) \\ \vdots \\ v_{M-1}(t) \end{bmatrix}$$

or $\boldsymbol{y}(t) = \boldsymbol{h}(\theta)s(t) + \boldsymbol{V}$, where k, d, and θ are the wavenumber, antenna element separation, and direction of arrival (DOA), respectively, and $\boldsymbol{h}(\theta)$ is called the steering vector. Note that $\boldsymbol{h}(\theta)$ must be

modified for each specific antenna array geometry to give proper delay characteristics in the direction θ. It is possible to find a filter $\boldsymbol{K}$ that amplifies the signals in certain directions. Therefore, in case of antenna arrays the term $\boldsymbol{K}^*\boldsymbol{h}(\theta)$ represents the array gain.

3.2 Power Gain of Antenna Arrays

Antenna arrays act as directional amplifiers, with a voltage amplification factor of $\boldsymbol{K}^*\boldsymbol{h}(\theta)$, also known as the Array Factor (AF), which is a function of θ (assuming 2D patterns). The coefficients of the filter $\boldsymbol{K}$ are the antenna weights $\boldsymbol{w} = [w_0, w_1, \dots, w_{M-1}]^T$, therefore, $AF = \boldsymbol{w}^T\boldsymbol{h}(\theta)$. Most of the literature like [6] [11] [15] [20] [21] considers the antenna array gain to be equal to either the array factor or the power gain, $G_p(\theta,\phi) = |AF(\theta,\phi)|^2 G(\theta,\phi)$, where $G(\theta,\phi)$ is the power gain of a single element of the array. These representations of the antenna gain provide accurate directional characteristics and signal-to-noise ratios (SNRs) but fail to preserve the actual power amplification provided by the antenna. The array factor provides the complex amplitude gain for an array and does not directly relate to the power gain. The solution to this problem is addressed in [22]. They show that the power gain of an antenna array is

$$G_p(\theta) = 2\pi \frac{|AF(\theta)|^2}{\int_0^{2\pi} |AF(\theta)|^2 \, d\theta} P_{fact}. \tag{2}$$

where $P_{fact} = \frac{1}{M}\sum_{j=0}^{M-1} |w_j|$, and M is the number of antennas in the array.

In order to synthesize the antenna array beam pattern, the two parameters that can be modified are the antenna weights, $\boldsymbol{w}$ and the steering vector, $\boldsymbol{h}(\theta)$. As shown in section 3-A, the steering vector is dependent on the antenna array geometry and is fixed for a given antenna array. The flexibility of antenna arrays lies within the fact that complex antenna weights can be modified to obtain the desired beam pattern.

There are several ways to find the weight vector, $\boldsymbol{w}$. For example, it is possible to find $\boldsymbol{w}$ that minimizes the output noise power while holding unit gain in the signal direction. This is called the "Minimum Variance Distortion-less Response" filter. Numerous other beam synthesis techniques like the Schelkunoff polynomial method [23], Fourier transform method [24], Woodward-Lawson method [25] [26], etc. have been extensively studied over the years. The problem with most of the methods is that there is no absolute guarantee the solution is globally optimal unless the problem is convex [27] [28], and they also assume the knowledge of the noise covariance matrix, which requires complex and expensive hardware for realization.

In this paper, we use the convex optimization [11] technique for synthesizing beam patterns for design problems that are convex. However, the problem of computing phase-only weights is non-convex; therefore, the Nelder-Mead simplex search [12] is also used for minimizing the desired fitness function in such cases.

3.3 Convex Optimization

A set, C is convex [11] if and only if for any two points $x_1, x_2 \in C$ and any θ where $0 \le \theta \le 1$, the point $\theta x_1 + (1-\theta)x_2$ also is an element of C. In other words, this means that a set is convex if the direct path between any two points in the set is entirely included in the set. For a function f, if the line segment between $(x, f(x))$ and $(y, f(y))$, which is a chord from x to y, lies above the graph of f, then the

function is defined to be convex. Mathematically, a function f is convex on a convex domain if for all $x, y \in \mathbf{dom}\, f$, and θ with $0 \leq \theta \leq 1$, the following inequality holds:

$$f(\theta x + (1-\theta)y) \leq \theta f(x) + (1-\theta) f(y). \tag{3}$$

The convex optimization problem involves minimizing the convex function over its domain, which is a convex set. The convex optimization problem is defined using the following notation, which is often referred to as disciplined convex programming [29] [30]:

$$\begin{aligned} &minimize\ f_0(x) \\ &subject\ to\ f_i(x) \leq 0, \quad i = 1, \dots, m \\ &\qquad\qquad h_i(x) = 0, \quad i = 1, \dots, p \end{aligned} \tag{4}$$

and the objective is to find the value x that minimizes $f_0(x)$ satisfying $f_i(x) \leq 0, i = 1, \dots, m$, and $h(x) = 0,\ i = 1, \dots, p$. It is always possible to find the global minima of convex functions as the local minima itself is the global minima as per the definition of convex functions. Many optimization problems like least squares techniques, linear programming, conic optimization, etc., fall into the category of convex optimization, and computing the weights of an antenna array can be treated as a convex problem by relaxing the constraints.

3.4 Nelder-Mead Simplex Method

While the convex optimization approach of computing the optimal antenna weights finds solutions with relaxed constraints, it requires using step attenuators or amplifiers that increases the hardware cost and complexity of the antenna system. Therefore, it is sometimes desirable to find antenna weights that are phase-only, so that the system could be realized using only the phase shifters. However, constraining the weights to have unit magnitude makes the optimization problem to be non-convex as discussed previously. Hence, we make use of the Nelder-Mead algorithm to perform an unconstrained search for phase-only weights.

The Nelder-Mead (NM) algorithm [12] is one of the most widely used methods for non-linear unconstrained optimization. The Nelder-Mead method attempts to minimize a scalar valued non-linear function of n variables using only the function values without any derivative information. This algorithm uses a simplex of n-dimensional vectors $\boldsymbol{x}$**.** Let x_i, denote the list of points in the current simplex, with $i = 1, \dots, n+1$. Our objective is to minimize the function f such that $\boldsymbol{x} \in \mathbb{C}^{\boldsymbol{n}}$ is the domain of f, therefore, x_i is referred to as the best point, and x_{n+1} as the worst point. Four scalar parameters $reflection\ (\rho), expansion\ (\chi), contraction\ (\gamma)$, and $shrinkage\ (\sigma)$ are specified for Nelder-Mead method.

The following indicates one iteration of the Nelder-Mead algorithm [31]:

- The $n+1$ vertices are ordered such that $f(x_1) \leq f(x_2) \leq \cdots \leq f(x_{n+1})$.
- The reflection point, x_r is computed as $x_r = \bar{x} + \rho(\bar{x} - x_{n+1}) = (1-\rho)\bar{x} - \rho x_{n+1}$, where $\bar{x} = \sum_{i=1}^{n} \frac{x_i}{n}$. Evaluate $f_r = f(x_r)$. If the value $f_1 \leq f_r \leq f_n$, the reflection point x_r is accepted and the iteration terminates.

- The expansion point is computed as $x_e = \bar{x} + \chi(x_r - \bar{x}) = \bar{x} + \rho\chi(\bar{x} - x_{n+1}) = (1 + \rho\chi)\bar{x} - \rho\chi x_{n+1}$, if $f_r < f_1$ and the value of the function f_e at x_e is evaluated. The iteration is terminated after retaining either x_e $(f_e < f_r)$ or x_r $(f_e > f_r)$.
- Contraction is performed by computing the contracted point $x_c = \bar{x} + \gamma(x_r - \bar{x})$. A new simplex is obtained by using the contracted point, x_c, if it is better than the worst point.
- The function is evaluated by replacing all the points by $v_i = x_1 + \sigma(x_i - x_1)$, $i = 2, \dots, n+1$, except for the best point. The new vertices $x_1, v_2, \dots, v_{n+1}$ are used for update in the next iteration.

4 Simulation Results and Analysis

The simulations were performed in Matlab with the following system parameters. The WIM was used to compute the path losses with a base station height of 50 m, receiver height of 3 m, and the frequency of operation was set to 900 MHz. The building heights and street widths were varied according to the desired terrain. Different antenna array geometries were tested, and the antenna weights computed using convex optimization and NM simplex method were compared.

The optimal antenna weights can be found by minimizing the squared error between the gain pattern that compensates for the path losses as given by equation (1) and the estimate of the gain obtained using the antenna with limited degrees of freedom. The constraint on the weights, $\boldsymbol{w}$ determines the requirement of amplifiers or attenuators in the system. For example, if the magnitude of the weights is constrained to be less than or equal to 1, then the system could be realized using only phase shifters and attenuators without the need for amplifiers. On the other hand, having fixed constraints for magnitudes (phase-only weights) makes the optimization problem to be non-convex. The optimization problem for finding the optimal antenna weights using convex optimization was set up as follows:

$$\xi(\theta) = \boldsymbol{w}^T \boldsymbol{h}(\theta) - \sqrt{G_t(\theta)} \tag{5}$$

$$minimize \ \|\boldsymbol{\xi}\|_2$$

$$subject \ to \ |w_i| \leq 1, \quad i = 0, \dots, M-1$$

In our simulations, a 2-norm penalty function is used to penalize the errors. If the function f is a norm function and $0 \leq \theta \leq 1$, then from triangle inequality, $\|\theta x + (1-\theta)y\| \leq \|\theta x\| + \|(1-\theta)y\| = \theta\|x\| + (1-\theta)\|y\|$ is true, where the equality follows from homogeneity of a norm. Therefore, the norm function satisfies equation (1) and is convex by definition. Hence, we can solve for the antenna weights using standard convex optimization solvers.

The solutions developed in this paper uses CVX [32] [33], which is a Matlab based modelling system for convex optimization. CVX supports disciplined convex programming [29] [30], where the objective functions and constraints are identified as convex from the outset of the problem and can be specified as standard Matlab expressions.

To enforce the phase-only constraint, the NM simplex method was used to find the optimal value of the weights that minimizes the absolute value of error between the desired gain obtained using equation (1) and the achieved gain. The problem was set up as follows – the phase-only weights of the antenna array are given by

$$\boldsymbol{w} = e^{j\boldsymbol{\phi}}, \tag{6}$$

where $\boldsymbol{\phi} = [\phi_1, \phi_2, \dots]$ are the individual antenna phases. The estimate of the gain with limited degrees of freedom is computed as $G_{est}(\theta) = |\boldsymbol{w}^T \boldsymbol{h}(\theta)|^2$, and the objective function is defined as

$$\xi = \frac{1}{n}\sum_{i=1}^{n} |G_t(\theta_i) - G_{est}(\theta_i)|. \tag{7}$$

The error function $f = \xi$ is minimized using the NM algorithm to find the optimal value of antenna weights. The antenna weights will be constrained to be phase-only due to the way in which the weights are defined in equation (6), i.e., setting the magnitude to be unity. The results in this paper are developed using Matlab's implementation of the NM algorithm utilized through the $fminsearch()$ function.

Using the suburban terrain setting, a circular antenna array with 36 elements was used and the achieved gain pattern was compared with the ideal desired pattern. Figure. 5 shows the ideal and the achieved gain patterns using the convex optimization and the NM simplex approach. The ideal gain pattern computed using equation (1) is used to compensate for path losses and makes the terrain apparently flat for radio communication at the VR. However, the ideal gain requires very high power for realization (Figure. 5: $\frac{1}{2\pi}$ × (Area under the blue curve in Watts)), and therefore, is not practical. Hence, the achieved gain pattern of a passive array can only achieve the desired directivity (shape), but does not meet the power amplification level as shown in Figure. 5. The achieved gain pattern shows increased directivity in the desired directions while conserving the total power of the system to be equal to the transmitter power (passive antenna gain). We can see from Figure. 5 that the convex optimization approach provides a smooth pattern compared to the NM approach that tries to enforce the phase-only constraint at the optimization stage.

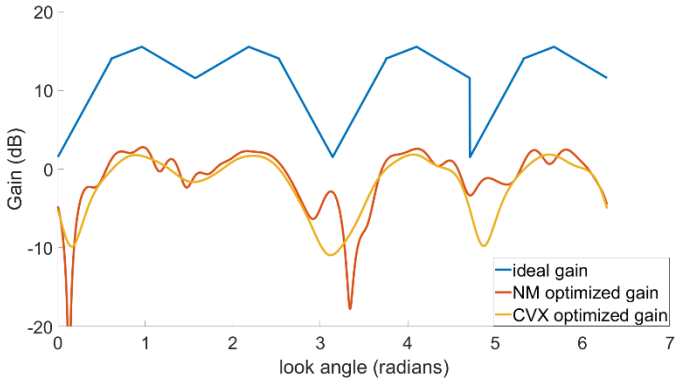

Figure. 5: Ideal and achieved beam patterns.

The power received using the achieved gain pattern in the suburban setting at a distance of 1 km from the transmitter is shown in Figure. 6, and is compared with the received power using an omni-directional antenna for transmission. A 10 W transmitter is used, and the WIM to compute the path losses. Figure. 6 shows that VTL tries to provide a flat response by directing the gain towards increased path losses. Also, the power received with the CVX optimized array has a lower but smoother response due to the relaxed optimization constraints compared to the NM optimized array that constrains the weights to be phase-only. The convex optimization approach constrains the weights to be less than or equal to one. In other words, the weights are realized using step attenuators in hardware. That is why the power received from

the CVX optimized array is lower than the power received from the phase-only NM array, which does not use any attenuators.

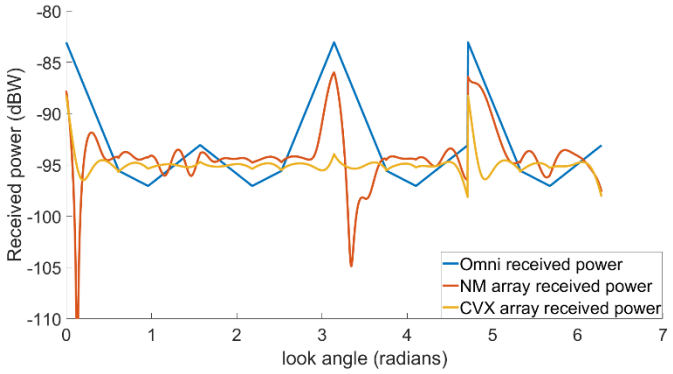

Figure. 6: Received power at a distance of 1 km from the transmitter.

As a measure of performance, the percentage of look-angles above the threshold of -95 dBW is plotted as a function of distance and is shown in Figure. 7. The threshold of -95 dBW was arbitrarily chosen to represent the sensitivity of modern receivers. VTL tries to increase the power received up to the VR from the transmitter. In our simulations, the VTL power gain was computed to achieve a uniform response up to a distance of 1 km from the transmitter. It can be seen from Figure. 7 that the received power with VTL is higher than the received power with omni-directional antennas up to 1.05 km. The power rapidly drops with increasing distances, which is a desirable behavior to avoid interference and for better frequency reuse in wireless networks. Therefore, with VTL, fixed infrastructures like cell-phone base stations will be able to provide increased reception within the cell, at the same time reducing interference to the neighboring cells.

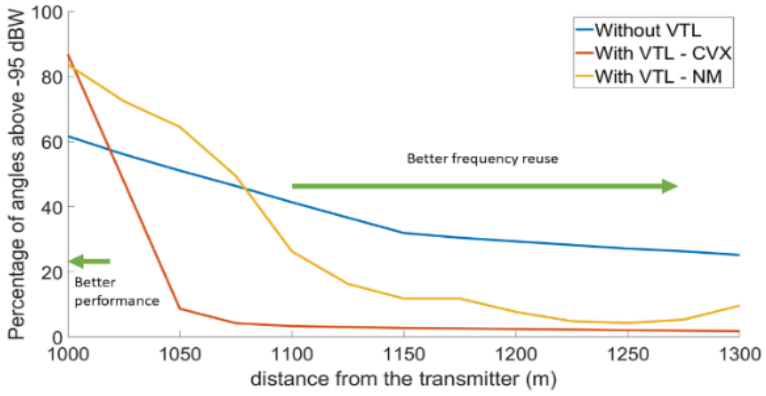

Figure. 7: Percentage of look angles above the threshold of -95 dBW for arrays optimized using different techniques as the distance from the transmitter varies.

Further, the variation of the percentage of look-angles as a function of total power was examined and is shown in Figure. 8. The performance of the VTL antenna system with weights computed using either the CVX or NM approach is evaluated using the power injected into antenna system and the corresponding signal power delivered to the receiver. With very low transmitter powers (less than 6 W), the percentage

of angles below the threshold with VTL is less than the percentage of angles below the threshold with omni-directional transmission. This is because, VTL tries to provide a flat gain pattern rather than increasing the coverage of signals above the desired threshold. As the transmitter power increases, the response with VTL gets significantly better. We can also see that the relaxed constraint system using convex optimization for finding the weights provide slightly better response than the NM optimized arrays with fixed constraints.

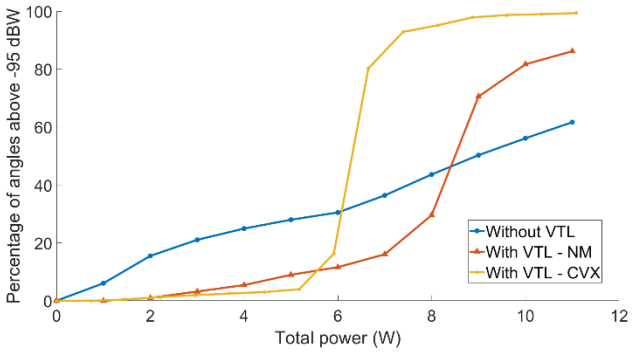

Figure. 8: Percentage of look-angles above the threshold of -95 dBW for arrays optimized using different techniques measured at a distance of 1 km from the transmitter.

As previously discussed, the antenna gain is dependent upon the antenna weights and the steering vector, which in turn depends on the antenna array geometry and the number of antenna elements in the array. In order to see the influence of varying the steering vector on VTL performance, the number of antenna elements and the array geometry were varied, and the weights were computed using the CVX and NM techniques for each case. Different array geometries of linear, square, and circular antenna arrays were investigated. Figure. 9 shows the comparison of various antenna array geometries with 36 antennas and weights computed using different techniques. The CVX optimized array with the relaxed constraint shows more variation with changing geometries compared to the NM optimized array. Also, the arrays symmetric with respect to 2D axes like square and circular arrays perform better than linear arrays that are symmetric with respect to only one axis and this is clearly reflected in Figure. 9.

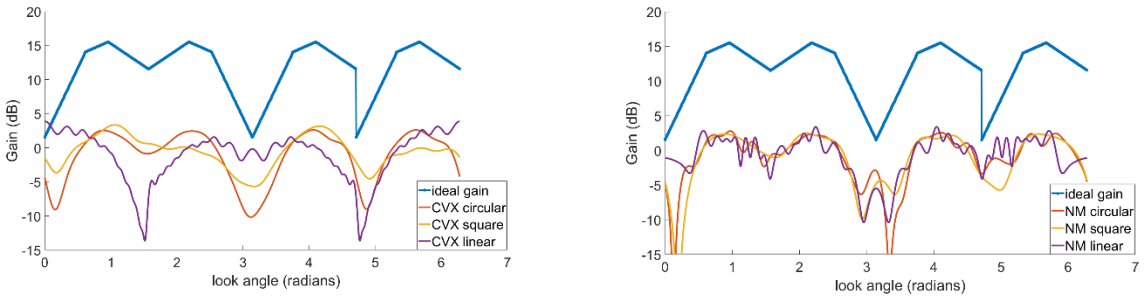

(a) (b)

Figure. 9: Antenna gain patterns for varying array geometries containing 36 elements estimated using (a) convex optimization (b) NM simplex method.

Increasing the number of elements in the array increases the degrees of freedom of an antenna array, thereby, providing an estimate that closely matches the ideal antenna gain. With increasing number of array elements, the maximum directivity of an array in a particular direction also increases. Figure. 10

shows the ideal and the achieved beam patterns of a circular antenna array with varying array elements computed using different optimization methods. It is clear from Figure. 10 that increasing the number of array elements provides a better estimate of the gain pattern.

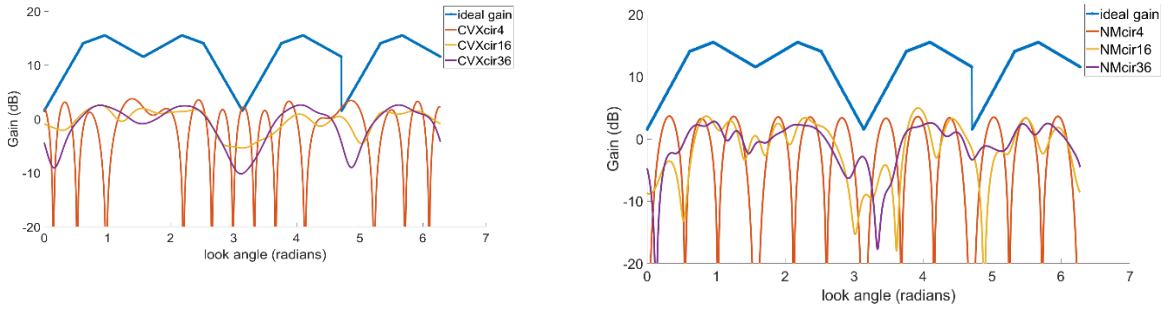

(a) (b)

Figure. 10: Antenna gain patterns of a circular array geometry for varying number of array elements estimated using (a) convex optimization (b) NM simplex method.

As an objective measure of performance, and to complement the graphs in Figure. 9 and Figure. 10, Table 1 and Table 2 show the percentage of look-angles above the threshold of -95 dBW measured at a distance of 1 km from the transmitter with power, $P_t = 10\ W$ for varying antenna array geometries and array elements, respectively.

Table 1. Percentage of look-angles above -95 dBW with varying antenna array geometry (# of antenna elements = 36

Array Geometry	CVX	NM
Linear	46.53	67.36
Square Grid	74.24	83.05
Circular	92.99	79.58

Table 2. Percentage of look-angles above -95 dBW with varying number of antenna elements.

Number of Antenna Elements	CVX	NM
4	56.81	52.53
16	72.64	62.98
36	92.99	79.58

VTL does not perform well with rapidly varying terrain. The passive antenna arrays will not be able to provide variable gain in different directions with abrupt or large changes in terrain. Using active antenna arrays with power amplifiers in the system can improve the response. Figure. 11 shows the comparison of the active antenna gain patterns with the ideal and passive gain patterns. The active antenna weight computation was set up using convex optimization by having the constraint on the weights to be $|w_i| \leq k$, where $k \geq 1$. The power used by the amplifiers is proportional to $|w_i|^2$. Simulations were conducted for the cases when $k = 1, 2, 3$ and the results are shown in Figure. 11. It can be seen that with increasing power, the computed gain patterns move closer to the ideal gain pattern that makes the terrain apparently flat for radio communication.

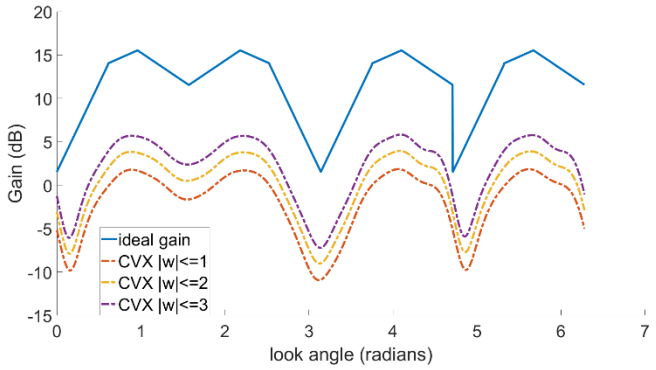

Figure. 11: Antenna gain patterns for increasing amplitude of weights.

5 Conclusion

The novel approach of VTL is proposed that uses phased array antennas to virtually nullify the effects of terrain. The terrain is approximately flattened for radio communication up to the VR from the transmitter. VTL compensates for the communication path losses using antenna array gain. The WIM was used in our simulations for computing the path losses. A hybrid low complexity digital/analog beamforming approach was used for implementing VTL that reduces the hardware cost and complexity of implementation. Two different optimization approaches of using convex optimization and the NM simplex method were employed for estimating the desired beam pattern. The convex optimization approach uses a relaxed constraint to maintain convexity of the problem, whereas, the NM simplex method performs an unconstrained search to find the phase-only weights for the antenna array. The benefits of these two methods can be compared based on the trade-off between increased hardware complexity using convex optimized results, and lower hardware complexity but heavier computational burden of NM.

The power gain of the antenna array was used instead of the normalized array factor to compute the actual received power at a given distance from the transmitter. The gain plots show that the achieved beam patterns try to closely match the ideal beam patterns. The performance of the VTL system was analyzed using the total power injected into the system and the corresponding received power. The percentage of look-angles above the threshold at the receiver was investigated with and without VTL by varying the total power injected into the system and also by increasing the transmitter-receiver separation. VTL shows significant improvement in the percentage of look-angles above the threshold up to the specified VR from the transmitter, and the percentage drops quickly as distance increases. This shows that VTL can potentially mitigate issues like interference in mobile ad hoc networks.

Simulations were conducted to study the benefits of increasing the number of antennas in the array and it was evident from the results that increasing the number of antennas increases the number of degrees of freedom, thereby, providing a better estimate of gain patterns. Various antenna array geometries were also tested and arrays that are symmetric with respect to the 2D axes provided better response compared to linear arrays. One of the limitations of VTL is that it does not perform well in the presence of rapidly varying terrain. Active arrays were also tested and were shown to provide better results in high loss scenarios.

REFERENCES

[1] D. Tate, L. Joneckis, J. Fregeau, C. Kramer and D. Sparrow, "Impact of Terrain Features for Tactical Network Connectivity," Institute for Defense analyses, Alexandria, Virginia, 2013.

[2] J. Pontes, M. Porebska, T. Fugen and W. Wiesbeck, "Base Station Antenna Synthesis for High Sites CDMA Networks," in *European Conference on Antennas & Propagation EUCAP*, Nice, 2006.

[3] J. Pontes, S. Schulteis, M. A. Baldauf and W. Wiesbeck, "Evaluation and Optimization of CDMA System Performance in Macrocell Environments based on Antenna Radiation Pattern.," in *German Microwave Conference*, Karlsruhe, 2006.

[4] J. Pontes, A. Lambrecht, M. Rutschlin, S. Schulteis, M. Porebska, T. Fugen and W. Wiesbeck, "Synthesized Antenna Arrays for Future Mobile Networks.," in *2nd International ITG Conference on Antennas. INICA'07*, 2007.

[5] C. Kosta, B. Hunt , A. U. Quddus and R. Tafazolli, "On interference avoidance through inter-cell interference coordination (ICIC) based on OFDMA mobile systems.," *IEEE Communications Surveys & Tutorials,* vol. 15, no. 3, pp. 973-995, 2013.

[6] S. Y. S. Bhamidipati, "Low Complexity Hybrid Digital/Analog phased array for Ad Hoc networks," University of Wyoming, Laramie, May 2012.

[7] V. B. Ramakrishnaiah, R. F. Kubichek and S. S. Muknahallipatna, "Nelder-Mead Based Iterative Algorithm for Optimal Antenna Beam Patterns in Ad Hoc Networks.," *Journal of Computer and Communications,* vol. 5, no. 07, p. 117, 2017.

[8] V. B. Ramakrishnaiah, R. F. Kubichek and S. S. Muknahallipatna, "Optimization of antenna beam pattern in ad hoc networks for optimal global performance," in *IEEE 58th International Midwest Symposium on Circuits and Systems (MWSCAS)*, Ft. Collins, 2015.

[9] F. Wang, V. Balakrishnan, P. Y. Zhou, J. J. Chen, . R. Yang and C. Frank, "Optimal array pattern synthesis using semidefinite programming.," *IEEE Transactions on Signal Processing,* vol. 51, no. 3, pp. 1172-1183, 2003.

[10] V. B. Ramakrishnaiah, R. F. Kubichek and S. S. Muknahallipatna, "Virtual Terrain Nullification Using Phased Array Antennas for Wireless Ad Hoc Networks," in *The 43nd IEEE Conference on Local Computer Networks (LCN)*, Chicago, USA, October 1-4, 2018.

[11] S. Boyd and L. Vandenberghe, Convex Optimization, Cambridge university press, 2004.

[12] J. A. Nelder and R. Mead, "A simplex method for function minimization," *The computer journal,* vol. 7, no. 4, pp. 308 - 313, 1965.

[13] J. Miles, S. S. Muknahallipatna, R. F. Kubichek, J. McInroy and H. Muralidhara, "Use of radio propagation maps in a single moving beacon assisted localization in MANETs.," in *International Conference on Computing, Networking and Communications (ICNC)*, 2014.

[14] V. B. Ramakrishnaiah, S. S. Muknahallipatna and R. F. Kubichek, "Adaptive Region Construction for Efficient Use of Radio Propagation Maps.," *Journal of Computer and Communications,* vol. 5, no. 8, p. 21, 2017.

[15] D. J. Sadler, "Sector beam synthesis using antenna arrays.," *The IEE Signal Processing Professional Network and EURASIP,* pp. 29/1-5, 2005.

[16] F. J. Ares-Pena, J. A. Rodriguez-Gonzalez, E. Villanueva-Lopez and S. R. Rengarajan, "Ares-Pena, Francisco J., et al. "Genetic algorithms in the design and optimization of antenna array patterns.," in *IEEE Transactions on Antennas and Propagation*, 1999.

[17] S. . Y. S. Bhamidipati, R. F. Kubichek and S. S. Muknahallipatna, "Antenna array geometry for mobile ad-hoc networks.," in *International Conference on Computing, Networking and Communications (ICNC).*, 2014.

[18] J. Walfisch and H. L. Bertoni, "A theoretical model of UHF propagation in urban environments," *IEEE Transactions on antennas and propagation,* vol. 36, no. 12, pp. 1788-1796, 1988.

[19] E. Damosso and L. M. Correia, "Digital Mobile Radio Towards Future Generation Systems Communications. COST 231 Final Report.," CEC, Brussels, Belgium., 1999.

[20] S. J. Orfanidis, Electromagnetic Waves and Antennas., New Brunswick, NJ: Rutgers University, 2002.

[21] S. F. Maharimi, M. F. A. Malek, M. F. Jamlos, S. C. Neoh and M. Jusoh, "Impact of spacing and number of elements on array factor.," in *Proc. of Progress in Electromagnetics ResearchSymposium.*, 2012.

[22] V. B. Ramakrishnaiah, R. F. Kubichek and S. S. Muknahallipatna, "Correction Factor for Power Gain in Antenna Arrays.," *International Journal of Communications, Network and System Sciences,* vol. 11, no. 3, 2018.

[23] S. A. Schelkunoff, "A mathematical theory of linear arrays.," *Bell Labs Technical Journal,* vol. 22, no. 1, pp. 80-107, 1943.

[24] H. G. Booker and P. C. Clemmow, "The concept of an angular spectrum of plane waves, and its relation to that of polar diagram and aperture distribution.," in *Proceedings of the IEE-Part III: Radio and Communication Engineering*, 1950.

[25] P. M. Woodward, "A method of calculating the field over a plane aperture required to produce a given polar diagram.," *Journal of the Institution of Electrical Engineers-Part IIIA: Radiolocation,* vol. 93, no. 10, pp. 1554-1558, 1946.

[26] P. M. Woodward and J. D. Lawson, "The theoretical precision with which an arbitrary radiation-pattern may be obtained from a source of finite size.," *Journal of the Institution of Electrical Engineers-Part III: Radio and Communication Engineering,* vol. 95, no. 37, pp. 363-370, 1948.

[27] O. M. Bucci, G. D'Elia and G. Panariello, "Antenna pattern synthesis: A new general approach.," in *Proceedings of the IEEE*, 1994.

[28] H. Lebret and S. Boyd, "Antenna array pattern synthesis via convex optimization.," in *IEEE transactions on signal processing*, 1997.

[29] M. Grant, "Disciplined Convex Programming," Stanford University, 2004.

[30] M. Grant, S. Boyd and Y. Ye, "Global Optimization: from Theory to Implementation," in *Nonconvex Optimization and Its Applications*, L. Liberti and N. Maculan, Eds., Springer, 2006.

[31] J. C. Lagarias, J. A. Reeds, M. H. Wright and P. E. Wright, "Convergence properties of the Nelder--Mead simplex method in low dimensions," *SIAM Journal on optimization,* vol. 9, no. 1, pp. 112 - 147, 1998.

[32] M. Grant and S. Boyd, "{CVX}: Matlab Software for Disciplined Convex Programming, version 2.1," March 2014. [Online]. Available: http://cvxr.com/cvx.

[33] M. Grant and S. Boyd, "Graph implementations for nonsmooth convex programs," in *Recent Advances in Learning and Control*, V. Blondel, S. Boyd and H. Kimura, Eds., Springer-Verlag Limited, 2008, pp. 95-110.

SOCIETY FOR SCIENCE AND EDUCATION
UNITED KINGDOM

TNC TRANSACTIONS ON NETWORKS AND COMMUNICATIONS

VOLUME 6, NO. 6
ISSN: 2054 -7420

Forwarding with Prediction over Machine Learning based Nodes in Wireless Mesh Networks

[1]Jianjun Yang, [2]Ju Shen, [3]Mengyi Ying
[1]University of North Georgia, Gainesville, GA, USA
[2]University of Dayton, Dayton, OH, USA
[3]University of North Georgia, Dahlonega, GA, USA
jianjun.yang@ung.edu; jshen1@udayton.edu; mengyi.ying@ung.edu

ABSTRACT

As part of the next generation Internet, Wireless Mesh Networks have emerged as a key technology to deliver Internet broadband access, wireless local area network coverage and network connectivity at low costs. The capacity of a wireless mesh network is improved by equipping mesh nodes with multi-radios tuned to non-overlapping channels. Hence the data forwarding between two nodes has multiple selections of links and the bandwidth between the pair of nodes varies dynamically. The new technology makes mesh nodes cognitive, thus a mesh node is able to adopt machine learning mechanisms to choose the possible best next hop which has maximum bandwidth when it intends to forward data. In this paper, we present a new forwarding algorithm by which a forwarding node dynamically select its next hop with highest potential bandwidth capacity to resume communication based on learning algorithm. The efficiency of this approach is that a node only maintains three past status, and then it is able to learn and predict the potential bandwidth capacities of its links. Then, the node selects the next hop with potential maximal link bandwidth. Additionally, a geometrical based algorithm is developed to let the forwarding node figure out the best forwarding region in order to avoid flooding. Simulations demonstrate that our approach significantly outperforms peer algorithms.

Keywords: mesh networks, machine learning, forwarding, highest bandwidth capacity, geometrical routing.

1 Introduction

Wireless mesh networks(WMNs) have emerged as one of the key technologies for wireless communications. They are undergoing rapid development and have inspired numerous applications because of their advantages over other wireless technologies. The networks, such as WiFi, 802.15, 802.16 and sensor networks, can be integrated into the WMN through gateways and mesh routers. Mesh clients, either stationary or mobile, can form client mesh networks among themselves and with mesh routers. WMNs are anticipated to significantly improve the performance of ad hoc networks, wireless local area networks (WLANs), wireless personal area networks (WPANs), and wireless metropolitan area networks (WMANs).

DOI: 10.14738/tnc.66.5653
Publication Date: 09th December 2018
URL: http://dx.doi.org/10.14738/tnc.66.5653

In wireless networks, devices (nodes) remain connected to the network through wireless links. The critical issue is to provide high bandwidths for nodes to communicate with each other. A wireless mesh network (WMN) is a communication network made up of nodes organized in a mesh topology[1]. WMNs are capable to connect diverse network nodes such as desktops, laptops, iPads, and smart phones. Mesh routers and client devices are self-organized and self-configured to form wireless mesh networks(WMNs) [1]. A device is called a node in WMNs. Each node is equipped with multiple radios to improve the whole capacities in WMNs [5]. The radios in WMNs are cognitive radios, by which the radio devices are capable of learning from their environment and adapting to the environment[2]. Cognitive radio is also called programmable radio because such radio has the ability of self-programming[3], learning and reasoning [2].

Machine learning has been studied for many years. It evolved from simple artificial intelligence to a wide variety of applications in image processing, vision, networking, and pattern recognition. In this paper, we propose a learning algorithm for a forwarding node to find one of its links with possibly maximal bandwidth, and then choose next forwarding node and then forward the message to that node. Each node only saves the last three changed bandwidth status of its links. Then the forwarding node learns the three status and predict the potential bandwidth of its links. So the forwarding node is able to find the neighbor with highest link bandwidth as its next hop. We further devise an algorithm to let the source node figure out the forwarding region in order to avoid flooding.

The rest of the paper is organized as follows. Section 2 discusses the related research on this topic. Section 3 proposes our novel forwarding method that selects the best next hop. We evaluate the proposed schemes via simulations and describe the performance results in Section 4. Section 5 concludes the paper.

2 The Existing Ranking Methods

Scholars have conducted research on machine learning, wireless forwarding and related work[6][7][8][9][10][11]. Wang Y. et al. [12] proposed a machine learning based mechanism that was used to supervise given input and output. The input includes the factors of memory utilization, channel loading evaluation, and signal strength. The output includes the transmissions on the channels where the packet is received. The authors created a machine learning based algorithm to automatically find out the relationship between input and output, making a new routing protocol with high efficiency. Further, they implemented their mechanism as MetricMap, which adopted knowledge acquired from a training phase.

Sawhney A. et al. [13] presented a machine learning algorithm to handle congestion controlling in wireless networks. Their approach learns many factors that have impact to congestion controlling, and then uses the parameters in a fuzzy logic to generate better result when congestion takes place. The efficiency is assessed with machine learning tools.

3 The Mechanism of Learning Based Forwarding with Prediction

3.1 The Forwarding Problem

In wireless mesh networks(WMNs), the communications are over links. Link bandwidth is critical for transmission speed. Since each node may be equipped with multiple network interfaces with different radios and the radios are switchable, the bandwidth over two neighbor nodes may vary from time to time.

The radios in WMNs are cognitive radios and then the nodes are able to learn the changes of past bandwidths and can further predict and select the desired link with potential highest bandwidth.

Fig. 1 shows an example of WMN, the dotted lines illustrate that there could be multiple possible channels to be assigned to a node, thus a node may have multiple choices for next step with different bandwidth in forwarding process.

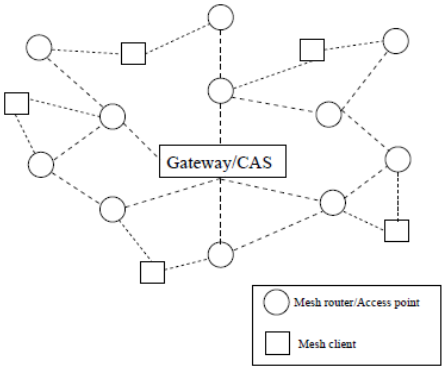

Figure. 1. An example of Wireless Mesh Network

As shown in Fig. 2, assuming a source node s intends to send data to a destination node d, many traditional routing algorithms set up the forwarding path by simply selecting the shortest route. For example, $s-c-g-h-d$ is the forwarding path in Fig. 2. However, it may not be the best path in WMNs. In WMNs, the bandwidth over two nodes changes frequently. The bandwidth of the link sc is possibly much lower than that of sa. Or the past bandwidth of sc is higher than sa but too much traffic is over sc now so the available bandwidth of sc is going down while that of sa is going up.

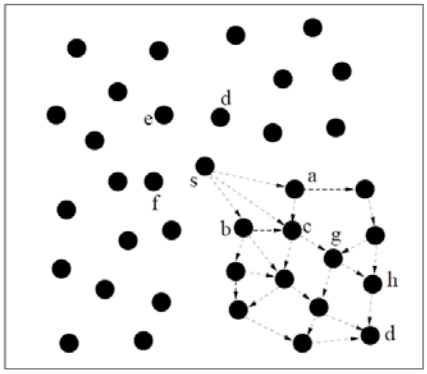

Figure. 2. Topology of Wireless Mesh Networks

Our goal is to let each forwarding node select the link for next hop with the highest potential bandwidth. In our approach, each node learns its links' past bandwidths and then predict their potential bandwidths. Then the forwarding node figures out its next hop with highest potential bandwidth.

3.2 Prediction for Future Bandwidth

Suppose node i saves the bandwidth changes of its links of the last three times $t_0, t_1,$ and t_2. Then for any of its neighbor$j$, i predicts the potential bandwidth of linkij. By computational method[14], we define

$$\alpha_{i,j,k}=\sum_{m=0}^{k}\frac{B_{i,j,m}}{\prod_{n=0}^{k}(t_m-t_n)} \quad (1)$$

at time t_k, where $B_{i,j,m}$ is the bandwidth between node i and node j at time m. Then the bandwidth of link ij at future time p can be calculated and predicated as:

$$B_{i,j,p} = \alpha_{i,j,0}+\alpha_{i,j,1}(t_p - t_0) + \alpha_{i,j,2}(t_p - t_1)(t_p - t_2) \quad (2)$$

Algorithm 1 describes node i learns the bandwidth of link ij in the last three changes and then it predicts the bandwidth of next time$p$.

Algorithm 1: Prediction for future bandwidth of link *ij*

Step 1: Learn and keep the bandwidth changes of link ij at the last three times 0,1, and 2.

Step 2: Calculate $\alpha_{i,j,k}$ with equation (1)

Step 3: Calculate the predicted bandwidth of link ij of time p with equation (2)

3.3 Forwarding Region

When a node s intends to send data to node d, it selects the neighbor node with highest potential link bandwidth as its next hop and then same metric continues to select the best next forwarding node . Apparently, s will not select any nodes in the opposite direction from s to d. How is node s aware of the region where the next hop falls? In current WMNs, each device is equipped with GPS and hence it knows its location. We assume that the sender knows its own location and the location of the receiver. The assumption is very common in geographic routing[6]. Fig. 3 shows the scenario. Suppose node s intends to send data to node d, it figures out the forwarding region as algorithm 2.

Algorithm 2: Figure out the region for next hop

Step 1: s connects d.

Step 2: sd makes 45^o anticlockwise rotation, the ray is l'.

Step 3: sd makes 45^o degrees clockwise rotation, the ray is l''.

Step 4: The intersection region with l' and l'' will be the forwarding area.

Suppose the coordinates of nodes s and d are $s(x_s, y_s)$ and d(x_d, y_d), respectively. Then line sd, say l can be described as the following equation.

$$\frac{y - y_s}{y_d - y_s} = \frac{x - x_s}{x_d - x_s}$$

It can be written as:

$$(y_d - y_s)x - (x_d - x_s)y + (x_d y_s - x_s y_d) = 0 \quad (3)$$

When (3) makes 45^o anticlockwise rotation, the line, say l' is represented as the equation:

$$(x_d + y_d - x_s - y_s)x - (x_d - y_d - x_s + y_s)y + \frac{\sqrt{2}}{2}(x_d - y_d)(x_s + y_s)$$

$$-\frac{\sqrt{2}}{2}(x_s - y_s)(x_d + y_d) = 0 \quad (4)$$

When (3) makes 45^0 clockwise rotation, the line, say l'' is represented as the equation:

$$(x_d - y_d - x_s + y_s)x - (x_d + y_d - x_s - y_s)y + \frac{\sqrt{2}}{2}(x_d + y_d)(x_s - y_s)$$

$$-\frac{\sqrt{2}}{2}(x_s + y_s)(x_d - y_d) = 0 \quad (5)$$

Hence the forwarding region of the intersection area with l' and l'' can be simply figured out by (4) and (5). However, if no such a node qualified for next step in the forwarding area, the forwarding will be changed to traditional GPSR[15].

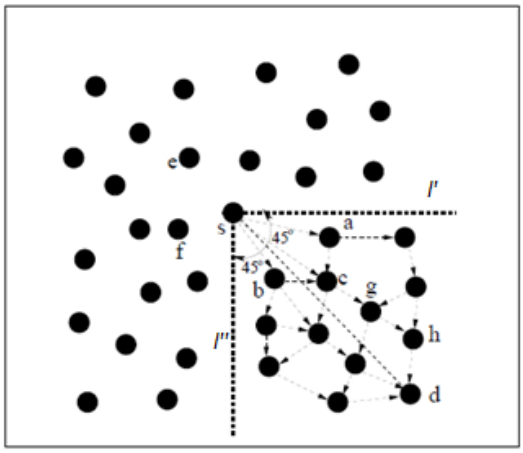

Figure. 3. Forwarding Region

3.4 Forwarding algorithm

Suppose each node in a Wireless Mesh Network regularly maintains the last three changes of bandwidths of all its links that connect its neighbors. When node s intends to send data to node d, s first uses algorithm 2 to figure out the region where the forwarding will be performed. Then s calls algorithm 1 to find the node with potential highest bandwidth among all its neighbors as next hope. When the selected node relays the forwarding, it only considers its neighbors in the forwarding region as forwarding candidates, and it calls algorithm 1 to forward the data to next hop with potential highest bandwidth. The forwarding resumes until the packets arrive destination node d.

Algorithm 3: Forwarding algorithm

Step 1: s calls algorithm 2 to figure out the forwarding region.

Step 2. if no node exists in such region, change to traditional GPSR and go to step 4; otherwise go to step 3.

Step 3: s calls algorithm 1 to find the node n with potential highest bandwidth of link sn as next hope, where n is in the forwarding region.

Step 4: if n is d, end the algorithm; otherwise $s = n$, go to step 2.

4 Experiments and Analysis

We evaluated our mechanism in a simulated noiseless radio network environment by MATLAB. We create a topology that consists of a number of randomly distributed nodes. We compare our approach (ML Forwarding) with two other algorithms. One is congestion control and fuzzy logic with machine learning for wireless communications, say Fuzzy Logic. The other one is supervised learning approach for routing optimization in wireless networks, say Supervised Learning. The compared metrics are transmission delay (Milliseconds) and transmission speed (MBs/Millisecond). We performed a sequence of experiments in which the number of nodes varies from 100 to 300 in increments of 25 over an area of 100x100 meters in the reference network. For each number of mobile users, we conduct our experiments 10 times and present the average value.

Fig. 4 shows that our approach results in the least delay. It is because our approach selects the link with potential maximum bandwidth of each hop. Fig. 5 shows that with the same reason, our approach generates the maximal transmission speed among the three approaches.

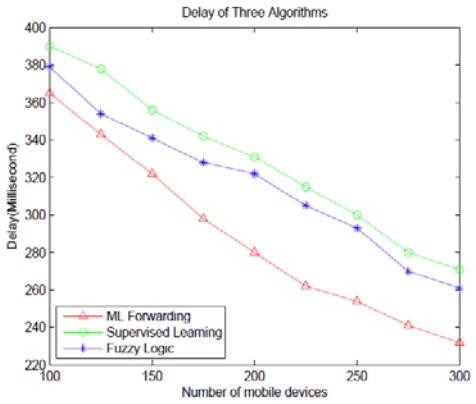

Figure. 4. Transmission Delay of the Three Algorithms

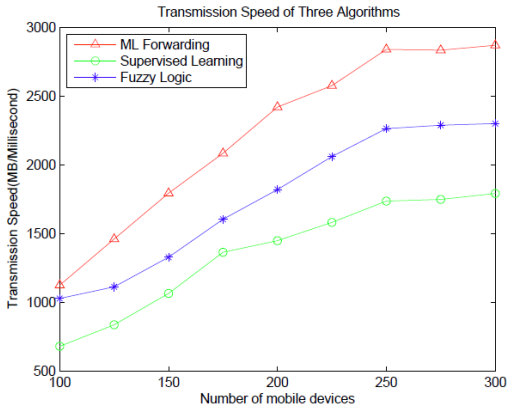

Figure. 5. Transmission Speed of the Three Algorithms

5 Conclusion

We present a machine learning based forwarding algorithm with cognitive radios in in wireless mesh networks in this paper. In this algorithm, each mobile device keeps the last three bandwidth changes of its links that connect its neighbors. Then when a node intends to forward data, the node learns the historical changes of bandwidth and then predicts the possible future bandwidths of the links with neighbor nodes. Hence the forwarding node is able to select the next hop with highest bandwidth. We also designed a geometrical algorithm to let the source node figure out the forwarding region in order to avoid unnecessary flooding. Simulation results demonstrate that our approach outperforms peer approaches.

REFERENCES

[1] Akyildiz I.F. , et al., *A Survey on Wireless Mesh Networks*, IEEE Commu-nications Magazine,2005.

[2] Mitola, J, *Cognitive radio: An integrated agent architecture for software defined radio*, Ph.D. dissertation, Royal Institute of Technology (KTH), Stockholm, Sweden, 2000.

[3] Costlow, T, *Cognitive radios will adapt to users*, IEEE Intelligent Systems, vol. 18, no. 3, p. 7, May-June ,2003.

[4] Ayodele, T. O, *Introduction to machine learning*, New Advances in Machine Learning. InTech, 2010.

[5] Yang, J., et al., *Fair Gain Based Dy-namic Channel Allocation for Cognitive Radios in Wireless Mesh Networks,* Journal of Computers, 2014.

[6] Yang, J., et al., *HDAR: Hole detection and adaptive geographic routing for ad hoc networks*, Computer Communications and Networks (ICCCN), 2010 Proceedings of 19th International Conference, pp. 1-6. IEEE, 2010.

[7] Yang, J., et al., *Broadcasting with prediction and selective forwarding in vehicular networks*. International journal of distributed sensor networks, 2013.

[8] Yang, J., et al., *Bipartite graph based dynamic spectrum allocation for wireless mesh networks*. In Distributed Computing Systems Workshops, 2008. ICDCS08. 28th International Conference, pp. 96-101. IEEE, 2008.

[9] Shen, J., et al., *Layer depth denoising and completion for structured-light rgb-d cameras*. In Computer Vision and Pattern Recognition (CVPR), 2013 IEEE Conference on, pp. 1187-1194. IEEE, 2013.

[10] Jianjun Yang, et al., *A Machine Learn ing Based Forwarding Algorithm Over Cognitive Radios in Wireless Mesh Networks,* EAI International Conference on Machine Learning and Intelligent Communications, Shanghai, 2016.

[11] Shen, J., et al., *Image-based indoor place-finder using image to plane matching*, 2013 IEEE International Conference on Multimedia and Expo, 2013.

[12] Wang, Y., et al., *A supervised learning approach for routing optimizations in wireless sensor networks.* Proceedings of the 2nd international workshop on Multi-hop ad hoc networks: from theory to reality, pp. 79–86,2006.

[13] Sawhney, A., et al., *Congestion Control in Wireless Communi-cation Network Using Fuzzy Logic and Machine Learning Techniques*, International Journal of Advanced Research in Electrical, Electronics and Instrumentation Engi-neering Vol. 3, Issue 11, October, 2014.

[14] Kincaid, D., et al., *Numerical Analysis: Mathemat*

[15] B. Karp, et al., *GPSR: Greedy perimeter stateless routing for wireless networks*, ACM/IEEE International Conference on Mobile Computing and Networking, 2000.

SOCIETY FOR SCIENCE AND EDUCATION
UNITED KINGDOM

TNC TRANSACTIONS ON NETWORKS AND COMMUNICATIONS

VOLUME 6, NO. 6
ISSN: 2054 -7420

SDN/NFV Based Internet of Things for Multi-Tenant Networks

Do Sinh[1], Luong-Vy Le[2], Bao-Shuh Paul Lin[1,3], Li-Ping Tung[3]
[1]Department of Computer Science, National Chiao Tung University, Hsinchu, Taiwan
[2]College of Electrical and Computer Engineering, National Chiao Tung University, Hsinchu, Taiwan
[3]Microelectronics & Information Research Center, National Chiao Tung University, Hsinchu, Taiwan
dosinhuda.cs04g@nctu.edu.tw, leluongvy.eed03g@nctu.edu.tw, bplin@mail.nctu.edu.tw, lptung@nctu.edu.tw

ABSTRACT

The Internet of Things (IoT) refers to variety of smart devices such as smartphones, tablets, and sensors that can interact and exchange of data among devices through the Internet. The diversity of IoT devices and their services have posed a larger range requirements of availability, throughput, latency, and performance in heterogeneous connectivity environments. Meanwhile, the existing networks often struggle with such of limitations in complex control protocols and difficulty in internetworking with billions of smart devices with different requirements such as latency and bandwidth allocations. These obstacles become substantial barriers to deploy services, as well as isolate between multiple co-existing tenants on the same physical network, deploy simultaneous protocols in the network, be stable to maintain the bandwidth and latency according to predefined QoS demands. These obstacles have recently been facilitated by Software Defined Network (SDN) and Network Function Virtualization (NFV) technologies that enable the programming and monitoring in data plane. In this study, firstly, the authors investigate and propose a SDN/NFV based architecture for multi-tenant networks with plenty of network slices working in a shared physical infrastructure. Secondly, P4 and ONOS Controller are used to implement a deep programming in BMv2 devices to efficiently maintain the network motoring in order to guarantee the E2E latency of communicating channels. Finally, the VXLAN technologies are exploited to for network slicing with different purposes and applications, and Inband Network Telemetry (INT) is used to monitor network latency.

Keywords: Software Defined Network (SDN); Software Defined Mobile Network (SDMN), Network Function Virtualization (NFV); Internet of Things (IoT); Wireless Sensor Network (WSN); P4; PSA(Portable Switch Architecture); ONOS.

1 Introduction

Recently, SDN[1] and NFV[2] are considered as key technology and promising enablers for network deployment, operation, and management with the full capacity of advanced programmability, flexibility, and elasticity. Therefore, they are expected to address different challenges in the next generation network (5G) and the Internet of Things[3][4][5][6].

DOI: 10.14738/tnc.66.5695
Publication Date: 23rd December 2018
URL: http://dx.doi.org/10.14738/tnc.66.5695

SDN is a new paradigm for network processing, it decouples the data and control planes to simplify network configuration and encourage evolution. It provides a new model for network providers to program the control plane for managing data plane devices and optimizing network resources automatically. OpenFlow[7] is a popular API network protocol for SDN to control data plane devices that bring significant benefits for future network deployment such as reduce OPEX (Operating Expense) and CAPEX (Capital Expense). Moreover, P4[8] is a domain-specific language (DSL), multi-platform, protocol, target independent, and re-configurable which is designed to allow the programming of data plane devices with different targets such as software switches, FPGA-based NICs (Field-Programmable Gate Array based Network Interface Cards) or switches based on reconfigurable ASICs (Application-Specific Integrated Circuit)[9]. Therefore, it provides an efficient way to configure the packet processing pipelines to improved network programming in both data and control planes that can achieve such benefit from network performance and encourage high speed network innovation.

NFV (Network Function Virtualization) is an approach to virtualize network element that mean billions of complex dedicated network appliances such as middleware boxes, firewalls, and even routers, switches, etc., are replaced by software running on commodity hardware. As a result, NFV has important roles in reducing the deployment cost and power consumption, and increasing network scalability, network efficiency, and services deployments.

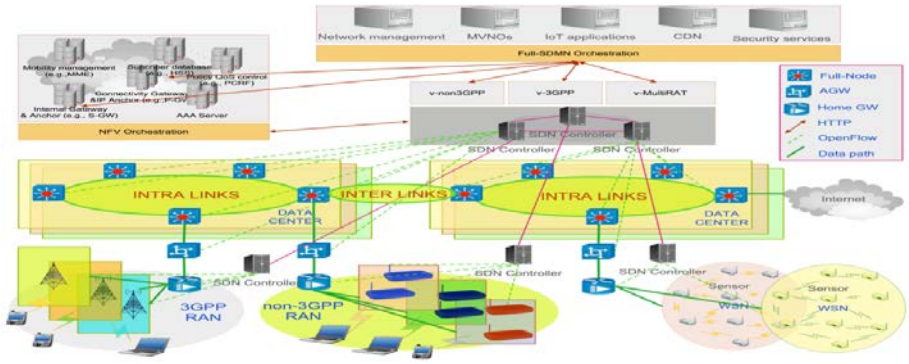

Fig. 1. Full-SDMN Architecture

Figure 1. Full-SDMN Architecture

On the other hand, the Internet of Thing has been growing rapidly in the number of IoT devices, applications, and data collection. With billions of heterogeneous IoT devices connected to networks for exchanging data with different protocols can cause many challenges about the system management and orchestration. Fortunately, SDN/NFV can be exploited as a promising and effective solution to handle the concern. For example, they allow various E2E (End-to-End) communication with different technologies in term of a protocol-independent to interconnect simultaneously through a controller's application that is used to control and manage underlying devices such as P4. The SDN/NFV architecture for 5G and IoT called Full-SDMN (Full-Software Defined Mobile Network) shown in Fig.1 was proposed and described in our previous study[4], in that SDN/NFV were applied for 5G network and served as a tool for deploying IoT applications.

In this paper, firstly, we propose the Full-SDMN architecture for 5G and IoT, and illustrate how an IoT application can be deployed as an SDN controller application on top of SDN network under

the synergy of NFV orchestration, Full-SDMN orchestration, and SDN controller. Secondly, a framework integrating state-of-the-art SDN/NFV components for monitoring IoT applications of multiple tenants with diversity requirements on the same physical network is proposed. In this architecture, the PSA[10] and BMv2[11] P4-based switches are exploited in the data plane to perform multiple protocols services, that mean packets of each path of a service are processed according to its predefined requirements , such as throughput and E2E latency. Moreover, VXLAN (Virtual eXtensible Local Area Network) and VXLAN GPE (Generic Protocol Extension for VXLAN)[12], which have been recently explored by network developers, are considered as key technologies for extending network slicing services to tackle the limitation number of the current VLAN (Virtual Local Area Network). They allow end devices communicate without being limited by distance. In this study, VXLAN and INT[13][14] are chosen as a new integrated solution to monitoring the E2E latency of different services. Finally, several experiments are implemented in the new environment P4-BMv2 target and ONOS Controller[15] to evaluate framework performances.

The remainder of the paper is organized as follows: Section 2 presents the related work; Section 3 proposes and describes the Full-SDMN architecture for the multi-tenant networks; Section 4 implements experiments and performance analysis; Section 5 addresses challenges of the model and discusses the future works; Section 6 concludes the present study.

2 Related Work

SDN/NFV architecture for IoT has recently attracted a lot attention from academia, for example, research [16] proposed a general SDN/NFV-based framework for IoT, in which various IoT devices were connected through SDN/NFV-based gateways, and a framework over wireless sensor networks (WSN) were introduced in study [17] introduced; for more detail, research [18] developed a three-level hierarchical fog architecture applying for smart grids, vehicular networks, and WSN, and research [19] described how SDN-based sensor nodes operate in SDN networks; [20] introduced SDN/NFV-based architecture for supporting network slicing applications. [21] proposed an architecture that can co-operate between SDN and NFV, and they also defined E2E logical network slicing running on a common underlying network. On the other hand, many studies focused on analyzing and deploying the quality of service (QoS) demands for the wide range requirements of diversity E2E slices using SDN/NFV approaches [22][23][24][25][26][27]. However, there are several challenges still need more concentrated effort to overcome: i) a comprehensive IoT framework with a deep programmable data plane to easily implement independent protocols for diversity of IoT devices and services. ii) E2E network virtualization and isolation network or E2E network slicing for multi-tenant applications working under the same physical infrastructure. iii) Effective methods for resource monitoring and optimizing in IoT networks with a huge number of smart devices and connections and complicated service requirements. INT, a new approach based the handshaking between data and control planes, is used to control the E2E latency. iv) Practical models based on SDN/NFV and SDN controller applications to prove the effectiveness of state-of-the- art SDN technologies in providing managing and programing the data plane to supporting different policies on requested IoT services such as multi-tenant services.

To deal with these issues, the Full-SDMN architecture shown in Fig.1 can be considered as a suitable solution supporting independent protocols and less hardware dependent. Especially, the

recent integration of P4 based BMv2 switches to the architecture is an essential innovation to overcome the complexity in pipeline of the existing OF- (OpenFlow Data Plane Abstraction)[28] and OpenFlow-based switches. The reprogrammable pipeline is a crucial step motivating service providers to define new protocols so that network programming, controlling, and DPA management become more flexible by using SDN applications with the co-operation of the NFV orchestrations, SDN controllers, and Full-SDMN orchestration. Based on the application, the Full-SDMN orchestration creates original policies to manage and control network elements and services such as MVNOs (Mobile Virtual Network Operators), and IoT applications, and then it generates flows to program the elements to create virtual network slices. Meanwhile, the management of NFV orchestration ensures those element are created and operated normally underlying network. Finally, SDN controller application controls physical components and network function

3 Proposed SDN/NFV Based Internet of Things Architecture for Multi-Tenant Networks

Fig.2 illustrates our proposed SDN/NFV-based IoT architecture for multi-tenant networks, which comprises three main planes: Data plane, Control plane, and Management plane.

3.1 Data plane

WSNs comprise billions of devices/sensors with different types and abilities of computing, sensing, and communicating for various types of applications such as smart-home, e-healthcare, and autonomous cars. In this scenario, the HomeGWs (Home Gateways), which reside at edge network have significant roles connecting the IoT devices, WSNs, and the core network. the HomeGWs work as the gateway supporting for different type of edge networks such as 3GPP RAN (Radio Access Network) and non-3GPP RAN. Therefore, they must satisfy such capacity of flexibility, and scalability for hosting various applications. They are also responsible for

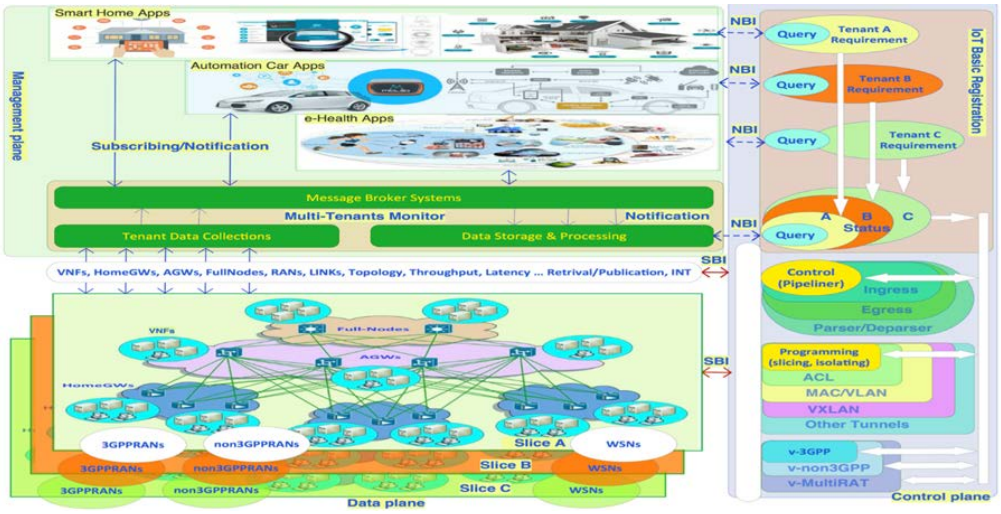

Fig. 2. SDN/NFV Based IoT Architecture for Multi-Tenant networks

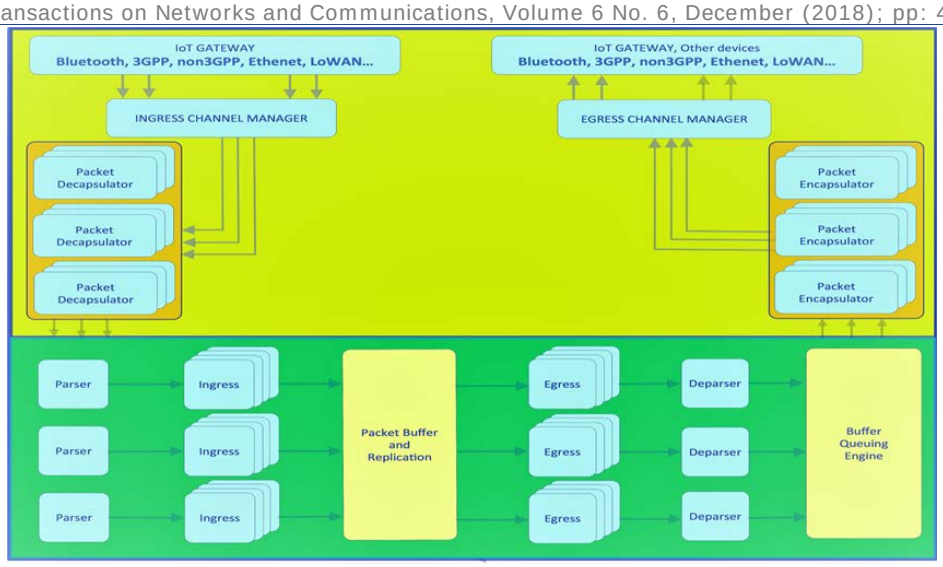

Fig. 3. Multi-protocols and SDN-enabled HomeGWs

processing data generated by WSNs to the Internet. As a result, a huge amount of data generated by IoT devices is pre-processed at each HomeGW so that the data processing at the core network will be significantly reduced. Hence, the HomeGW must be powerful enough to satisfy these requirements. Fig.3 shows our proposed HomeGW architecture based on SDN technology and describes how to process and modify packets of various services in HomeGWs.

In this architecture, Portable Switch Architecture (PSA) model, which has six programmable P4 blocks and two fixed-function blocks with multiple-pipelines, Packet Buffer, and Buffer Queuing Engine are used for installing QoS policies at the data plane. Moreover, the separation of ingress and egress pipelines make the process, modify and management flow packets more flexible and efficient. This is an essential characteristics to support programming interfaces among IoT services regardless of various services with different requirements, that means a service request is independently allocated appropriate resources. For example, Fig.4 describes how to apply different IoT applications in a multi-tenant framework, here, each IoT application such as Automation Cars, Smart Home, and e-HealthCare only intercommunicate with its components (services and IoT devices). Each application usually expects a network performance guarantee like throughput and latency based on the characteristic of services. For example, the vehicular communication, cars need to communicate with one another (Vehicle to Vehicle or V2V), and with the network infrastructure (V2I) for supporting safety services

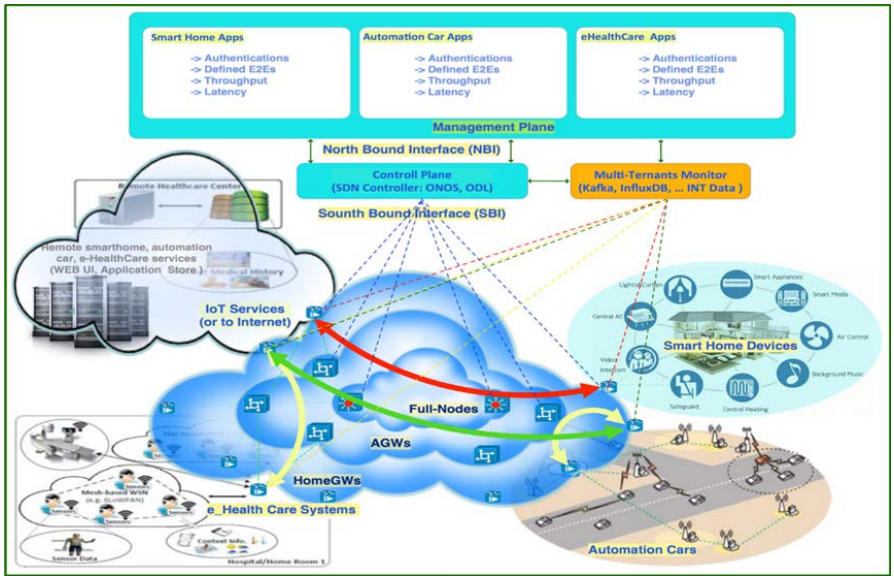

Fig. 4. An example for applying IoT Architecture for Multi-Tenants

(i.e., real-time dangerous warning of on the road) and non-safety services (i.e., local traffic, road map, local weather, car parking areas, popular news)[29][30]. On the other hand, the servers of different applications are often allocated at different positions in the networks. For example, with safety services, their servers must be located at the edge network to reduce latency, while for non-safety services like entertainments, these servers are usually located On the Internet. Therefore, it is necessary to create some virtual RANs (VRAN) and virtual core network (VCN) with different VLAN ID under the data plane of access technologies and core networks such as v-3GGP, v-non3GPP, and v-Multi-RAT. Those VLAN are created and controlled by controller applications based on several methods such as MAC/VLAN tag, VXLAN and VXLAN GPE[12].

Similarly, Applying IoT for eHealth systems is complicated due to network communications, data collection and processing from a massive types of smart sensors and actuators (i.e., heartbeat sensors, body sensors, blood pressure devices, wearable smart medical sensor devices, wire or wireless medical instruments) [31]. Among the common access technologies or WSN for eHealth system, ZigBee, Bluetooth, and LPWAN (Low-Power Wide Area Network) are the most popular due to the fact that they are low energy and low-cost wireless networking standards. [32][33]. In eHealth networks, health data and patient information such as electronic health records and electronic medical records are collected and sent via HomeGWs to Remote Healthcare Center or Internet without caring about latency, while telehealth, telemedicine, and connected health services need a real-time communication [34].

The last IoT scenario discussed in this subsection is IoT for Smart Homes in which smart sensors are embedded in the smart home environment like central power, sight, heating devices, and even other multi-media systems such as background music, and smart appliances to bring more benefits, comfortable, and secure for household users [35][36]. Smart sensors communicate over IoT to systems and usually provide as web server- client modes.

Table 1. IoT applications and requirements

ID	Different Requirements of each IoT services in network			
	Application domains	***Descriptions***	***Data rate***	***Tolerable delay***
1	Automation car and safety services.	real-time warning, roadside functionalities, real-time emergency respond	high	Low (milliseconds)
2	non-safety services for vehicles.	local traffic, road conditions, road map, local weather, car parking areas, popular news.	normal	Normal (seconds)
3	e-Healthcare:alarmand emergencyrespond.	AAL (ambient assisted living), remote diagnosis, disable assistance	normal	low
4	e-Healthcare: data collection and context information storage.	Remote Healthcare Center or Internet for purposes of storing medical history and giving appropriate medical treatments later.	normal	normal
5	Smarthome: data collection, remote controlling, energy management	Central AC, light, central heating, smart appliances, air control.	low	normal
6	Smarthome for Entertainments and comfortableliving	Video Intercom, smart Media, Background Music	high	normal
7	Smarthome for safety	security and video surveillances,, access managment	high	low

Table 1 summarizes different requirements (throughput and latency) for typical IoT application domains; therefore, IoT platforms must provide the flexibility for the planners, designers, and implementers that they can employ emerging industrial IoT applications under suitable performance network slices. However, with the increase in IoT devices and services, the current methods for virtualizing network such as VLAN are no longer relevant and substituted by new approach such as QinQ and VXLAN. Moreover, a comprehensive IoT platform supporting a deep programming in the data plane is an essential requirement to implement network slicing and multi-protocol IoT application such as VLAN tagging, VXLAN, and VXLAN GPE.

3.1 Control Plane

The control plane is described as in Fig.2, in which SDN controllers work as a distributed controlling system. They play three significant roles in the network: Program the data plane; manage flows across the network nodes; and provide the platform for hosting controller applications. They co-operate with one another to create on demand and monitor VRAN architectures, such as 3GPP, non-3GPP, and MutiRAT, using SDN controller applications without the need to alter the data plane components. Practical SDN controllers that can meet such wishing of providing the flexibility to easily build and deploy new dynamic IoT services with simplified programmatic interfaces are ONOS and OpenDayLight (ODL)[37]. For example, ONOS, a distributed control architecture, supports both configuration and real-time control of the data plane to deploy of new IoT software, hardware, and applications. In this study, the authors use ONOS controller to build VRAN as v-3GPP, non-3GPP, and v-MultiRAT applications in which the standards are defined by software or SDN applications. These applications modify and control packets though match and actions (parser, ingress, egress, and deparser) in the pipeline of OpenFlow Switch or slice network by using ACL, MAC/VLAN ID Tagging, VNI - VXLAN Network Identifier and VNI-VXLAN GPE).

The first approach use ACL to program the data plane, this application is a built-in ONOS application including rules to allow or deny IP traffic at relevant devices. Through the Multi-

Tenants application, SDN controller conducts real-time measurements over fast varying parameters such as the queues in BMv2 switches, links states. Moreover, it uses Round Robin, Kalman filter algorithm to control each slice to fulfill the services with respect to application characteristics. Thank for P4 - INT [13][38], a powerful network monitoring mechanism implemented in P4, can be injected to every packet to specify the type of metadata such as switch ID, ingress timestamp, hop latency, etc.

The second approach is VLAN, which (Virtual Local Area Network) is an isolation approach to separate different classes of packets. Network providers use VLAN as a group identifier to apply different policies such as QoS to different groups. A VLAN-based slicing is deployed with VLAN IDs tagged to packets to represent for each tenant , [39]. Otherwise, a slice can be defined as a group of devices' MAC addresses or IP addresses pre-defined in the IoT controller application. Moreover, QinQ is used to extend the VLAN numbers up to 4096 x 4096 to solve the limitation of number VLANs (4094 VLAN IDs).

The last approach is VXLAN or VXLAN GPE, which is designed to provide layer 2 overlay network on top of the layer 3 network using MAC-in-UDP encapsulation, in which a 24-bit VNI field can be used to define the number of LAN segments (up to 16 million) to meet the demand on network scales.

Another important component in control plane is the IoT Basic Registration controller application for providing query points to interconnect applications and Multi-Tenants Monitor controller applications to monitor the network slices, which will be explored in the next section.

3.2 Management plane

The management is implemented in two main phases. The first phase aims to set up the virtual E2E transmissions between end users via HomeGWs, AGWs, and Full-Nodes. In this phase, IoT controller applications define the requirements physical resources such as E2E transmissions and its QoS (throughput, latency). Firstly, the requirements are sent to IoT Basic Registration Application to implement application

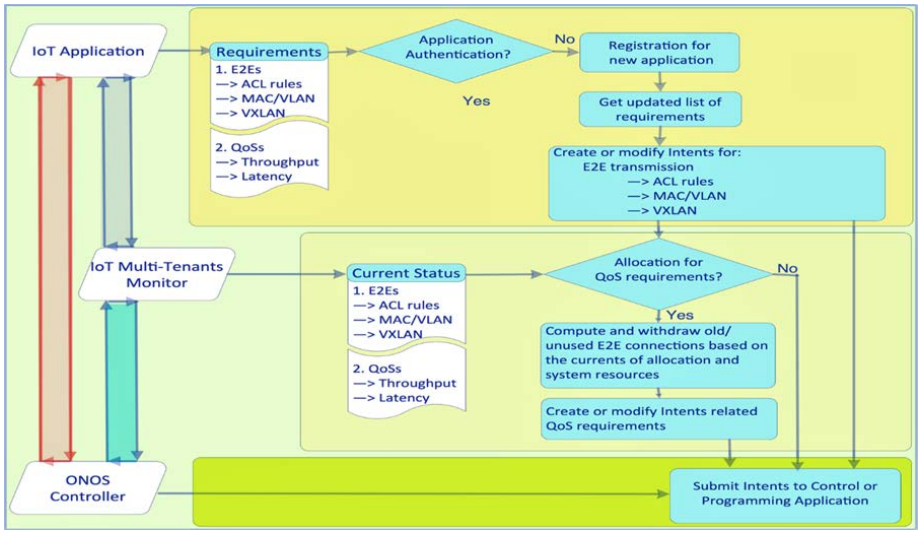

Fig. 5. Application Registration and Monitoring QoS

authentication, modify Intents as shown in Fig.5, and then create network slices applied to Control and Programming Applications based on several methods such as ACL rules, MAC/VLAN, QinQ, and VXLAN.

The second phase aim to maintain the QoS of E2E transmissions, in this phase the Basic Registration Application continuously check the current QoS of E2E transmission from a Multi-Tenants Monitor Application, and optimize network efficiency by creating or modifying Intents that are related to QoS requirements based on the current system resources.

In this architecture (Fig.5), different IoT applications include smart home, automation car, e-Health applications associate with their requirements and the authentication procedure for their end-users. Moreover, their current E2E channel status are provided via notification of the Multi-Tenants Monitor Application to track their services deployed at data plane.

The Multi-Tenants Application plays the main roles in collecting data from Tenants such as VFNs, HomeGW, AGW, Full-Node devices, links, topology events via SDN Controller. The notations are shifted to IoT applications through the Message Broker Systems. It also processes and stores data for QoS controlling purposes at the IoT Basic Registration Application. In this architecture, P4 INT mechanisms are applied for collecting and reporting network states by data plane without requiring intervention or work from the control plane.

To clearly explore how a user can access and use services and network slicing according to its demand,

Fig.6. shows an example of Automation Car User (UE) that want to access Automation Car Services stored in the Server. The process is explained bellows:

Firstly, the UE sends a packet to its destination via RANs such as SDN based eNBs, or SDN based APs, or SDN based WSN nodes, etc.. And then RANs send a packet-in to SDN Controller (step 2) for authentication and virtual E2E channel establish. Here we assume that Automation Car Controller Application was accepted by IoT Basic Registration Application. Step 3, IoT application implements UE authentication and send back a message to IoT Basic Registration Application for creating or modifying intents of the virtual E2E channel (step 4). Here, if the IoT application does not have any QoS requirement, then the intents created at step 4 will be submitted to Control Application and Programming Application (in SDN Controller) to establish virtual E2E channel (step 5- 12).

Otherwise, if the IoT application requires a QoS control, Multi-Tenants Monitor Application will implement data collection such as devices, links, topology via SDN Controller (step 13-15), then shifts notification to Automation Car Application (step 16) and IoT Basic Registration Application (step 17, 18). After receiving requirements of the IoT application (step 19), the IoT Basic Registration Application re-computes, modifies, and creates Intents for QoS requirements, and then submits it to the Control and Programming Applications to slice and control the virtual E2E channel based on-demand services (step 20-24)

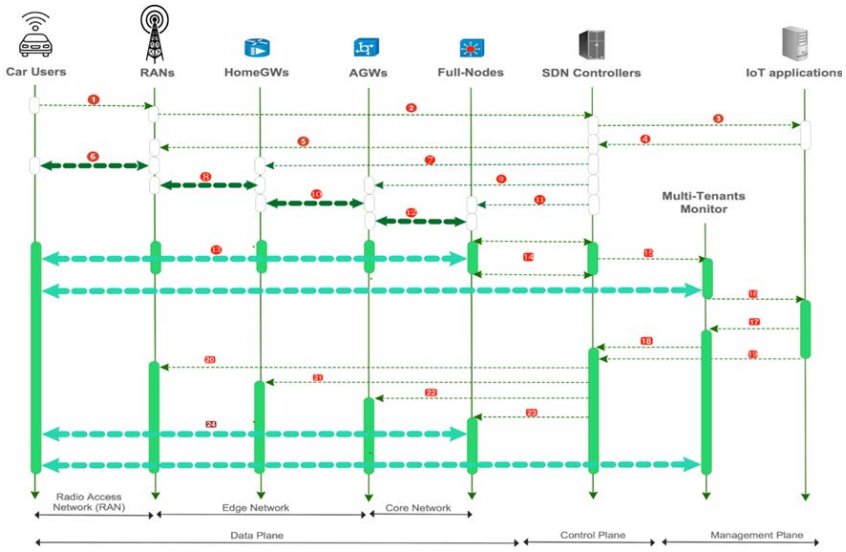

Fig. 6 An example for Automation Car Processing

In summary, the proposed SDN/NFV-based Internet of Things architecture for Multi-Tenants satisfies the trend of 5G, and be completely suitable for multiple providers.

4 Implementation and Evaluation

In this section, we implement an experiment in the standard P4-BMv2 target environment for core networks to perform network slicing and isolating via VXLAN and inject INT for monitoring QoS of multiple E2E channels. The authors used the open source P4 BMv2 switches model available at https://github.com/opennetworkinglab/routing/ and Mininet[40] to create each P4 BMv2 switches in the different trellis topologies to implement the experiments on different spine-and-leaf with the same number of Full-Nodes (spines) and AGWs (leaves). All tests were deployed on the off-the-shelf Dell PowerEdge 1950 III Server platform with two quad-core Intel Xeon 5400, CPU 3.16GHz, and 64GB memory running Linux 4.15, Mininet version 2.2.2, P4 Runtime package, and ONOS Controller version 1.13.2. Moreover, the INT over VXLAN GPE is suitable for virtualized data centers in building the Multi-Tenants Monitor application. Here, the VXLAN GPE (generic protocol extensions) is used to carry INT Headers between VXLAN GPE header and payload. The designed pipelines, INT and VXLAN GPE are used to reduce the complexity in network performance and forward packets transparently over the whole network that be suitable for implementation in virtualized datacenters. Fig.7.a shows the concept of modified BMv2 for multiple pipelines, and the pipeline processing is shown in Fig.7.b. Fig.8. shows a standard packet framework that formats for L2 Frame crossing whole network including the detail explanation of VXLAN header and INT header as bellow:

The modified VXLAN GPE Header is redefined within fields bellow: P bit (Next Protocol Bit) is set to indicate that the Next Protocol field is present; VXLAN Next Protocol bits defined values as 0x01 for next protocol is IPv4; 0x02 for IPv6; 0x03 for Ethernet; and 0x05 for In-band Network Telemetry Header (INT Header); O bit (OAM Flag Bit) is set to indicate that the packet is an OAM packet. In this case, this packet is sent to the ONOS Controller for controlling purposes; otherwise, it is a normal packet that must be forwarded. B bit is defined as BUM bit or a Flag bit. When B bit is set to 1, the packet is marked as a replicated-packet that need to be processed at the Packet Buffer and Replication Function for Multicast traffic purposes.

Instance bit (I bit) is set to indicate a valid VNI, which is a 24-bit field to identify the VXLAN overlay network and indicate that inner packets belonging to different VNIs cannot communicate with each other.

INT header is defined as sub-fields, INT's Type is an 8-bit field. Here, we reserve two types: hop-to-hop INT header and destination INT header type; INT Length is an 8-bit field indicating the actual INT data following the INT header ((0xFF – 4) * 32 bit); Max Hop Count is an 8-bit field indicating the maximum number of hops; Total Hop Count is an 8-bit field indicating the total number of hops that have added their metadata instances to the INT packet; Rep is a 2-bit field for replication requested; C is a 1-bit field indicating the packet that is a copy packet if C is set to 1. The sink HomeGW must be able to distinguish the original packets from replicas to process appropriately; E is a 1-bit flag to indicate that whether a device can prepend its own metadata due to reaching the Max Hop or not; Instruction Count is a 5-bit field indicating the number 1's bit in the Instruction Bitmap; and Instruction Bitmap is a 16-bit INT Instruction field, each bit. Correspond to a specific standard metadata such as bit 0 indicating the Switch ID, bit 1- the Ingress port ID and Egress port ID, bit 2- Hop latency, bit 3 defines Queue Occupancy, bit 4- Ingress timestamp, bit 5- Egress timestamp, bit 6- Queue congestion status, bit 7- Egress port tx utilization, and the remaining bits are reserved.

There are metadata fields defined by HomeGWs, AGWs, and Full-Nodes that enable the P4 program to specify where each packet arrived on, and control where it will go next. The P4 programmer defines objects in P4 that conforms to APIs, and the inputs and outputs of the programmable blocks such as Parser, Ingress, Egress, and Deparser based on user-defined headers and metadata.

After parsed by the Parser, packets are fed to the Ingress block for forwarding step. In this context, the standard packet format and forwarding process are implemented as the main roles of the Ingress block. In the next step, the forwarding process, firstly, verifies the header of the packets to determine what kind of packets and their functionalities. After that, the forwarding process uses a basic forwarding match-action table to find the egress port forwarding packets to destinations. This forwarding mechanism is supported on P4 programming and ONOS services, such as link layer discovery and reactive forwarding.

After processed at two fixed functions: PBR (Packet Buffer and Replication) and BQE (Buffer Queuing Engine), packets are sent to the programmable Egress block for removing the INT header (at HomeGWs) or cloning packets to egress ports. At Egress pipeline, the header is updated and then sent out of Egress to Deparser. Finally, at the Deparser, the packets are serialized and sent out of relevant egress ports.

In this test, the network consists of 16 nodes as shown in Fig.9. a). Fig.9. b) evaluate the latency of E2E communication in the UDP/VXLAN/INT test case, respectively; Fig.9.c), d) and e) show the test result of

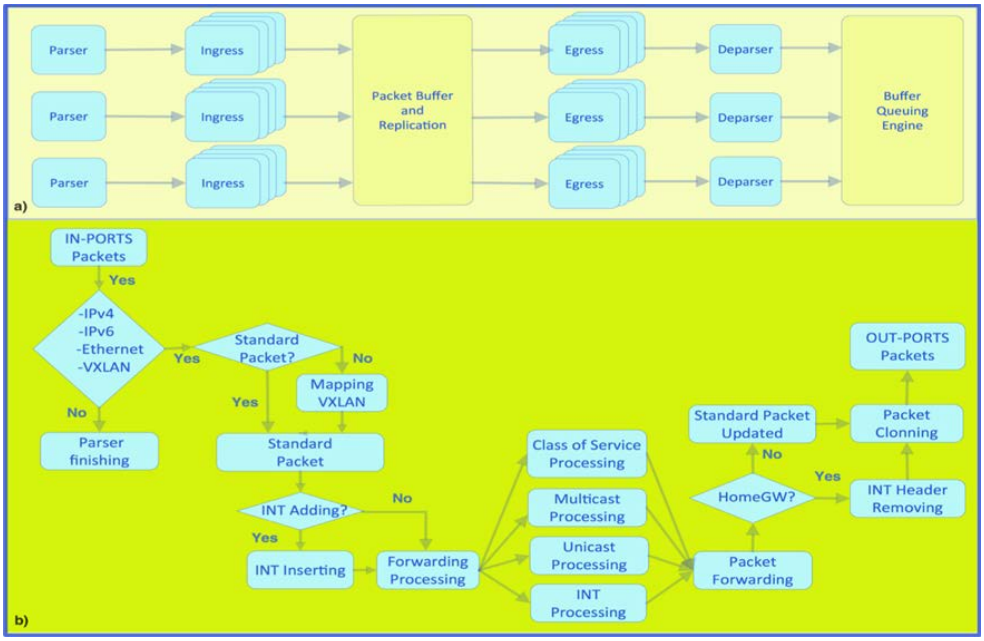

Fig. 7. a) The Concept of Modified BMv2 and b) A modified BMv2 pipeline processing

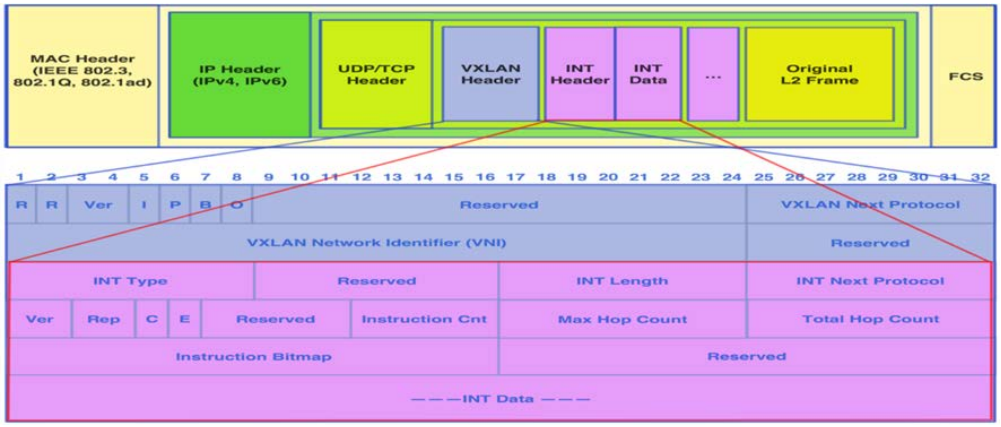

Fig. 8. A standard packet that format for L2 Frame crossing the whole network

UDP/VXLAN/INT after adding latency at source AGWs and AGWs, and Full-Nodes, respectively.

Next experiment, the Multi-Tenants Monitor implements QoS control for 8 different levels based on the 3 bit-QoS priority field predefined from QoS_class0 to QoS_class7, in each class the latency is predefined according to the customer demands. Fig. 10 and 11 show the testing results of some classes with a duration of 20 minutes for each class (QoS_class0, QoS_class2, QoS_class5, and QoS_class7). In the Maximum QoS (QoS_class7) require sink AGWs have to process amount of bigger data than other QoS _classes.

The last experiment, we choose different numbers of VNI-VXLAN at the highest variety of CDF of different cases to test the variable maximum QoS (QoS_class7) as shown in Fig 12. As can be seen, when the numbers of communicating VNIs channels increases, the processing load of the Full-Node also increases. Therefore, the latency at Full-Node is the main latency, result in the increase of E2E latency. Fig. 13. a) and b) show the testing results for 32 VNIs and for 64VNIs in the network, respectively. The E2E latencies

are stable until the last duration (n=64; p=0.7), where increase among of source, sink AGWs and Full-Nodes caused by low performance of deploying in this demo.

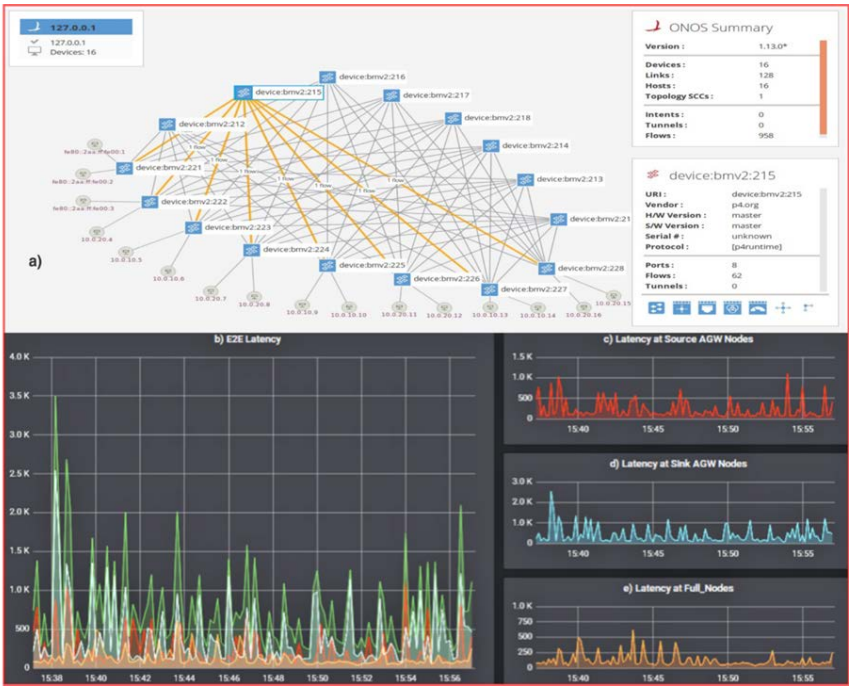

Fig. 9. a) A test case on a topology 16 nodes; b) 250 Byte-UDP/VXLAN/INT packets to test the latency at End to End host communication (10-3 ms); c) the latency at source AGWs; d) the latency at sink AGWs; e) the latency at source Full-Nodes.

Fig. 10. A test case for QoS_Class0 and Qos_Class2. a) the latency at End to End host communication (10-3 ms); b) the latency at source AGWs; c) the latency at sink AGWs; d) the latency at Full-Nodes.

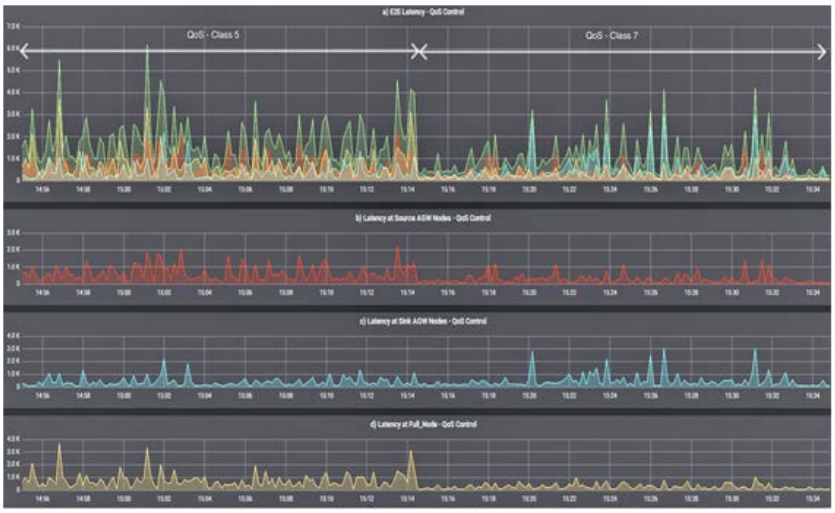

Fig. 11. A test case for QoS_Class5 and Qos_Class7. a) the End to End latency (10-3 ms) hosts communicating; b) the latency at source AGWs; c) the latency at sink AGWs; d) the latency at Full-Nodes

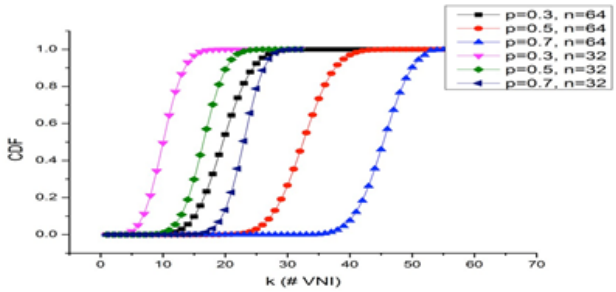

Fig. 12. A test choosing for Qos_Class7 with different VNI cases

5 Future Works

Our future work focuses on investigating and deploying components in customers' side and edge cloud, and integrating different IoT technologies to turn the HomeGWs into a multi-protocols gateway for plenty of IoT technologies and devices. On the other hand, we continue explore programmable data planes like Mobile CORD with P4 and various kinds of SPGW (Serving and Packet Gateway) and build applications on core networks such as traffic flow monitoring, traffic congestion control, QoS and QoE (Quality of Experience) control. Moreover, network slicing implemented at the Full-Nodes and AGWs different RANs is an essential technology for developing multiple protocols (both stateful and stateless protocols) in the network to meet diversity demands of applications in new scenarios.

6 Conclusion

A deep programmable data plane for deploying new network protocols, reprogramming pipelines and developing network services is crucial in opening new features for network innovation, availability, and scalability to satisfy the rapid increase in IoT devices and protocols. In this paper, the authors proposed a

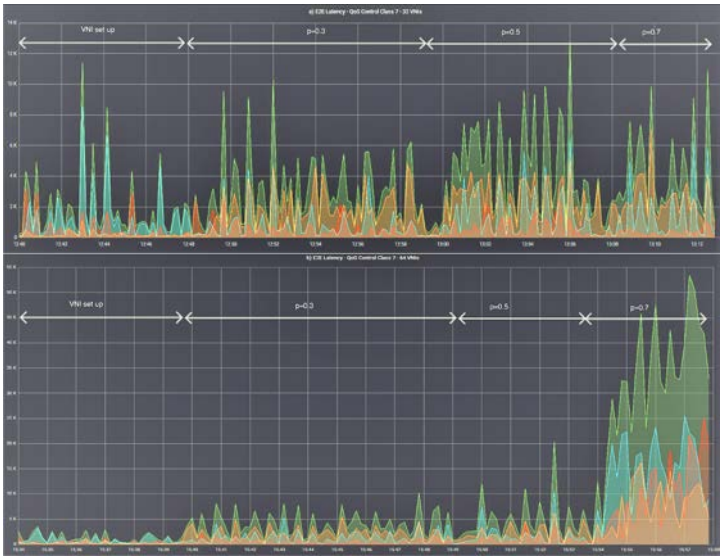

Fig. 13. A test case for QoS_Class7 with different VNIs. a) the End to End latency (10-3 ms) in case 32 VNIs deploying; b) in case 64 VNIs deploying

network architecture that completely suitable for multi-tenant networks, in which SDN/NFV play important roles in orchestrating entire network via SDN controller applications, and then, based on this architecture, network slicing associated with QoS control and network monitoring were implemented. We also recognized that, VXLAN, a new technology supporting a huge number of slices (sixteen millions), is a perfect solution for network slicing in datacenters and metropolitan environments. In addition, INT is a powerful approach for monitoring QoS of channels in the data plane, and then, the controller application can give timely respond to modify the network. The development of open sources such as P4-BMv2, ONOS is considered as key element and solution for new protocols, QoS monitoring mechanism for multi-tenant networks.

ACKNOWLEDGMENT

This paper is particularly supported by “the Center for Open Intelligent Connectivity from The Featured Areas Research Center Program within the framework of the Higher Education Sprout Project” by the Ministry of Education (MOE) in Taiwan, and the Ministry of Science and Technology of Taiwan under Grants: MOST 107-2221-E-009-056.

REFERENCES

[1] Open Networking Foundation, “SDN Architecture Overview,” *Onf*, no. 1, pp. 1–5, 2013.

[2] ETSI, “Network Functions Virtualisation (NFV); Architectural Framework,” *ETSI GS NFV 002 v1.2.1*, vol. 1, pp. 1–21, 2014.

[3] B. P. Lin, F. J. Lin, and L. Tung, “The Roles of 5G Mobile Broadband in the Development of IoT , Big Data , Cloud and SDN,” no. February, pp. 9–21, 2016.

[4] D. Sinh, L. Le, L. Tung, and B. P. Lin, "The Challenges of Applying SDN / NFV for 5G & IoT," *14th IEEE – VTS Asia Pacific Wirel. Commun. Symp. (APWCS), Incheon, Korea, Aug 2017*, pp. 138–142, 2017.

[5] L. Le, B. P. Lin, L. Tung, and D. Sinh, "SDN / NFV , Machine Learning , and Big Data Driven Network Slicing for 5G," IEEE 1st 5G World Forum, Santa Clara, CA, July 9-11,2018

[6] D. Sinh, L. Le, B. P. Lin, and L. Tung, "SDN / NFV - A new approach of deploying network infrastructure for IoT," *27th Wirel. Opt. Comminications Conf. (WOCC 2018)*, pp. 124–128, 2018.

[7] Z. L. K. Ben Pfaff, Bob Lantz, Brandon Heller, Casey Barker, Dan Cohn, Dan Talayco, David Erickson, Edward Crabbe, Glen Gibb, Guido Appenzeller, Jean Tourrilhes, Justin Pettit, KK Yap, Leon Poutievski, Martin Casado, Masahiko Takahashi, Masayoshi Kobayashi, Nick M, "OpenFlow Switch Specification," *Open Netw. Found.*, pp. 1–56, 2011.

[8] P. Bosshart, G. Varghese, D. Walker, D. Daly, G. Gibb, M. Izzard, N. McKeown, J. Rexford, C. Schlesinger, D. Talayco, and A. Vahdat, "P4: Programming Protocol-Independent Packet Processors," *ACM SIGCOMM Comput. Commun. Rev.*, vol. 44, no. 3, pp. 87–95, 2014.

[9] "P4 Brigade," no. https://wiki.onosproject.org/display/ONOS/P4+brigade, p. 4.

[10] C. S. Architecture, "P4 16 Portable 1 Switch Architecture," pp. 1–12, 2016.

[11] "Barefoot Networks. P4-bmv2. Website. https://github.com/p4lang/behavioral-model.," p. 4.

[12] https://datatracker.ietf.org/doc/draft-ietf-nvo3-vxlan-gpe/?include_text=1, "vxlan-gpe-6.pdf."

[13] Changhoon Kim, Parag Bhide, Ed Doe, Hugh Holbrook, Anoop Ghanwani, Dan Daly, Mukesh Hira, and Bruce Davie, "In-band Network Telemetry (INT)," no. September, pp. 1–28, 2015.

[14] "https://wiki.onosproject.org/display/ONOS/%28INT%29+In+Band+Network+Telemetry+with+ONOS+and+P4#id-(INT)InBandNetworkTelemetrywithONOSandP4-InstallBPFCollector," p. 29.

[15] P. Berde, M. Gerola, J. Hart, Y. Higuchi, M. Kobayashi, T. Koide, and B. Lantz, "ONOS: towards an open, distributed SDN OS," *Proc. third Work. Hot Top. Softw. Defin. Netw. - HotSDN '14*, pp. 1–6, 2014.

[16] M. Ojo, D. Adami, and S. Giordano, "A SDN-IoT architecture with NFV implementation," *2016 IEEE Globecom Work. GC Wkshps 2016 - Proc.*, 2016.

[17] F. Granelli, A. A. Gebremariam, M. Usman, F. Cugini, V. Stamati, M. Alitska, and P. Chatzimisios, "W IRELESS A CCESS IN F UTURE W IRELESS N ETWORKS : S CENARIOS AND S TANDARDS," no. June, pp. 26–34, 2015.

[18] I. Stojmenovic, "Fog computing: A cloud to the ground support for smart things and machine-to-machine networks," *2014 Australas. Telecommun. Networks Appl. Conf. ATNAC 2014*, pp. 117–122, 2015.

[19] H. I. Kobo, A. M. Abu-mahfouz, and G. P. Hancke, "A Survey on Software-Defined Wireless Sensor Networks: Challenges and Design Requirements," *IEEE Commun. Surv. Tutorials*, vol. 5, no. Submitted for publication, 2017.

[20] L. Velasco, L. Gifre, J.-L. Izquierdo-Zaragoza, F. Paolucci, A. P. Vela, A. Sgambelluri, M. Ruiz, and F. Cugini, "An Architecture to Support Autonomic Slice Networking," *J. Light. Technol.*, vol. 8724, no. c, pp. 1–1, 2017.

[21] J. Ordonez-Lucena, P. Ameigeiras, Di. Lopez, J. J. Ramos-Munoz, J. Lorca, and J. Folgueira, "Network Slicing for 5G with SDN/NFV: Concepts, Architectures, and Challenges," *IEEE Commun. Mag.*, vol. 55, no. 5, pp. 80–87, 2017.

[22] W. Miao, F. Agraz, S. Peng, S. Spadaro, G. Bernini, J. Perelló, G. Zervas, R. Nejabati, N. Ciulli, D. Simeonidou, H. Dorren, and N. Calabretta, "SDN-Enabled OPS With QoS Guarantee for Reconfigurable Virtual Data Center Networks," vol. 7, no. 7, pp. 634–643, 2015.

[23] M. Gramaglia, I. Digon, V. Friderikos, D. Von Hugo, C. Mannweiler, and M. A. Puente, "Flexible Connectivity and QoE / QoS Management for 5G Networks : the 5G NORMA view."

[24] S. S. Kumar, "Investigation of Security and QoS on SDN Firewall Using MAC Filtering," pp. 0–4, 2017.

[25] N. Ul Hasan, W. Ejaz, I. Baig, M. Zghaibeh, and A. Anpalagan, "QoS-aware channel assignment for IoT-enabled smart building in 5G systems," *Int. Conf. Ubiquitous Futur. Networks, ICUFN*, vol. 2016– Augus, pp. 924–928, 2016.

SOCIETY FOR SCIENCE AND EDUCATION
UNITED KINGDOM

TNC TRANSACTIONS ON NETWORKS AND COMMUNICATIONS

VOLUME 6, NO. 6
ISSN: 2054 -7420

Simulation on Collective Panic Behavior Based on PI

Wen ZHENG, Da ZHU
(Management Department, Northeastern University at Qinhuangdao, Qinhuangdao, 066004, P. R. China
zhengwen@neuq.edu.cn, 1433137831@qq.com

ABSTRACT

The collective panic behavior, which is caused by PI (Propagation Intensity), influences the welfare of citizens and the stability of the society (business). A well-known challenge is to understand the spreading mechanism of the panic behavior. In this work, the PI is classified as f and g, defined in the coefficient f (Promotion Intensity) and g (Inhibition Intensity) in the probability. MAS (multi-agent-simulation) model/tool is used to construct the systematic structure composed of four types of the participants (the individuals, the mass media, the social leaders, and the supervisors).This tool stimulates the collective panic behavior from the initial coefficient f and g, showing the different results in the condition of the population size and the conformity. Through setting up the rules and the strategies in an emergency, the framework stimulates the interaction between the agents (e.g. between the individuals, between the individuals and the mass media, between the individuals and the social leaders, between the individuals and the supervisors). The results advocate that the current simulator might be an appropriate first step towards the simulation and analysis of the combination of rules and strategies in panic behavior.

Keywords: Collective Panic Behavior, MAS(Multi-Agent-Simulation), PI(Propagation Intensity), *NetLogo* Platform

The project is funded by National Natural Science foundation, Code NO. 71473032.

1 Introduction

Nowadays, understanding the spreading mechanism of individual irrational behavior and the collective panic behaviors in an emergency is still an open challenge. China is a relation-society and the people in this country will share their feelings in an incredible way. When an emergency comes, a rumor is like a gem(seed). It can be spread heavily in a positive or negative way. It is absurd that many people rushed to buy the salt in China after the nuclear leakage accident in Fukushima (Japan)in case of the rumor" using iodized salt can prevent the harm of iodine -131" in 2011. The rumor (three days without daylight) leaded to the panic buying of the candles in some cities in China in 2012. What is the reason and the mechanism of the abnormal, large-scale panic behavior for some certain ordinary situations in an emergency? The current work presents an MAS tool, which aims at stimulating and analyzing the collective panic behavior in an emergency. The paper concludes four parts. First, we give the background of the study. Second, the framework of the CPBsim (Collective Panic Behavior Simulation) is given. Third, MAS model is constructed to explore the impact of the PI(Propagation Intensity). Last, it gives some discussions and conclusions.

DOI: 10.14738/tnc.66.5740
Publication Date: 23rd December 2018
URL: http://dx.doi.org/10.14738/tnc.66.5740

2 Background

2.1 Literature Review

In the literature, the researches on the abnormal phenomena of panic behavior had been analyzed before this study(Chen et al, 2007; Dai et al, 2015; Kou et al, 2012).They can be classified among: (a) the ones, those proposed the practical cases for the panic behavior,(Thomas et al, 2002;Edward et al, 2005; Li et al, 2009), and (b) the ones, those analyzed the different facets of the theoretical models in mathematics(Bergemann et al, 1996; Barabasi et al, 1999; Kirman et al, 2001;Yuan et al, 2005; Izquierdo et al, 2005), and (c) the studies based on the model of the simulation in individuals(Du et al, 2011; Zhang et al, 2011; Liu et al, 2014; Zhang et al, 2014;Zheng et al, 2016; Carlos et al, 2016). The practical cases are as following: after terrorist attacking in the "9.11", the purchase of gas masks in the shopping centers and the ciprofloxacin and other drugs in drug stores in United States increased rapidly(Thomas et al, 2002).The phenomenon of gasoline buying came after Hurricane Karina hit the United States(Edward et al, 2005). Some other theoretical researches in mathematics gave answers in, such as: establishing and solving the consumer decision-making behavior model to explain the phenomena of collective buying from the economic point of view(Yuan et al, 2005), and establishing the model and simulating the impact on the psychological expectations of panic behavior in context of an emergency (Sun et al,2006; Dai et al, 2015; Zhuang et al, 2013; Zhang et al, 2015; Kou et al, 2012; Liu et al, 2014; Chen et al, 2007; Qiang et al, 2014; Chang et al, 2011). The risk of the perceptions as the core of the intermediary variables would have a significant impact on people's mental state and the process of individual decision-making behaviors in the tsunami, the earthquake and other disasters (Li et al, 2009; Liu et al, 2013; Xu, 2003; Bi, 2007; Li, 2008). A three-level index evaluation system was established, pointing out the characteristics of the individual behaviors in an emergency and considering the external material environment and the individual's personality traits and other related factors(Zhao et al, 2010). The microscopic discrete dynamics concept model was deduced in the Internet surrounding in analyzing the interrelationship between Internet users' behaviors and the social dynamics factors. It can quantify the perceived information of the Internet users(He et al, 2010). Other researchers introduced the group behavior dynamics in constructing the dynamic theoretical model of the evolution of the collective behavior. (Wei et al, 2011; Xie et al, 2013; Lu et al, 2011). The modeling method was used in the microscopic perspective in constructing the simulation model of individual, revealing the behavior of individual and the interaction among them, as well as the whole situation of rumor propagation(Liu et al, 2014; Du et al, 2011; Zhang et al, 2016; Zhang et al, 2014; Zhang et al, 2011). Furthermore, the population model under the uncertain environment was done by proposing the fuzzy membership functions for the uncertainty movement of the microcosmic individuals(Chen et al, 2007).Based on the bounded trust rules, the conceptual model of noisy heterogeneous bounded trust was established(Zhao et al, 2015). With the method of Multi-Agent modeling, the public opinion evolution based on Internet were constructed(Du et al, 2015; Zhang et al, 2011; Yang et al, 2010; Chen et al, 2015).

The existing researches showed the collective panic behavior, which was caused by the rumors in context of an emergency. From the perspective of the systematic dynamics, the existing work explored the influence of the effective transmission intensity of rumors on the different amount of the participants in

the collective panic behavior. The paper is based on the *NetLogo* platform on giving t the simulation results.

2.2 Assumption

1) In an emergency situation, individuals, who are in the initial population of the spatial range (Li et al,2014), are divided into two categories: the participants with the collective panic behavior or with no-involving in it. The participants, who are in the collective behavior, are not only in joining in but also in affecting the surrounding neighbors. The participants at t time accounts for the Initial Population Size(IPS) $s(t)$. The ones, who do not participate in the panic behavior at t time, account for the proportion of the initial population in $1-s(t)$. The potential degree, which will be affected by the collective panic behavior of the population size, is basically stable. The initial population size is W.

2)The concentration of the population in the space is large and the spatial distribution is relatively uniform. The number of the neighbors of each individual is tiny, and at any time t, each participant of the panic behavior can communicate with the k individuals in the initial population of the space.

3) The collective panic behavior is affected by PI, which is cited as the positive one as the promotion intensity and the negative one as the inhibition intensity. And PI i expressed as the promotion intensity $f(r,e)$ and the inhibition intensity $g(c,l)$, respectively. Where r is the credibility of the rumor, e indicates the degree of the negative impact of the panic event itself, c represents the credibility of the government administration, and 1 indicates the disposition of the government administration. $f(r,e)$ and $g(c,l)$ are monotonically increasing functions of r, e and c. (In scope of $0 \le r,e,c,l \le 1$, $0 \le f(r,e) \le 1$, $0 \le g(c,l) \le 1$).

4) Assuming that the probability of the initial group does not participate in the panic behavior(Yan et al, 2010; Zheng et al, 2016). The participants are only related to the credibility of the rumors and the negative impact of the panic (Virginia et al, 2016) event itself. The value is the proportion of $f(r,e)$. In the initial group, the probability of panic behavior participants become the withdrawal from the panic and the credibility of government administration, as well as the intensity of disposal of government departments, and its value is proportion of $g(c,l)$.

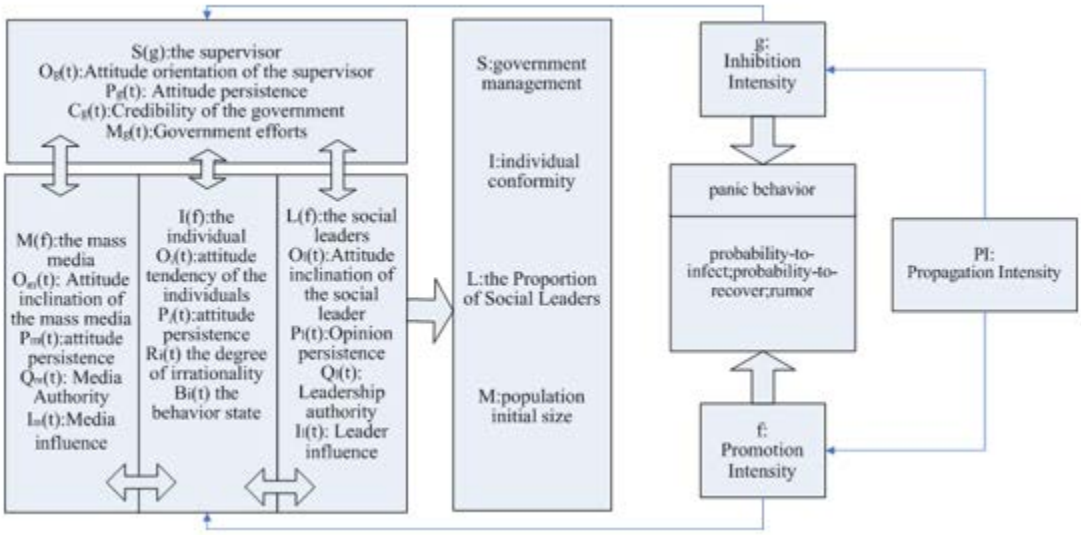

Fig.1 Class diagram of the CPB/Panbeh-agents

3 CPBsim/PanbehSim

CPBsim/PanbehSim is the simulation tool on the framework of the Collective Panic Behavior.

3.1 The Agents

3.1.1 Individual

The value is within continuous range.

1) Attitude tendency of the individual: $O_i(t)$ indicated the attitude of individual i to panic behavior at moment t. Attitude tendency is divided into three kinds: negative, neutral, and positive. The value is in continuous range, and the initial attitude tends to uniform random distribution.

2) Attitude persistence: $P_i(t)$ indicates the persistence degree of the attitude of individual i towards the panic at moment t. Attitude persistence is divided into three categories: lower, general, and higher. It is within the continuous range.

3) The degree of irrationality: $R_i(t)$ represents the degree of irrationality of the individual i at time t. The value is in continuous range.

4) The behavior state: $B_i(t)$ represents the behavior state of the individual i at time t. Behavior states are divided into three types: ①it does not yet involve in the collective panic behavior;②it has involved in the collective panic behavior; ③it has withdrawn from the collective panic behavior.

3.1.2 Mass Media

The value is in the continuous ranges.

1) Attitude inclination of the mass media: $O_m(t)$ represents the attitude of the mass media j at the t moment to the information (the facts or the rumor), which is in contacted with. The value is in continuous intervals.
2) Attitude persistence: $P_m(t)$ stands for the degree to which the mass media j maintains its attitude toward the information (facts or rumor). The value is in the continuous intervals.
3) Media Authority: $Q_m(t)$ represents the authority size of the mass media j at the t moment. The value is in the continuous range.
4) Media influence: $I_m(t)$ represents the spatial range, which the mass media j can influence the group at the t moment.

3.1.3 Social Leader

1) Attitude inclination of the social leader: $O_l(t)$ stands for social leaders' attitudes towards their own exposure to information (facts or rumors) at t. The values are in the successive intervals.
2) Opinion persistence: $P_l(t)$ refers to the degree to which social leaders adhere to their information (facts or rumors) set at 1.
3) Leadership of the authority: $Q_l(t)$ shows the authority size of the social leaders at the t moment in the continuous range of the values.
4) Leader influence: $I_l(t)$ represents social leaders' influence at the t moment in the groups in the continuous range of the values.

3.1.4 Supervisor

1) Attitude orientation of the supervisor: $O_g(t)$ indicates the attitude of the supervisor to the information that they have at the t moment. The government is positive in the process of the collective panic behavior.
2) Attitude persistence: $P_g(t)$ stands for the degree to which government authorities adhere to the information they spread.
3) Credibility of the government: $C_g(t)$ means that the confidence of the individual in the crowd to the government management will change with the management of the panic incident, and take the value in the continuous range.
4) Supervisor's efforts: $M_g(t)$ stands for the government's management of the negative information (rumors and related rumors) to deal with the intensity, in the continuous range of $[0,1]$.

3.2 The Rules

3.2.1 Rule 1

$$agent \in \{\Omega, B, C, E, \Psi, F\} ,$$

1) Ω ($\Omega = \{agent_1, agent_2, \cdots, agent_W\}$) is the whole group space, which is composed of a collection of all agents.
2) B ($B = \{b_0(t), b_1(t)\}$) is the individual behavior strategy state space. $b_0(t)$ indicates that the individual takes the panic behavior without taking part in at the t moment. And $b_1(t)$ stands for

the individual at the t moment to take part in the panic behavior. Three agents, which are indicated in colors of green, red, and gray on programs. Green indicates that the behavior of the agent is not yet involved. Red indicates that the behavior of the agent is participating. Grey indicates that the agent has withdrawn from the panic behavior.

3) C ($C=\{c(1),c(2)\}$) represents the possibility that individuals are infected by the other panic neighbors. Among them, $c(1)$ is a rational type, and $c(2)$ is an irrational type.
4) E ($E=\{f,g\}$) is the external environment function, where f ($0\le f\le 1$) is the promotion intensity, and g ($0\le g\le 1$) is the inhibition intensity.
5) Ψ ($\Psi=\{\Psi_1,\Psi_2,\cdots,\Psi_k\}$) is the space function of the agents and their neighbors.
6) F ($F:\{(C_i,E_i,\Psi_i)\to B_i(t)\}\times t\to B_i(t+1)$) is the behavior state transition function. The behavior state of agent at t = 1 is related to its own individual characteristics, surrounding neighbors, and external social environment at the t moment.
7) t ($t=\{1,2,3,\cdots\}$) is the system time pointer. During the evolution of the simulation system, Ω and Ψ are fixed, and the parameters of B are changed with the simulation system clock. C and E are the external adjustable parameters of the simulation system. And they are given before the simulation system is running. Because of the individual learning, the behavior strategy of the agent will take in the collective panic behavior under the circumstances of an emergency. The system is designed as a learning mechanism in updating rules, which take consideration the status of the individual, the neighborhood, and the external social environment.

3.2.2 Rule 2

The characteristics of the decision-making of the indifferent rationality and the herd irrational individual are recorded as $c(i),(i=1,2)$, $c(1),c(2)\sim U(a,b)$, and ordered as $c(1)\sim U(0,0.5)$, $c(2)\sim U(0.5,1)$.

The size of C reflects the size of individual conformity, which means the smaller value of C is, the less likely it is to learn from the surrounding individuals. The greater value of C is, the more it is likely to learn from the surrounding individuals.

3.2.3 Rule 3

The trait of individual conformity is q_i, and n is the total number of neighbors of the individual $agent_i$. And $\sum_{k=1}^{n} b_{ik}^{(0)}$ indicates the number of neighbors who do not participate in the panic behavior.
Individual changes from the panic behavior to withdrawal from the panic behavior. The renewal probability is:

$$P\{b_1(t)\to b_0(t+1)\}=\begin{cases}P_1 & P_1>0\\ 0 & P_1\le 0\end{cases} \quad (1)$$

The update probability of the behavioral strategy of the individual who changes from the no-involving one in the panic behavior to the involving one is:

$$P\{b_0(t) \to b_1(t+1)\} = \begin{cases} P_2 & P_2 > 0 \\ 0 & P_2 \le 0 \end{cases} \tag{2}$$

$$P_1 = q_i[\frac{1}{n}\sum_{k=1}^{n} b_{ik}{}^{(0)} + (g - f)] \tag{3}$$

$$P_2 = q_i[\frac{1}{n}(n - \sum_{k=1}^{n} b_{ik}{}^{(0)}) + (f - g)] \tag{4}$$

In (3) and (4), q_i stands for the subjective character of the individual to reflect the possibility of the individual conformity, which is affected by the panic infection.; $\frac{1}{n}\sum_{k=1}^{n} b_{ik}{}^{(0)}$ represents the proportion of neighbors in the neighborhood of $agent_i$, who do not participate in the panic behavior strategy. $\frac{1}{n}\sum_{k=1}^{n} b_{ik}{}^{(0)}$ reflects the local spatial environment of the individual; $g - f$ is the difference between the inhibition intensity and the promotion intensity, and reflects the external social environment.

Simulation system in the initial state, according to the above rules to update the evolution, if most of the agent's behavior strategy tends to participate in panic behavior strategy, the collective panic behavior is formed.

3.3 The Interactions among the Agents

In simulation model of the Multi-Agent of collective panic behavior, individual behavior changes are influenced by attributes of their own, of the surrounding neighborhood individuals, of the mass media, of the government management, and of the social leaders. The propagation of a rumor or a truth is a process of a individual choice. It can continue to be convinced in the group. And the performance of the individual within the group take the action strategy to evolve in the panic behavior or exit the group(not following group's strategy) .

3.3.1 Interaction between individuals

Referring to Coulomb's law, the degree of persistence of an individual's attitude toward collective panic behavior is analogous to the amount of charge in a vacuum neutral point charge, and the gap between individual attitudes is analogous to the distance between vacuum point charges, and the influence of individual attitudes is analogous to the interaction force between point charges, which reflects the change in attitudes towards panic behavior among individuals at the t and $t+1$ moments. The influence function S_i' of individual j on individual i is set at the moment of t :

$$S_i' = \sum_{j=1}^{N} (\frac{1}{N}) \frac{(1 - P_i)P_j}{\sqrt{d_{ij}}} \tag{5}$$

Among them, P_i is the attitude persistence degree of individual i , $1 - P_i$ is the attitude shift degree of individual i , P_i is the attitude persistence degree of individual i , d_{ij} is the attitude gap between individual i and j , and N is the number of neighbors that can be contacted by the peripheral area of individual i . When $d_{ij} = 0$,the attitude gap between individual i and individual j is 0, that is individual

i and j have the same attitude towards collective panic behavior, while individual i still adheres to its original attitude, that is $O_i(t+1) = O_i(t)$.

3.3.2 Interaction between individuals and the mass media

1) The extent to which the individual is influenced by the mass media is related to the authority of the mass media and the influence of the mass media. The influence function S'_M of the mass media on the individual i is:

$$S'_M = \sum_{m=1}^{s} \frac{1}{s} (c_1 Q_m(t) + c_2 \mathrm{Im}(t)) \bullet (1 - P_i(t)) \tag{6}$$

Among them, $Q_m(t)$ is the authority of mass media, $I_m(t)$ is the mass media influence, and s is the number of mass media involved in collective panic behavior. The influence of mass media on individuals is directly proportional to the authority of the mass media and the influence of the mass media. c_1 and c_2 are the ratio coefficients, $c_1 + c_2 = 1$, which are set by weight.

2) The attitude of the mass media at the $t+1$ moment tends to be influenced by the management of the sudden panic behaviors at the t moment, that is:

$$O_m(t+1) = f_1 O_m(t) + f_2 M_g(t) \tag{7}$$

Among them, $M_g(t)$ is the disposal efforts of the government towards to the sudden panic behavior of the group at the moment of t, f_1 and f_2 for the scale factor, $f_1 + f_2 = 1$, and set by the weight. Because the mass media and individual belong to two different behavior subjects, the attitude gap between them is not taken into consideration.

3.3.3 Interaction between individuals and social leaders

The attitude of individual to collective panic behavior is influenced by the authority of leaders and the influence of leader, and the influence function S'_L of the social leader on individual i is :

$$S'_L = \sum_{l=1}^{n} \frac{1}{n} (b_1 Q_l(t) + b_2 I_l(t)) \bullet (1 - P_i(t)) \tag{8}$$

Where $Q_l(t)$ is the authority of the social leader at time t, n is the number of social leaders in the group, $I_l(t)$ is the influence of the social leader at time t, Leadership authority and leadership influence are invariable, b_1 and b_2 are proportional factors, $b_1 + b_2 = 1$, and are set by weight. Since social leaders and individuals belong to two different actors, the attitude gap between them is not taken into consideration.

3.3.4 Interaction between individuals and government authorities

1) The influence function S'_G of government management on the individual attitude is:

$$S'_G = (a_1 M_g(t) + a_2 C_g(t)) \bullet (1 - P_i(t)) \tag{9}$$

Among them, $M_g(t)$ is the disposing of the government at time t, $C_g(t)$ is the government credibility in the time of t, $1-P_i(t)$ stands for the transfer of individual attitude on the moment of t, a_1 and a_2 are the proportional factors, $a_1+a_2=1$. Because of the government departments and individuals belonging to two different subjects, therefore the gap between the two attitude will not be considered.

2) The credibility of the government at the next moment is influenced by the credibility of the government at the moment and the government's supervision of sudden panic behavior, that is:

$$C_g(t+1)=e_1C_g(t)+e_2M_g(t) \tag{10}$$

Among them, e_1 and e_2 are the ratio coefficient, $e_1+e_2=1$.

3.3.5 Interaction between the group attitude and the group behavior

The theorem of Kinetic Energy is used to describe the transition of individual behavior during the evolution of panic behavior. The individual attitude is analogous to the quality of the subject, the irrational degree of the individual is analogous to the velocity of the moving object, and the individual's behavior state is analogous to the kinetic energy of the object:

$$B_i(t)=(1-O_i(t))\bullet R_i^{\,2}(t) \tag{11}$$

Among them, $B_i(t)$ is the behavior state of the individual i at the moment of t, $O_i(t)$ is the attitude of individual i at the moment of t, and $R_i(t)$ is the irrational degree of the individual i at the moment of t.

4 MAS model in exploring PI's Impact

Take the individual conformity as the research variable, and consider the individual characteristics and the external social environment characteristics in order to establish Multi-Agents simulation model. The agent has the ability to learn and can make independent decision of the individual, with closed two-dimensional grid community in infinite space (which can carry a agent) to represent the spatial environment of agent, each agent can move in any direction and randomly, and they can adopt two kinds of behavior strategies: take part in panic behavior and do not participate in panic behavior. Among them, do not participate in panic behavior should include all the time not involved in the panic behavior, but also has been involved in panic behavior but now opt out of panic behavior. The criterion of formation of collective panic behavior is that people with relatively stable scale take part in the panic behavior.

There are four categories of subjects in the mimic system. These are: the individual, the mass media, the social leaders, the supervisor. In order to ensure the simulation effect of panic behavior, the Agents' attributes are the constant value, and the other values of the Agents' attributes are generated by the random number generator during the operation of the simulation.

Based on the simulation platform, the simulation model of collective panic behavior caused by rumors in emergencies is established. The model stimulate the influence of the initial population size(IPS), the initial population conformity(IPC), the proportion of the social leader's influence(PSL). f is the promoted intensity, g is the suppressed intensity, $initial-participation$ is the initial participation rate of the panic behavior, and $initial-conformity$ is the proportion of non-rational individuals in the population.

4.1 The Influence of promotion Intensity and suppression Intensity

The effect of the promoted intensity f and the suppressed intensity g on the number of participants in the group panic behavior is shown in Fig.2

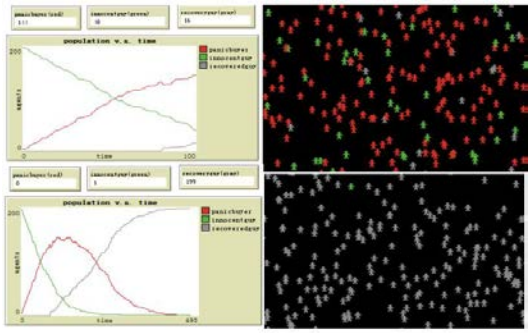

Fig. 2(a) Simulation results ($f = 0.5, g = 0.25$)

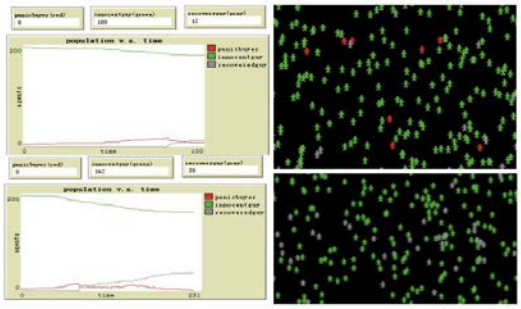

Fig. 2 (b) Simulation results ($f = 0.25, g = 0.5$)

when the behavioral strategies of the heterogeneous individuals in the population and the conformity of heterogeneous individuals are subject to the uniform distribution. When $f > g$, the number of the panic behavior in the crowd is greater than the number of the ones, who are not involved in the panic behavior, it indicates that the possibility of collective panic behavior is greater. When $f < g$, the number of panic behavior participant will reduce, interventions by government authorities have an inhibitory effect on the individual attitudes towards participating in the panic behavior. Part of the panic participants gradually withdraw.

Figure 2(a,b) effectively illustrates the control of the formation of the panic group. It is necessary in the initial stage of group in panic behavior to effectively control the spreading of the rumors. Those strategies are, to reduce the value of f, or to improve the degree of the government information disclosure, the government credibility, the government disposal efforts. In one word, that is, to increase the value of g.

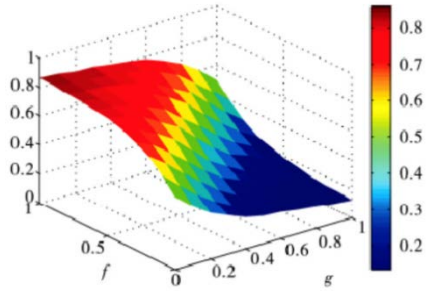

Fig. 3 The diagram of changing relationship in f, g, and participation rate

Figure 3 is a surface map, which indicates the participation rate of the group panic behavior changes with the promoting intensity and the inhibiting intensity. The abscissa represents the suppressing intensity of the behavior. The ordinate represents the promoting intensity of the behavior. The vertical coordinate represents the participation rate of the collective panic behavior in a stable stage. As it can be seen from the figure, even if the $f = 0, g = 1$, the participation rate of the group in the panic behavior is still greater than 0. The reasons are those, not only of the behavior to promote the intensity, but also of the panic behavior to suppress the intensity. The panic behavior is also subject to the individual's own state features and the impact of such factors. In addition, with the promoting the intensity of the behavior, the participation rate of the group panic will remain at a certain level. Even the power of the behavior, which leads to suppress the intensity, is close to 1. This is too tight in social structure because of the group in panic psychology leading to the whole. Although the intervention of the government management department controls intensity is too big, it cannot inhibit the formation of the collective panic behavior.

4.2 The Initial Size of the Population(ISP)

When $f = 0.5, g = 0.5$ is selected and the individual initial conformity characteristics obey the uniform distribution, the effects of initial panic behavior participation rate on the development trend of panic behavior are shown in Fig.4.

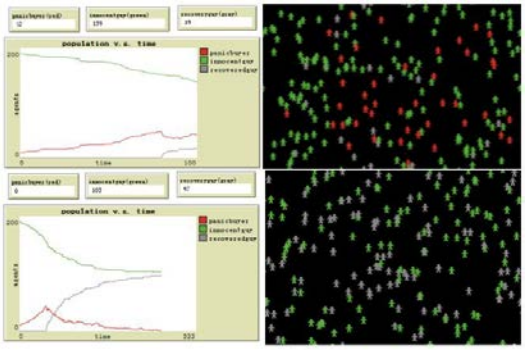

Fig. 4 (a) Simulation results ($f = 0.5, g = 0.5$, IPS rate = 5%)

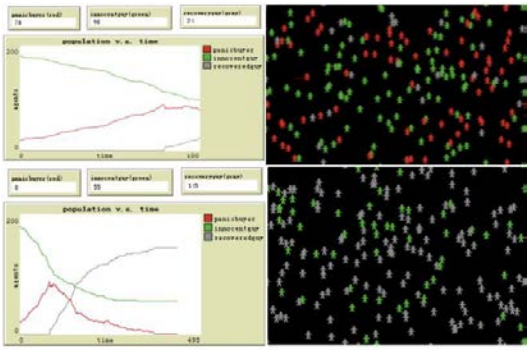

Fig. 4 (b) Simulation results ($f = 0.5, g = 0.5$,IPS rate= 10%)

When the inhibitory strength of participants is changed for $g = 0.25$ (Fig.6(a)) and $g = 0.15$ (Fig.6(b)), the government intervention is not in time, resulting in the number of collective panic behavior of participants increased rapidly. Even much number of the agents don't participant panic, it have an initial share advantage.

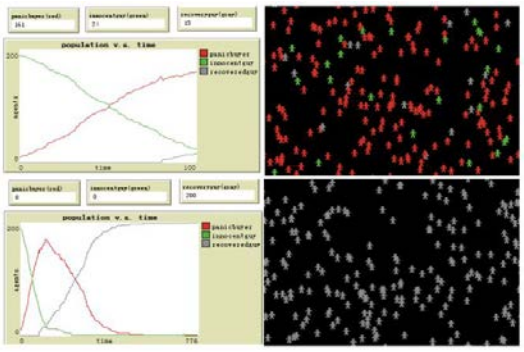

Fig. 5 (a) Simulation results ($f = 0.5, g = 0.25$, IPS rate= 5%)

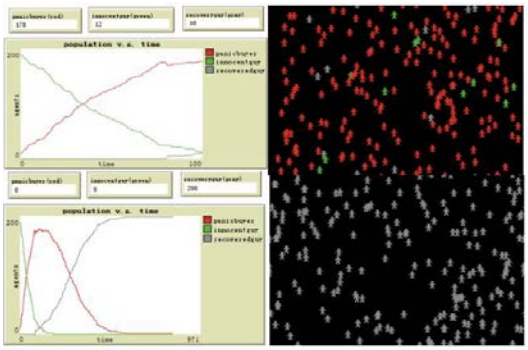

Fig. 5 (b) Simulation results ($f = 0.5, g = 0.15$, IPS rate = 5%)

It shows that the expanding of panic behavior is affected by the participation rate of the initial participants in space in fig.6, and the impact of government intervention on panic behavior. Even if the scale of the initial participation of collective panic behavior is not very large, it will lead to the scale of panic behavior expanding rapidly. And more people will involve in, if the government does not intervene.

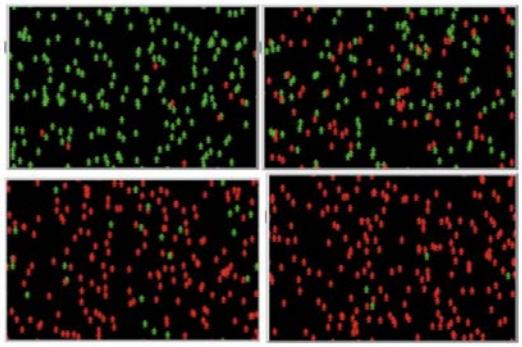

Fig.6 simulation results (IPS rate=5% to 98%, $f = 0.5, g = 0.25$)

4.3 The Initial Population Conformity(IPC)

Simulation parameters $f = 0.5, g = 0.25$, when the individual's initial behavior strategy is evenly distributed, the influence of individual conformity characteristics on the evolution results is revealed.

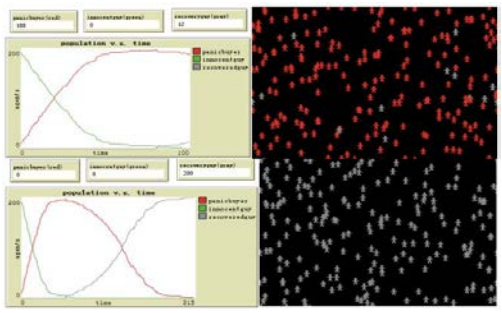

Fig. 7 (a) Simulation results ($f = 0.5, g = 0.25$, IPC = 25%)

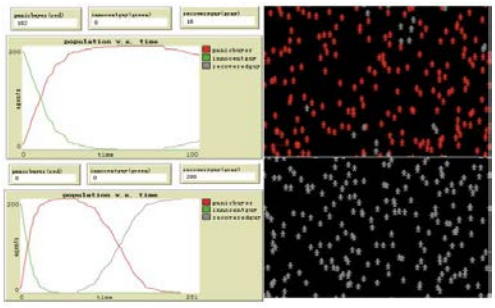

Fig. 7(b) Simulation results ($f = 0.5, g = 0.25$, IPC=50%)

It can be seen from the figure that under the same conditions, the proportion of irrational individuals in the initial population is greater, when the panic behavior involves a strong herd. In addition, Figure 7 (b) and Figure 2 (a) are two results of the simulation parameters of the same, the initial population size under the different conditions. By contrast, initial population conformity expands the scale of the participates in panic behavior. This is because when there are more non-rational individuals in the space group, the individual behavior strategy choice is more inclined to dominate the behavior strategy of most people. In this simulation experiment, due to the strength of promoting the panic behavior less than the strength of inhibiting one. The collective panic behavior after the short-term evolution was more dominant, so the individuals, who has herd characteristics, are more likely to take part in the panic.

4.4 The Proportion of Social Leaders(PSL)

Simulation parameters $f = 0.5, g = 0.25$, and when the individual's initial behavior strategy is distributed evenly, the influence of the proportion of social leaders in the group on the evolution results is considered. As the following Fig.8 show.

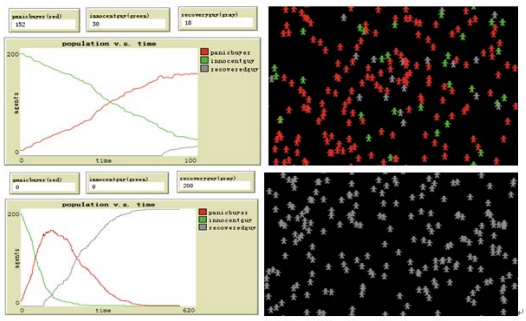

Fig.8(a) Simulation results ($f = 0.5, g = 0.25$, PSL= 5%)

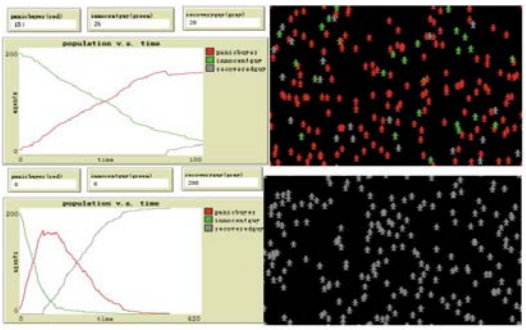

Fig. 8(b) Simulation results ($f = 0.5, g = 0.25$, PSL=10%)

It can be seen from the figure that under the same conditions, the proportion of social leader in the crowed is greater. When the leader was infected and transformed into the participants of panic behavior, due to its great social influence, more people around to spread rumors and related rumors. It results that more not involved are infected and turned into the panic participants. The expansion of the group panic is affected rapidly. And when social leaders are exposed to the truth and withdraw from the group panic behavior, because of its social influence, there will be more people around them will clarify the facts. The numbers of the collective panic behavior participants fall sharply and the panic behavior will gradually ease.

5 Discussions and Conclusions

The simulation results show the context of an accident. When the panic behavior occurred, which is caused by the rumors, the more the initial participation of collective panic behavior, the more conducive to induce the group spreading the rumors. The characteristics of the individual conformity can cause individuals, who have not yet participated in the panic behavior to support the dominant position of the party between promoting and suppressing the intensity of the panic behavior. If the proportion of social leaders in the crowed is great, the leader is infected and transformed into the participants of the panic behavior. Due to his(her) large social influence and wide network of connection, the more people around him are likely to spread the rumors, the more people are infected and transformed into the panic

participants. It leads to the scale of behavior in expanding the panic rapidly. Then the number of the panic behavior participants increased sharply. Furthermore, when the social leaders are exposed to the truth of the incidents and withdraw from the collective panic behavior, because of its social influence and wide social net connection, they will clarify the facts to more people. The rumors are self-defeated. The number of collective panic behavior participants declines sharply. Therefore, the collective panic behavior is gradually eased and subsided.

$f(r,e)$ and $g(c,l)$ in the evolution model represent two different "powers", which are the promotion and the suppression of the collective panic behavior. The regulation mechanism of the collective panic behavior caused by rumor can be considered in the following two aspects:

1. In the early stages of panic behavior, it should effectively reduce the intensity of rumor dissemination to achieve the purpose of $f(r,e)$.
2. Because of the low degree of controllability of rumor transmission, it needs a lot of auxiliary management tools and measures. Therefore, in the actual macro- management, scheme 1 is often difficult to implement in practice. In order to truly advance the prevention and effective control of the collective panic behavior, it also can improve the government's credibility and coping with crisis disposal efforts.

ACKNOWLEDGMENTS

The authors gratefully acknowledge the financial support from the NSFC (National Natural Science Foundation of China,71473032) and CSC(China Scholarship Council,201508130039) .

REFERENCE

[1] Barabási AL, Albert R. Emergence of scaling in random networks. Science 1999;286:509–12.

[2] Bergemann D, Valimaki J. Learning and strategic pricing. Econometrica 1996;64(5):1125–49.

[3] Bi Hongyin (2007).Analysis of the Group Influence in the Formation and Change of Network Public Opinion[J].Journal of TianJin University: (Social Sciences Edition),9(3):270-273.(in Chinese)

[4] Carlos Lemos, Rui Jorge Lopes, Helder Coelho (2016). On Legitimacy Feedback Mechanisms in Agent-Based Modeling of Civil Violence[J]. International Journal of Intelligent Systems, Vol.31,106-127.

[5] Chang Qin, Dang Huisen (2011).Research on population clustering model based on grid agent[J]. Journal of the People's Public Security University(Natural Science Edition), 17(3):71-74. (in Chinese)

[6] Chen Peng, Chen Jianguo (2015).Research on Multi - Agent Modeling of Sudden Group Violence[J].Computer Simulation, 32(1):377-381.(in Chinese)

[7] Chen Shiming, Huang Jiangping, Jiang Hong (2007). Research on modeling and simulation of swarm behavior in uncertain environment[J]. Computer Engineering and Applications, 43(21):32-35. (in Chinese)

[8] Dai Wei, Yu Lean, Tang Ling, Shen Yan (2015).A Study on the Public Information Strategy of Public Panic in Unconventional Emergencies: Based on Multi-Agent[J]. System Engineering-Theory &Practice, 35(3):641-650.(in Chinese)

[9] Du Rong, Liang Hongxia (2011).Simulation Government's Guide Effect on Network Opinion of Public Crisis[J]. Journal of Intelligence, 30(11):61-66. (in Chinese)

[10] Du Rong, Liang Lei,Wang Ning (2015). A Simulation Study on the Mass Emergency Evolution Based on the Social Physics——Evolution of Community Advice and Behavior[J].Complex Systems and Complexity Science, 12(3):61-69.(in Chinese)

[11] Edward Chow, Jonathan Elkind (2005). Hurricane Katrina and US Energy Security[J].Survival, 47(4):145-160.

[12] He Xiaoyuan, Hu Xiaofeng, Si Guangya (2010). Research on network information communication behavior based on social physics[J]. Journal of System Simulation, (12):2957-2962.(in Chinese)

[13] Izquierdo SS, Izquierdo LR, Galán JM, Hernández C(2005). Market failure caused by quality uncertainty. In: Mathieu P, Beaufils B, Brandouy O, editors. Artificial economics — lecture notes in economics and mathematical systems 564. Berlin: Springer-Verlag; 2005.

[14] Kirman AP, Vriend NJ (2001). Evolving market structure: an ACE model of price dispersion and loyalty. Journal of Economics Dynamic Control. 25(3–4):459–502.

[15] Kou Gang, Zhao Yiyi, Peng Yi (2012).Modeling and Analysis of Snapping Behavior under Sudden Incident[J]. Chinese Journal of Operations Research,20(1):85-91.(in Chinese)

[16] Li Huaqiang, Fan Chunmei, Jia Jianmin (2009). Public Risk Awareness and Emergency Management in Sudden Disasters: A Case Study of 5.12 Wenchuan Earthquake[J]. Management World, (6):52-63.(in Chinese)

[17] Li Lanying (2008).Based on CA's network of public opinion factors[J]. Science Technology and Engineering, 8(22):6179-6183.(in Chinese)

[18] Li Naiwen, Liu Yi, Huang Min (2014).A Study on Influencing Factors of Intrinsic Deviation in Individual Risk in Unconventional Emergencies[J]. Journal of China Safety Science, 24(5):10-14.(in Chinese)

[19] Liu Jia, Xie Kefan (2013).Study on influential factors of individual decision-making behavior of unconventional emergencies[J]. Soft Science, 27(3):50-54.(in Chinese)

[20] Liu Junguang, Ou Wei (2014). Research on Emergence Model and Simulation of Rumor Propagation of Sudden Incident[J]. Military Operations Research and Systems Engineering, 28(3):66-69. (in Chinese)

[21] LuQiaoyu, Shao Bo (2011).Analyzing public emergencies in the main behavior model based on the system thinking[J]. Public Management,(10):149-152.(in Chinese)

[22] Qiang Chaohua, Wu Peng (2014).A Study on the Behavior of Internet Users in the Process of Public Opinion Evolution of Sudden Events[J].Journal of Information Analysis and Research,(6):71-78.(in Chinese)

[23] Sun Duoyong (2006). The Economic Analysis on the phenomenon of individual buying in emergencies[J]. Economy and Management, (11):208-231.(in Chinese)

[24] Thomas A.Glass, Monica Schoch-Spana (2002). Bioterrorism and the People: How to Vaccinate City against Panic[J].Clinical Infectious Disease,34(2):217-223.

[25] Virginia Giorno, Serena Spina (2016). Rumor Spreading Models With Random Denials[J]. Physica A, Vol.461,569-576.

[26] Wei Jiuchang, Zhou Lei, Zhou Xin (2011). A Study on the Evolving Mechanism of Group Snapping in Public Crisis - A Case Study of Salt Selling in China Based on Japan's Nuclear Crisis[J]. Journal of management Case Study, 12(6):478-486.(in Chinese)

[27] Xie Liren, Chen Junmei, Zhang Minqin (2013).Research on influencing factors of sudden snapping behavior[J].Journal of XiAn University of Technology, 33(7):572-576.(in Chinese)

[28] Xu Zhiyu (2003).Compensation structure leads to control transfer - an analysis of SARS induced buying behavior [J]. Journal of FuZhou University (Philosophy and Social Sciences), (4):9-11.(in Chinese)

[29] Yang Zhimo, Si Guangya, Li Zhiqiang (2010).Design and implementation of large - scale group behavior simulation model[J].Journal of System Simulation,22(3):724-727.(in Chinese)

[30] Yuan Guiqiu, Pu Guohua (2005). Theoretical Explanation in Panic Buying[J]. Statistics and Decision, (1):56-57. (in Chinese)

[31] Zhang Fang, Si Guangya, Luo Pi (2011).A rumored propagation simulation model based on communication function[J].Journal of System Simulation, 23(11):2482-2486.(in Chinese)

[32] Zhang Yaofeng, Xiao Renbin (2014).Emergence mechanism of consensus synchronization in internet collective behavior based on cellular automata[J]. System Engineering - Theory & Practice, 34(10):2600-2608. (in Chinese)

[33] Zhang Yaofeng, Xiao Renbin (2015).Model and simulation of consensus evolution mass emergency[J]. Application Research of computers,32(2):351-355. (in Chinese)

[34] Zhao Laijun, Cheng Jingjing (2010). Research on Individual Behavior State under Unconventional Sudden Incident Based on Mutation Theory[J]. Journal of China Safety Science, 20(12):14-19. (in Chinese)

[35] Zhao Yiyi, Peng Yi, Xiao Lei (2015). Study on the Mechanism of Public Opinion Propagation of Group Snapping in Sudden Incident[J].System Engineering-Theory & Practice, 35(3):616-622. (in Chinese)

[36] Zheng Xiaojing, Zheng Junjun (2016).Criticality of symmetry breaking of collective behavior driven by Individual rules[J].System Engineering-Theory & Practice, 36(2):413-426. (in Chinese)

[37] Zhuang Yaming, Yu Hailin (2013). Research on Characteristics of Information Propagation Network of the Mass Unexpected Incident: A Case Analysis of Panic Buying of Candles[J]. Journal of Intelligence,32(7):37-42.(in Chinese)

APPENDIX

```
turtles-own [
infected? ;;if true, the person is either a panic buyer or a recovered guy.
  panicbuyer? ;; if true, the person is participating in the panic buying event.
  socialleader? ;; if true ,the person is a social leader which means he has greater influence on others.
  probability-to-infect ;; the probability of a normal guy to get infected
  probability-to-recover ;; the probability of a abnormal guy to get recovered
]
;;;
;;; SETUP PROCEDURES
;;;
to setup
clear-all
askpatches [ setpcolorblack ]
set-default-shapeturtles"person"
  setup-people
;; the original source rumor infectors of the whole panic buying event
askn-of ( round ( initial-participation /100* initial-people ) ) turtles [
set infected? true
set panicbuyer? true
    assign-color ]
askn-of ( round ( proportion-of-social-leader /100* initial-people ) ) turtles [
set socialleader? true ]
reset-ticks
end
to setup-people
create-turtles initial-people
  [ setxyrandom-xcorrandom-ycor
set infected? false
set panicbuyer? false
set socialleader? false
setsize1.5;; easier to see
    assign-color
set probability-to-infect 0
set probability-to-recover 0
  ]
end
to assign-color ;; turtle procedure
ifelsenot infected?
    [ setcolorgreen ] ;; it indicates that the person has not yet participated in panic buying event.
    [ ifelse panicbuyer?
      [ setcolorred ] ;; it indicates that the person is participating in panic buying event.
      [ setcolorgray ] ] ;; it indicates that the person has recovered from the panic buying event.
end
;;;
;;; GO PROCEDURES
;;;
to go
askturtles [ move ]
  getinvolved
  government-interfere
  getrecovered
askturtles [ assign-color ]
```

```
tick
;; if ticks = 100 [ stop ] ;; to get the temporary view and plot on the fly when ticks equal to one hundred.
;; when the count of panicbuyer less than or equal to the 1% of initial-people,
;; we can almost think the panic buying event is over.
if ( ticks>= government-interfere-time ) and ( notany?turtleswith [ panicbuyer? =true ]  )
    [ stop ]
end
;; people move about at random

to move  ;; turlte procedure
rtrandom-float360
ltrandom-float360
fd1
end
to getinvolved
;; because of touching rumor infectors,innocent guy have the probability1 to become a panic buyer
askturtleswith [ infected? =false ]
 [
ifrandom-float2< probability1
   [ set infected? true
set panicbuyer? true ]
 ]
end

to government-interfere
;; to research how to peace the panic buying behaviour,we start to consider this factor here
if ( ispublicized ) and ( ticks= government-interfere-time )
 [ askn-of ( round ( government-credibility /100* initial-people ) ) turtleswith [ panicbuyer? =true ]
   [ set panicbuyer? false ]
 ]
end

to getrecovered
;; because of touching truth,panic buyer starts to get recovered
ifany?turtleswith [ infected? =trueand panicbuyer? =false ] [
askturtleswith [ panicbuyer? =true ]
  [
ifrandom-float2< probability2
   [ set infected? true
set panicbuyer? false ]
  ]
 ]
end

;; the innocent guy has the probability1 to become a panic buyer

to-report probability1
askturtleswith [ infected? =false ] [
let number-a 0
let number-b 0
ifelse socialleader? =false
    [ set number-a (  count ( turtles-onneighbors4 ) with [ panicbuyer? =true ] )
set number-b ( countturtles-onneighbors4 )
```

```
ifelse number-b =0
      [ set probability-to-infect 0 ]
      [ set probability-to-infect ( initial-conformity /100 ) * ( ( number-a / number-b ) + (f /100 ) - ( g /100 ) ) ]
    ]
    [ set number-a (  count ( turtles-onneighbors ) with [ panicbuyer? =true ] )
set number-b ( countturtles-onneighbors )
ifelse number-b =0
      [ set probability-to-infect 0 ]
      [ set probability-to-infect ( initial-conformity /100 ) * ( ( number-a / number-b ) + ( f /100 ) - ( g /100 ) ) ]
    ]
 ]
report probability-to-infect
end

;; the panic buyer has the probability2 to get recovered

to-report probability2
askturtleswith [ panicbuyer? =true ] [
let number-a 0
let number-b 0
ifelse socialleader? =false
   [ set number-a ( count ( turtles-onneighbors4 ) with [ panicbuyer? =false ] )
set number-b ( countturtles-onneighbors4 )
ifelse number-b =0
      [ set probability-to-recover 0 ]
      [ set probability-to-recover ( initial-conformity /100 ) * ( ( number-a / number-b ) + ( g /100 ) - ( f /100 ) ) ]
    ]
    [ set number-a ( count ( turtles-onneighbors ) with [ panicbuyer? =false ] )
set number-b ( countturtles-onneighbors )
ifelse number-b =0
      [ set probability-to-recover 0 ]
      [ set probability-to-recover ( initial-conformity /100 ) * ( ( number-a / number-b ) + ( g /100 ) - ( f /100 ) ) ]
  ]
 ]
report probability-to-recover
end

;; Copyright 2017
;; Based on NetLogo platform
;; Simulation model of panic buying behaviour
;; By MMI.
```

SOCIETY FOR SCIENCE AND EDUCATION
UNITED KINGDOM

TNC TRANSACTIONS ON NETWORKS AND COMMUNICATIONS

VOLUME 6, NO. 6
ISSN: 2054 -7420

Research and Implementation of Bluetooth Indoor Auto-Tracking System

[1]Yen-Jen Chen, [2]Kai-Wen Zheng
[1, 2]Dept. of Electronics Eng., Ming Chi University of Technology, Taiwan, R.O.C.
yjchen@mail.mcut.edu.tw; wert880032@gmail.com

ABSTRACT

In recent years, outdoor positioning technology has been widely used and indoor positioning technology has gradually matured. Relevant applications such as: Indoor Location Based Service, Ambient Assistant Living, Indoor Navigation, Location Based Advertising, and the like have begun to show up in daily life and bring people with diversity and rich service content. The proposed study focuses on the research of real-time indoor dynamic positioning and dynamic tracking related mechanisms and algorithms, and uses the "microcontroller module" and "Bluetooth communication module" to actually detect the operational mechanism of the Bluetooth dynamic positioning system. This prototype system uses the smart phone as the locator of the traced person, named tracee (a new word created in this paper). The three-wheeled carrier acts as the tracer's body. On the locator, the processor is used to dynamically calculate the dynamic positioning of the tracee, and the calculated positioning result is transmitted to the tracer through the Bluetooth. The tracer calculates the distance and orientation, and then controls the axle motor so that the three-wheeled carrier closely follows the smart phone. Although many self-propelled vehicles have been sold on the market at present, and most of the follow-up signal uses infrared rays, ultrasonic waves, or Wi-Fi to complete the tracking action. However, the first two signals often require the tracee to carry an additional signal transmission device so as to assist in tracking. Due to the current popularity of mobile phones, although Wi-Fi and Bluetooth chips are already installed on the phone, yet the power consumption of Wi-Fi is still much higher than that of the Bluetooth. Therefore, in this study, Bluetooth was used to complete the indoor positioning system. Bluetooth belongs to 2.4GHz wireless technology; when using the Bluetooth signal for tracking, the signal strength is likely to cause many noises due to shielding, signal diffraction, or reflection, resulting in a deviation between the calculated transmission distance and the actual distance. The purpose of this study is to design a prototype of an Indoor Automatic Tracking System (hereafter named IATS) and explorer how to reduce the Bluetooth signal strength deviation so as to improve the accuracy of positioning is the main object of this study.

Keywords: Bluetooth, Auto-tracking System, RSSI, Indoor Location.

1 Introduction

Indoor positioning technology (IPT) [1] has gradually matured, with related applications such as: Indoor Location Based Service (ILBS)[2], Ambient Assistant Living (AAL) system[3], Indoor Navigation (IN)[4],

DOI: 10.14738/tnc.66.5808
Publication Date: 27th December 2018
URL: http://dx.doi.org/10.14738/tnc.66.5808

Location Based Advertising (LBA)[5] and the like services began to show up in daily life, and in the meantime, brought up more diversified and rich services content.

The origin of the present research is the observation of daily life such as: e-commerce shopping and warehouse management, home shopping for pre-school children, return of library books, nursing staff in medical centers, and other relevant staff all have the need to focus on other things in the work/family context and create the demand for an indoor automatic tracking system. The implementation of an Indoor Automatic Tracking System (IATS) must be supported by indoor positioning technology so that the IATS and tracee (a new word created in this paper, which means a traced person) can maintain proper distance under the auto-following operating mechanism. Using the pre-school children's home shopping as an exemplary, the IATS is a shopping cart, the tracee (parent) is the object to be followed. When the tracees move during the shopping process, the IATS can automatically position and control the IATS (shopping cart) to move or turn through control the motor so that the IATS (shopping cart) and the tracee is always at a fixed distance so as to achieve the object of automatic follow-up.

The indoor positioning technology uses the camera, infrared, laser (iGPS), ultrasonic or other communication technologies, in conjunction with corresponding spatial positioning algorithm to achieve indoor positioning. In the wireless communication technology portion, H. Liu [6] uses resolution and system scale to label the related technologies as shown in Fig. 1. Wherein, wireless communication technology with indoor positioning accuracy of less than 10 meters can be applied. From left to right, they are UWB, RF&IR, RF&Ultrasonic, WLAN, Bluetooth, DECT, ZigBee and other technologies, respectively. In accordance with recent academic research, UWB related research is mostly focused on algorithm improvement [7][8][9] and system design enhancement[10][11]; although RF&IR, RF&Ultrasonic can perform high-precision positioning, yet was not included in this study due to special device must be used to transmit the signal [12][13]; DECT [14] and ZigBee [15] are also constrained by the transmission device and the positioning accuracy is lower than RF&IR, RF & Ultrasonic, so they were not used in this study; WLAN and Bluetooth are supported by general smart phones, and their popularity is high. However, Bluetooth performance in terms of power consumption is more suitable for application program development [16][17], hence, this study uses Bluetooth as the communication technology for IATS implementation.

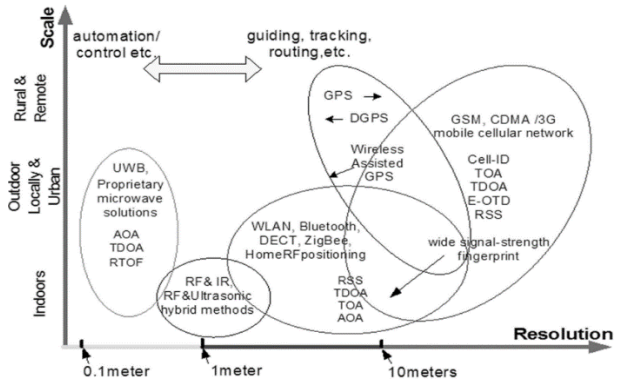

Fig. 1: Resolution and System Scale in Wireless Communication Positioning

In the recent academic research of Bluetooth, there is no lack of indoor positioning relevant research [18][19], but most of them are focused on the moving target with a fixed Bluetooth signal transmitter,

and the IATS proposed in this study has four features: 1) Virtual movement, 2) Instant positioning, 3) Closely following and 4) Dynamic environment. Details are described as follows:

a. Virtual movement: Both IATS tracer and tracee have the feature of being moved at any time.
b. Instant positioning: In terms of system computing capability, it must meet the requirements of the instance (less than 2 seconds per positioning).
c. Closely Following: The accuracy of the path calculation must in conformance with the condition of following in a short distance (less than 2.5 meters)
d. Dynamic environment: Barrier caused by the turn or movement of tracee will affect the tracking system operation

Up to the present, research on the use of Bluetooth in indoor positioning has not explored the 1), 3), and 4) items of the above features. Therefore, the research using Bluetooth technology aims to achieve indoor dynamic positioning and obstacle avoidance following shall be extremely challenging.

2 Background

The relevant technologies and research of the present paper are described as follows:

2.1 Bluetooth

Bluetooth is a wireless communication technology standard. It was jointly proposed mainly by the manufacturers of Ericsson, IBM, Intel, Toshiba and Nokia in 1998, and established the Bluetooth SIG to update and maintain technical specifications. Bluetooth technology alliance currently has more than 30,000 manufacturers in communications, computers, networks, and consumer electronics joined the membership. In terms of technology, Bluetooth uses Ultra High-Frequency radio waves as a transmission medium and operates in the Industrial Scientific Medical Band (2.4 to 2.485 GHz). It is used as the Personal Area Network (PAN) in stationary, mobile, and architectural applications. On the other hand, the current version used in the industry is Bluetooth 4.0 to 4.2, and the main difference between the 3.x and the current version is the improving power consumption and achieving a communication distance of 100 meters. Therefore, the Bluetooth 4.x version is called Bluetooth Low Energy (BLE).

2.2 Bluetooth Indoor Positioning System

The research of Bluetooth indoor positioning systems over the past few years is the system, through the signal transmitting device installed indoor, and based on the signal intensity to positioning. This type of method is called the Fixed Indoor Positioning System. Relevant research subjects are described as follows:

1) Positioning through the signal transmitted by the Bluetooth device beacon

Scholar P. Dickinson, et al [20] used low-power Bluetooth communication device beacon and install a beacon at the shopping corridor in the store every 5.4 meters or 8.1 meters, and use the pre-installed applications to transmit the Received Signal Strength Indicator (RSI) for various beacons at their current locations; the strongest beacon on the signal represents the consumer's proximity to the area, so as to understand the time and the path consumers spend and walk in various areas of the store.

2) Research using Wi-Fi and Bluetooth on Positioning

Scholar Vibhu Varshney et al [21] uses pre-arranged Wi-Fi and Bluetooth communication networks for positioning in the indoor environment. The positioning method was calculated using the most common RSSI in conjunction with triangulation method, and 10 measurements were performed. The experimental results indicate that at the area in space, the result for the coordinate of Wi-Fi positioning, the accuracy of the X-axis is 77.59%, the accuracy of the Y-axis is 88.41%, and in the Bluetooth portion, the accuracy of the X-axis is 89.1%, and the accuracy of the Y-axis is 73.3%.

The above-related studies are focused on the algorithm of the fixed Bluetooth positioning system and are different from the Bluetooth dynamic positioning system explored in this study. In accordance with the survey of this study, at present, there is no research concerning the use of Bluetooth for indoor tracking systems.

3 Methods

The present study focuses on the research of mechanisms and algorithms related to "instantaneous indoor dynamic positioning" and uses the "microcontroller module" and "Bluetooth communication module" to actually detect the operational mechanism of the Bluetooth dynamic positioning system. The system uses the smart phone as a tracee, and uses the three Bluetooth modules as a tracer body to be installed for dynamic positioning, and use algorithm the to instantly know the distance between the tracee and the tracer.

As shown in Fig. 2, the present study will install three Bluetooth modules on the auto-trace system. The Bluetooth module broadcasts the signal. The phone set detects the signal strengths of the three Bluetooth modules and derivate the current auto-trace system centered location information and transmitted back, when the auto-trace system receives the position message and controls the motor to automatically trace the smartphone held by the tracee to perform a three-wheeled carrier Bluetooth dynamic positioning system.

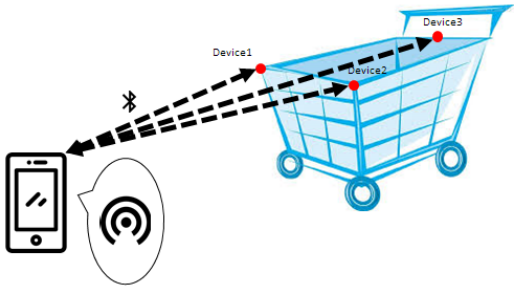

Fig.. 2: Schematic View of Bluetooth Dynamic Positioning System

The Bluetooth dynamic positioning system is composed of two systems: the Tracer and the Tracee. The system architecture is shown in Fig. 3. In practice, the tracee is a smart phone with Bluetooth module and has a smart phone mobile application (Mobile APP) to achieve Bluetooth reading and Real-Time Bluetooth positioning (RTBP) function; the tracer system is a microcontroller platform in conjunction with an external Bluetooth module. The microcontroller platform can be subdivided into two subsystems, namely Path Estimation (PE) and motor. Control (MC). Description is provided as follows: 1) Path estimation: This subsystem comprises four Bluetooth communication modules, three for indoor positioning and one for

communication. The trace system (namely, smart phone) forms a pair with the Bluetooth communication module and responsible for communication. After the smart phone completes the Bluetooth pairing, it will periodically capture the signal strength of the Bluetooth communication module used for indoor positioning, and calculate the position information of the current trace system and transmitted back to the subsystem, and this subsystem is based on trace system location information for motor control. 2) Motor Control: This subsystem is responsible for periodically receiving instructions for path estimation so as to control the axle motor to achieve the direction and speed required by the tracer.

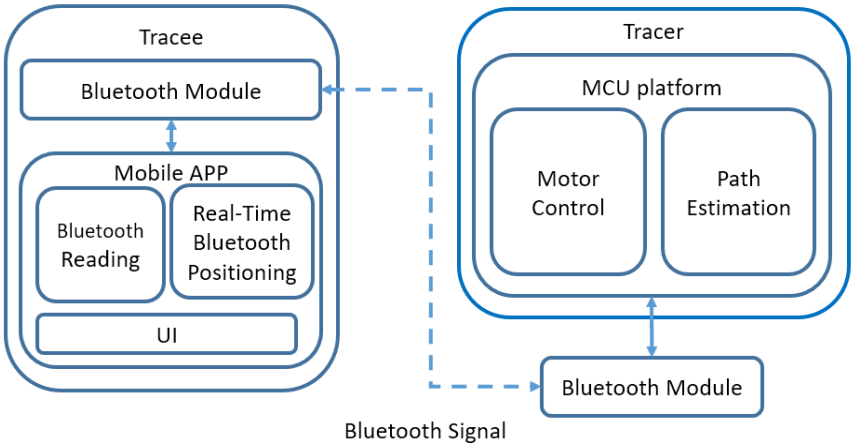

Fig. 3 System Architecture of Bluetooth Dynamic Positioning System

3.1 Real-Time Bluetooth Position

The most basic Bluetooth two-dimensional positioning system consists of one Positioning Node (PN) and three reference nodes (RNs)[22]. Under this architecture of the present study, a smart phone was used as a PN and the three vertices, AP1 to AP3, of the tracer were used as RNs. Based on the RSSI value measured by mobile phone for the three vertices to the tracer system to calculate the distance between the three vertices of the mobile phone to the tracer system, and then the coordinates of the mobile phone can be obtained through the trilateration method [23].

In indoor positioning related research, the signal sent by the transmitter is often converted to RSSI, the definition is shown as Equation 1:

$$RSSI = 10 \times \log(\frac{P_r}{P_{ref}}) \quad (1)$$

wherein, Pr is the power received by the receiver antenna, Pref is often 1mW.

The simplified relationship between received signal strength and distance can be expressed as Equation 2:

$$P_d = P_0 - 10 \times n \times \log_{10}(d) \quad (2)$$

Where P_d is the received signal strength (dBm), which is the distance from the transmitter source (dBm), that is, the so-called RSSI; P_0 is the received signal strength (dBm) from 1 meter from the transmitter; n is the path attenuation index. Equation 2 can be organized into the relationship between distance and RSSI as Equation 3:

$$d = 10^{\frac{P_0 - P_d}{10 \times n}} \quad (3)$$

On the basis of the trilateration method, the smartphone coordinates derived through three Bluetooth devices are shown in Fig. 4:

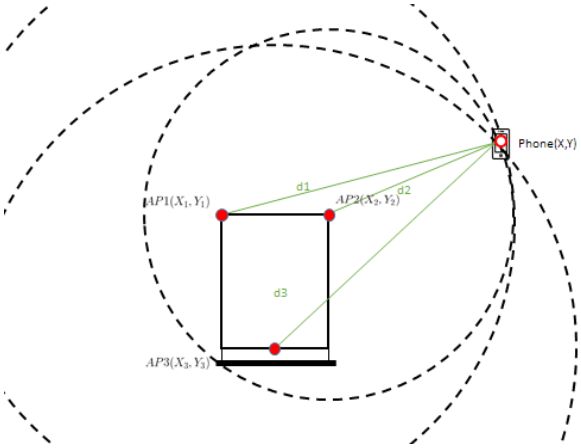

Fig. 4 Schematic Diagram of the Bluetooth Indoor Positioning Algorithm

The distance between each transmitter and receiver can be expressed as Equation 4, wherein the three devices are set to 1.2, 1.5, and 1.5, respectively. Substituting (x_i, y_i) into Equation 4 and solving 3 simultaneous equations can obtain the coordinates (x, y) of the mobile phone.

$$d_i^2 = (x - x_i)^2 + (y - y_i)^2, i = 1,2, \dots, N \quad (4)$$

The reason that the n path attenuation index is set in this way is due to the present study collects the RSSI values for each device at 1m, 2m, and 3m first, respectively and substitutes them into Equation 5 for the inverse n value.

$$n = \frac{P_0 - P_d}{10 \times \log(d)} \quad (5)$$

wherein, P_0 is derived by substituting the RSSI average value when the device distance is at 1m, and then substitutes the RSSI average of 2m and 3m into P_d to derive the value of n. Then, the resulting n value is fine-tuned so that the result of the RSSI transferring to distance formula is close to the actual value.

3.2 Enhance Positioning Accuracy

Bluetooth is a 2.4GHz wireless technology. This band is prone to many noises due to shield, signal diffraction or reflections. Therefore, the selection of signals and averaging are quite important. The present study uses Equation 6 to complete the average calculation.

$$X(t) = \alpha X + (1 - \alpha) X(t - 1) \; ; 0 < \alpha < 1 \quad (6)$$

wherein, X(t-1) is the average value obtained the previous time, X_(t) is the mean value obtained this time, and X is the RSSI value obtained this time..

However, how to set the value of the signal screening condition so will not exclude too much data. The process is shown in Fig. 5

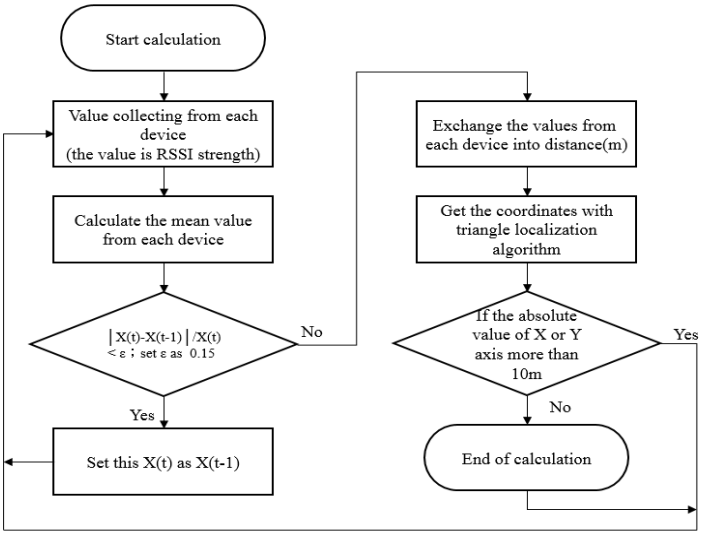

Fig. 5: Positioning Calculation Process Chart

Furthermore, after the mean value of each device is obtained, a filter condition is added to exclude the value that is too large due to excessive RSSI floating during the movement. The filter condition and the usage are shown in Equation 7.

$$\frac{|X(t)-X(t-1)|}{X(t-1)} < \alpha\ ;\ \alpha = 0.15 \tag{7}$$

4 Results

The test environment of the present study is located in a home with Wi-Fi, and the three Bluetooth devices used for positioning are placed on a plane with a length, width and height of 1m*1m*0.42m, and the three Bluetooth devices are placed in the same position on the plane. The tester holds the mobile phone with the positioning APP installed and stand to measure in front of the desk. Fig. 6 below shows the three device RSSI values measured at 1, 2 metrics and measured without any screening.

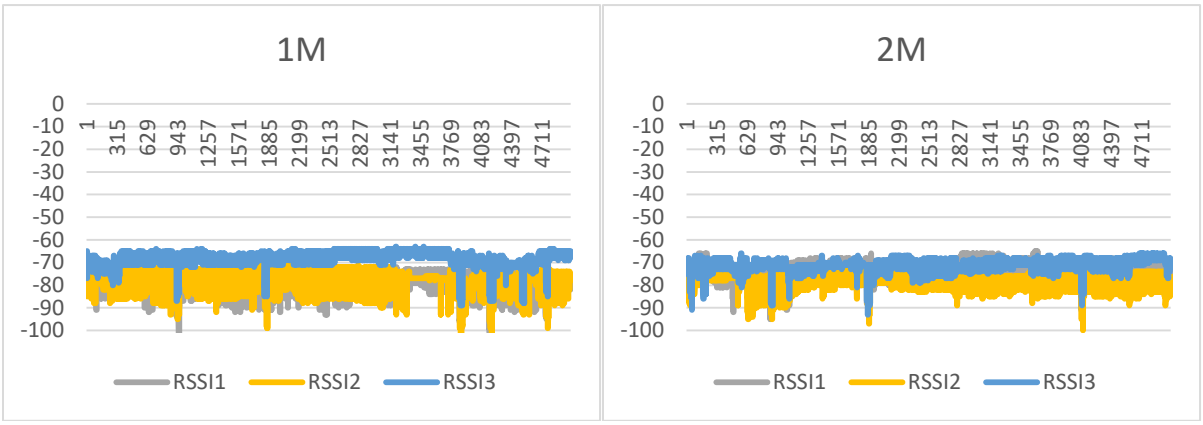

Fig. 6: RSSI Values for Three Devices

Fig. 6 contains 5,000 pieces of data in 1M and 2M respectively. It can be seen from the Fig. that the RSSI value is always up and down in one interval, wherein the standard deviations of devices 1 to 3 are 1M: 5.35, 5.99, 3.99, 2M: 4.49, 4.25, 3.46, respectively, in addition, the maximum deviation reaches up to 32%

for the consecutive data. However, the substitution of this equation into the distance equitation will make the difference more significant. Hereafter, it will cause using the trace to estimate the distance between the tracer and the tracee has too much deviation and not easy to control the output of the motor. Therefore, it is necessary to use the mean value calculation to reduce the standard deviation and the effect of consecutive data difference.

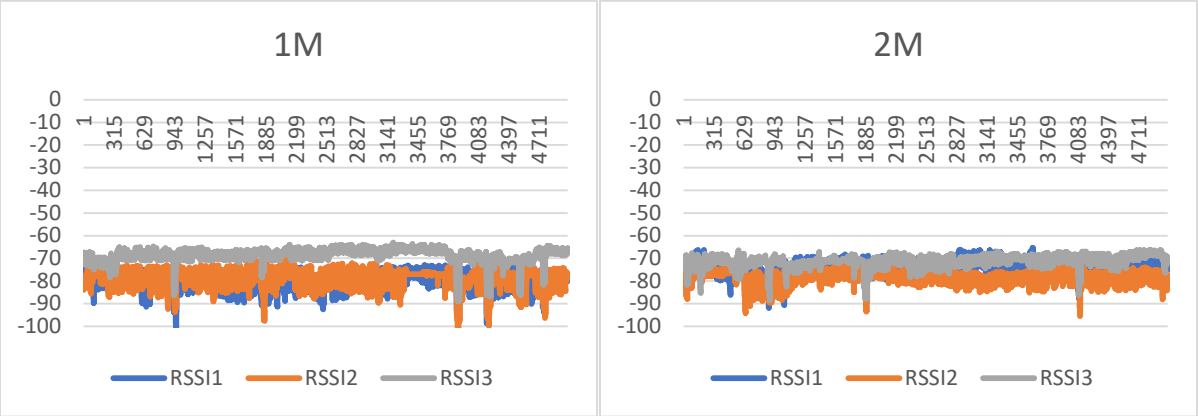

Fig. 7: RSSI Value after Averaging 3 Devices

After adding the average calculation, the standard deviation is 1M: 4.16, 4.4, 3.43, 4.25, 3.05, 2.71, and the consecutive data difference is reduced to 9%. It can be seen from the Fig. that after the screening, the numerical change (that mean the curve in the Fig.) is more gradual. However, the above is the result collected by the mobile phone in the fixed state. When the Bluetooth RSSI signal is in the moving state, the jump amplitude will be more proportional to the distance. Therefore, at present, the present study chooses the range of data difference within 15% to ensure that the data will not be deleted too much, and can have the function of excluding excessive changes.

Fig. 8 below shows the changes in the RSSI values presented by adding the average and the screening algorithm, and walking from distance 0M to 3M.

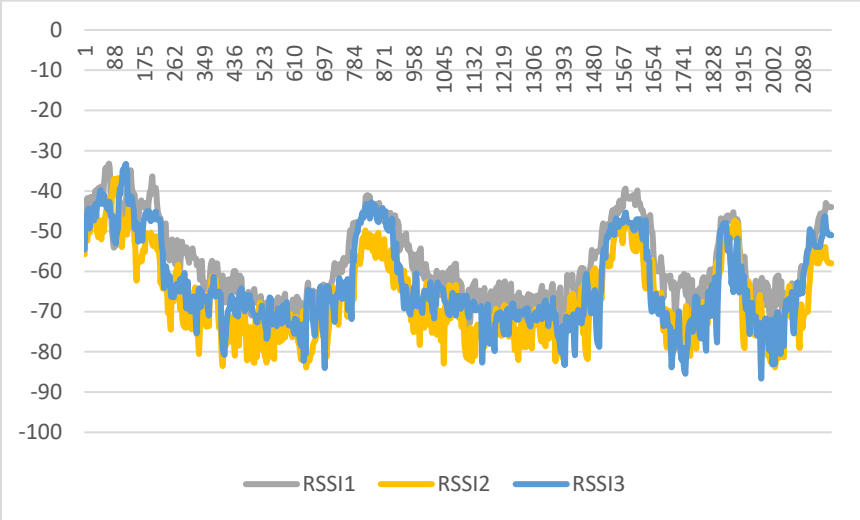

Fig. 8: RSSI Values from 0M to 3M Walking Back and Forth

Fig. 8 has a total of 2178 pieces of data, and its adoption rate is 90%. The screening condition is that when the data difference exceeds 15% before and after, the calculation results are excluded. After adding the

average calculation, the intensity of the Bluetooth RSSI signal will exceed 15% before and after the movement.

5 Conclusion

Indoor Positioning Technologies (IPT) is getting mature, relevant applications such as: Indoor Location Based Service (ILBS), Ambient Assistant Living (AAL) system, indoor navigation (IN), Location Based Advertising (LBA) and the like began to show up in daily life, and also brought more diversified and rich service content to people.

The purpose of the present study is to design a prototype of the Indoor Automatic Tracking System (IATS). The main object of the present study to explore how to reduce the deviation of the Bluetooth signal strength to improve the accuracy of positioning. The Bluetooth is a 2.4GHz wireless technology. This frequency band is prone to many noises due to shielding, signal diffraction or reflection. Therefore, the selection of the signal and the calculation of the average value are very important. The present study completes the average value calculation using Equation 6 and uses Equation 7 to add the screening conditions to eliminate the excessively large difference in RSSI due to excessive floating in the movement, so that the result will be up to 35% of the original data difference before and after calculation. After the algorithms is controlled at less than 10%, the utilization rate is 100%, and the difference between the data before and after moving will be higher than the 15% set in the present study, but the adoption rate is still 90%, and no excessive information will be excluded so as to make measurement data have a certain degree of accuracy.

REFERENCES

[1] Mautz Rainer, *Indoor Positioning Technologies*, 2012

[2] Ishida, S., Tagashira, S., Arakawa, Y. and Fukuda, A., *On-demand Indoor Location-Based Service Using Ad-hoc Wireless Positioning Network,* 2015 IEEE 17th International Conference on High Performance Computing and Communications, 2015 IEEE 7th International Symposium on Cyberspace Safety and Security, and 2015 IEEE 12th International Conference on Embedded Software and Systems, New York, NY, 2015: p. 1005-1013.

[3] Chen, H., and Cui, L., *DS-MMAC: A delay-sensitive multi-channel MAC protocol for Ambient Assistant Living systems*, in China Communications, vol. 13, no. 5 ,May 2016: p. 38-46,

[4] Caruso, D., Sanfourche, M., Le Besnerais, G., and Vissière, D., *Infrastructureless indoor navigation with a hybrid magneto-inertial and depth sensor system,* 2016 International Conference on Indoor Positioning and Indoor Navigation (IPIN), Alcala de Henares, Spain, 2016: p. 1-8.

[5] Liu, H., Darabi, H., Banerjee, P., and Liu, J., *Survey of Wireless Indoor Positioning Techniques and Systems,* in IEEE Transactions on Systems, Man, and Cybernetics, Part C (Applications and Reviews), vol. 37, no. 6, Nov. 2007: p. 1067-1080.

[6] Perera et al, A. A. G. A. K., *Ads-In Site: Location based advertising framework with social network analyzer,* 2014 14th International Conference on Advances in ICT for Emerging Regions (ICTer), Colombo, 2014: p.

116-123.

[7] Djaja-Josko, V., and Kolakowski, J., *A new transmission scheme for wireless synchronization and clock deviations reduction in UWB positioning system,* 2016 International Conference on Indoor Positioning and Indoor Navigation (IPIN), Alcala de Henares, 2016: p. 1-6.

[8] Djaja-Josko, V., and Kolakowski, J., *A new method for wireless synchronization and TDOA deviation reduction in UWB positioning system,* 2016 21st International Conference on Microwave, Radar and Wireless Communications (MIKON), Krakow, 2016: p. 1-4.

[9] Xie, Y., Janssen, G. J. M., and Veen, A. J., *A practical clock synchronization algorithm for UWB positioning systems,* 2016 IEEE International Conference on Acoustics, Speech and Signal Processing (ICASSP), Shanghai, 2016: p. 3891-3895.

[10] Chen, H. and H. Vun, C., *Compressive sensing techniques for UWB indoor positioning applications,* 2015 IEEE International Conference on Consumer Electronics (ICCE), Las Vegas, NV, 2015: p. 231-232.

[11] Piccinni, G., Avitabile, G., Coviello, G., and Talarico, C., *Distributed amplifier design for UWB positioning systems using the gm over id methodology,* 2016 13th International Conference on Synthesis, Modeling, Analysis and Simulation Methods and Applications to Circuit Design (SMACD), Lisbon, 2016: p. 1-4.

[12] Luo, Y., and Law, C. L., *Indoor Positioning Using UWB-IR Signals in the Presence of Dense Multipath with Path Overlapping,* in IEEE Transactions on Wireless Communications, vol. 11, no. 10, October 2012: p. 3734-3743.

[13] Khyam, M. O., Alam, M. J., Lambert, A. J., Garratt and M. R. Pickering, M. A., *High-Precision OFDM-Based Multiple Ultrasonic Transducer Positioning Using a Robust Optimization Approach,* in IEEE Sensors Journal, vol. 16, no. 13 July1, 2016: p. 5325-5336.

[14] Kranz, M., Fischer, C., and Schmidt, A., *A comparative study of DECT and WLAN signals for indoor localization,* 2010 IEEE International Conference on Pervasive Computing and Communications (PerCom), Mannheim, 2010: p. 235-243.

[15] Chung-Hsin, Liu., and Jian-Yun, Lo., *The study for the WLAN with ZigBee positioning system,* The 6th International Conference on Networked Computing and Advanced Information Management, Seoul, 2010: p. 520-525.

[16] Hieu, D. C., Van Tuan, Le., Thanh Hieu, Nguyen., Masuda, A., Rabarijaona, V. H., and Shimamoto, S., *Low power consumption Intelligent Local Avoided Collision (iLAC) MAC protocol for WLAN,* 2012 IEEE International Symposium on Signal Processing and Information Technology (ISSPIT), Ho Chi Minh City, 2012: p. 000001-000006.

[17] Nair et al, K., *Optimizing power consumption in iot based wireless sensor networks using Bluetooth Low Energy,* 2015 International Conference on Green Computing and Internet of Things (ICGCIoT), Noida, 2015: p. 589-593.

[18] Pei, L., Chen, R., Liu, J., Tenhunen, T., Kuusniemi, H., and Chen, Y., *Inquiry-Based Bluetooth Indoor Positioning via RSSI Probability Distributions,* 2010 Second International Conference on Advances in Satellite and Space Communications, Athens, 2010: p. 151-156.

[19] Varshney, V., Goel, R. K., and Qadeer, M. A., *Indoor positioning system using Wi-Fi & Bluetooth Low Energy technology,* 2016 Thirteenth International Conference on Wireless and Optical Communications Networks (WOCN), Hyderabad, 2016: p. 1-6.

[20] Dickinson, P., Cielniak, G., Szymanezyk, O., and Mannion, M., *Indoor positioning of shoppers using a network of Bluetooth Low Energy beacons,* 2016 International Conference on Indoor Positioning and Indoor Navigation (IPIN), Alcala de Henares, 2016: p. 1-8.

[21] Varshney, V., Goel, R. K., and Qadeer, M. A., *Indoor positioning system using Wi-Fi & Bluetooth Low Energy technology,* 2016 Thirteenth International Conference on Wireless and Optical Communications Networks (WOCN), Hyderabad, 2016: p. 1-6.

[22] Jian, S., Yongling, F., Lin, T., and Shengguang, L., *A Survey and Application of Indoor Positioning Based on Scene Classification Optimization,* 2015 IEEE 12th Intl Conf on Ubiquitous Intelligence and Computing and 2015 IEEE 12th Intl Conf on Autonomic and Trusted Computing and 2015 IEEE 15th Intl Conf on Scalable Computing and Communications and Its Associated Workshops (UIC-ATC-ScalCom), Beijing, 2015: p. 1558-1562.

[23] Al Nuaimi, K., and Kamel, H., *A survey of indoor positioning systems and algorithms,* 2011 International Conference on Innovations in Information Technology, Abu Dhabi, 2011: p. 185-190.

SOCIETY FOR SCIENCE AND EDUCATION
UNITED KINGDOM

TNC TRANSACTIONS ON NETWORKS AND COMMUNICATIONS

VOLUME 6, NO. 6
ISSN: 2054 -7420

Data Fusion in Wireless Communication Network Node Positioning

Ya Luo, Xiaoyang Liu, Chao Liu
School of Computer Science and Engineering, Chongqing University of Technology,Chongqing,400054,China
luoya@cqut.edu.cn; lxy3103@163.com

ABSTRACT

Aiming at the problems of low localization accuracy, high energy consumption and delay of transmission in wireless sensor networks, a wireless sensor network data fusion method is proposed. Combined with the theory of D-S argument, the wireless sensor network system model is first constructed. Then based on the analysis of ACO (Ant Colony Optimization) and MST (Minimum Spanning Tree) methods, a wireless sensor network data fusion method is proposed. The simulation results show that the larger the number of nodes in WSN is, the larger the energy consumption and delay are. As the moving speed of Sink node increases, the average transmission delay decreases and the useful data rate increases. The average energy The consumption is also gradually increasing; the performance of proposed WSN data fusion method is better than that of ACO and MST.

***Keywords**:* data fusion; algorithm design; mathematics modeling; wireless sensor network

1 Introduction

Wireless Sensor Network (WSN) is a distributed sensor network. It is a multi-hop self-organizing network formed by wireless communication. WSN can achieve target positioning. However, its positioning accuracy is the main indicator to measure the performance of WSN. Therefore, how to improve the positioning accuracy of WSN nodes is a key issue and a problem. WSN data fusion is one of the techniques to improve positioning accuracy.

The WSN is generally a single source node with multiple source nodes. This model can generally be regarded as the minimum Steiner Tree (MST) problem of covering the source node and the sink aggregation node [1-3]. The WSN data fusion algorithm is currently based on the traditional client/server (C/S) model. In this model, the sensor node is regarded as a Client, and the Sink node is regarded as a Server. The Sink node collects data transmitted from each sensor node according to a routing protocol, and performs centralized fusion processing. For

WSN, there are many problems in the C/S model [4-7]: (1) Network delay and energy consumption are large. Each sensor node can transmit data to the processing node at the same time, and the processing node can only receive the data sequentially. When the number of sensor nodes increases and the total amount of sensing data increases, the network delay and energy consumption increase. (2) Poor scalability. When the WSN supplements new sensor nodes, the network structure often needs to be

DOI: 10.14738/tnc.66.5833
Publication Date: 27th December 2018
URL: http://dx.doi.org/10.14738/tnc.66.5833

adjusted to maintain load balancing. (3) Node energy consumption is not balanced. Because the processing node needs to maintain the connection with each sensor node and process its data, it consumes more energy than the sensor node. This requires the node with preset super energy as the processing node or some algorithm to rotate the processing node, adding extra network overhead.

With the introduction of the mobile agent (Mobile Agent, MA)-based computing model in WSN, the problems caused by the traditional C/S model are solved to some extent [8-12]. In the WSN data fusion, the MA computing model is used, that is, the sensing data is kept locally at the node, and the MA is migrated to the data, and the appropriate algorithm is used for the fusion processing. The essence is to "move the fusion computing to the data", which enables It overcomes the shortcomings of traditional data fusion algorithms, reduces network bandwidth requirements, reduces energy consumption and delay, and enhances network stability while achieving better data fusion effects. After the MA-based data fusion is closely integrated with the routing strategy of the MA, it can effectively alleviate network congestion during data aggregation and ultimately prolong the network lifetime [13-15].

Diego V. et al. [15-16] proposed a multi-agent data fusion method based on the mobile-agent approach. The method has improved the energy elimination node reaction time and network lifetime. Habib M et al. [17-20] combined the static WSN with the dynamic WSN to analyze the complexity of node data fusion. First, define the boundary of the node in the static network, and then construct the topology domain of the dynamic network. Finally, the data fusion of the nodes is carried out according to the evolution graph. Sadia Din et al. [21-25] overcome the traditional single Sink deficiency based on practical applications. The multi-Sink node processing method of WSN is proposed, and the routing algorithm of multiple Sink nodes is proposed. M. Z. Zambian et al. [26-27] proposed a new energy-efficient structural data fusion protocol based on the energy consumption of the transmitted data, which consumes too much energy compared to the local data processing of the node. The simulation of the proposed data fusion protocol in energy consumption, reliability, the timeliness of data transmission has obvious advantages over traditional methods.

2 Data Fusion Mechanism and Method

There are three main data fusion mechanisms for WSN nodes: Tree-based, Cluster-based, and Centralized-based [27-28]. As can be shown in Fig.1.

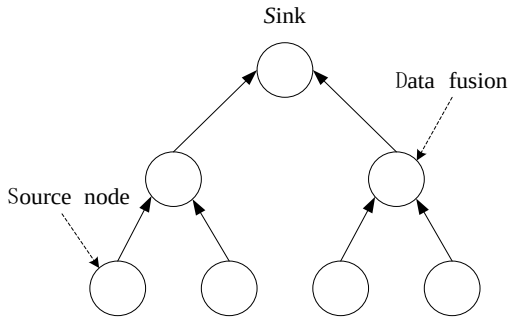

Fig.1 Tree-based data fusion

In Fig.1, there is a Sink node multi-source node situation. The node fuses the sensing data of multiple source nodes, and then transmits the merged data to the Sink node [29-31].

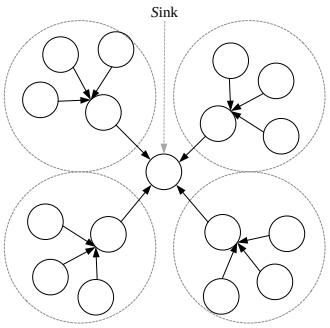

Fig.2 Cluster-type data fusion

In Fig.2, a clustering method is also a multi-source single-sink case. Each cluster contains multiple source nodes and one head node, and data fusion is performed at the head node. The data perceived by each source node is fused at the head node according to a certain data processing algorithm [32-37]. Each head node then transfers the merged data to the Sink node.

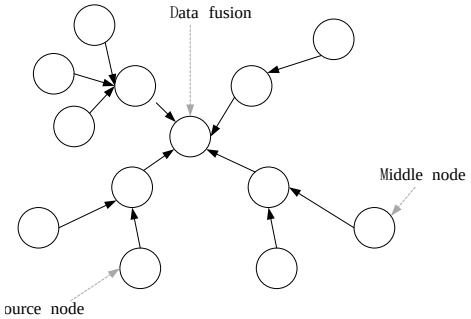

Fig.3 Centralized-based data fusion

In Fig.3, there is a central method. The model contains multiple branches. Each branch contains multiple source nodes and intermediate nodes. The data sensed by each branch node is transmitted to the head node and merged according to the data fusion mechanism and method.

Different fusion methods can be used for the perceived data. If there is complementary fusion, redundant fusion, cooperative fusion and other methods to analyze and process the event information, as shown in Fig.4[26-28].

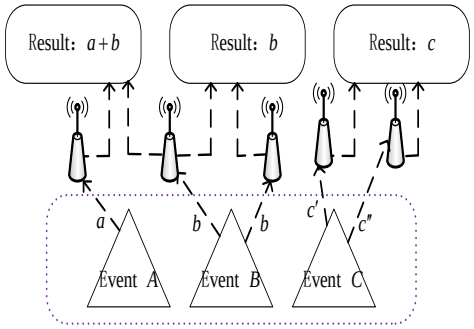

Fig.4 Data fusion based on time information source

3 Data Fusion Algorithm

3.1 Traditional methods

(1) ACO

The ACO algorithm adopts distributed parallel computer system and has strong robustness. The essence of the ACO algorithm optimization process is that the path with the larger amount of information has a higher probability of being selected; the amount of information above the path grows with the passage of ants and also decreases over time; the ants actually communicate and work together through the amount of information. Such a mechanism makes the ant colony algorithm have a strong ability to find better solutions.

(2) MST

The MST algorithm requires $n-1$ edges to be selected from a weighted undirected complete graph and the graph is still connected (that is, a spanning tree is obtained), and the weight of the tree is also considered to be minimized. The main idea is: First, use a node as the initial node of the minimum spanning tree. Then iteratively find the minimum edge with the weight of each node in the minimum spanning tree, and added to the minimum spanning tree. If a loop is generated after the join, skip this edge and select the next node. Once all the nodes have been added to the minimum spanning tree, the smallest spanning tree in the connected graph is found.

3.2 D-S argument theory

Dempster-Shafer (D-S) argumentation theory [18-20] can nonlinearly integrate data collected by different WSN sensing nodes. Dempster-Shafer theory can be applied in statistics, big data, information statistics and other related fields, and got a good development.

There are two trust function Bel_1 and Bel_2 under the same Θ, m_1 and m_2 are their credibility assignments. The focus elements of both are $A_1, A_2, \cdots, A_K$ and $B_1, B_2, \cdots, B_K$. Then the Dempster merge rule can be expressed as:

$$m(C)=\begin{cases} 0 & C=\varnothing \\ \dfrac{\sum_{i,j=1}^{n} m(B)_i m(A)_j}{1-K} & \forall C\subset U, C\neq\varnothing, A\cap B=\varnothing \end{cases} \tag{1}$$

In the above formula, K is a normalization constant. And the following formula is satisfied.

$$K=\sum_{i,j=1}^{n} m(B)_i m(A)_j<1 \tag{2}$$

In the formula $K\neq 1$, then m determines a basic probability assignment, indicating that the two sets of information m_1 and m_2 are identical or only partial information conflicts. The introduction of the canonical number K is actually to add the orthogonal and proportional proportions discarded by the empty set to the non-empty set, and make the $m(C)$ still satisfied:

$$\sum_{C\leq\varnothing}^{n} m(C)=1 \tag{3}$$

When D-S reasoning is used for data fusion of multiple WSN nodes, each node collects target information. Through D-S theory for data fusion, the feature vector of the target information can be calculated, so that accurate positioning can be achieved.

3.3 Node data fusion method

In the wireless sensing area, different sensing nodes are distributed, and the influence factor I_{jk} between two different sensing nodes j and k can be expressed as:

$$I_{jk}=e^{2}\frac{-(H_j^k-1)^2}{3\sigma^2} \tag{4}$$

Where, σ is the influence extent between j and k. H_j^k is the estimated hops between j and k. Which can be expressed as:

$$H_j^k=\frac{d^2(l-1,l)}{R_{\max}} \tag{5}$$

Where, $R_{\max}$ is the max transmission distance.

In communication area, The amount of energy E of a node during a data acquisition cycle is:

$$E=\eta h_{si}P_s t_s+\lambda\sum_{j\in N}^{n}\eta h_{ji}P_j t \tag{6}$$

Where, λ is the random modify variable, $0\le i\le 1$, $0<\eta<1$ is energy conversion coefficient. h_{si} and h_{ji} is the wireless communication link gain between different nodes. t_s denotes the time slot. P_s is the power of sink node. P_j is the transmit power of node j. Node energy consumption $E_{consume}$ can be denoted as

$$E_{consume}=v_i\varepsilon+\sum_{k=0}^{n}v_k e+P_i t \tag{7}$$

Where, ε and e is the unit energy consumption. Is the transmit power of node i. v_i and v_k is the amount of data collected at different nodes.

According to Shannon Formula:

$$C=B\log_2(1+\frac{S}{N}) \tag{8}$$

It can be concluded that the maximum data transmission rate of a node in the WSN area is:

$$\zeta_i=B\log_2(1+\frac{P_i h_{id}^{\ 2}}{\delta_{id}^3}) \tag{9}$$

In equation (9), δ_{id} is the noise power between two different nodes, and h_{id} is the link gain between two different nodes. B is the bandwidth of the wireless communication channel.

In the wireless communication sensing area, it takes a certain amount of time to complete a round of data collection. The average time interval required to complete a round of data collection can be expressed as:

$$T=\varepsilon\frac{\sum_{i=1}^{r}\max_{1\le j\le k}\{T_{i,j}\}}{r} \tag{10}$$

Where, ε obey the power law function distribution. r is the number of data acquisition rounds for data fusion in the communication network, and k is the number of proxy nodes.

It is assumed that the wireless communication channel bandwidth of the communication network is B(b/s), the time at which the proxy node transmits the data packet can be expressed as:

$$T_{\text{packet}} = \varepsilon \sum_{i=1}^{n} (T_{proc} + ((S_{ini}{}^{2} + \frac{i \cdot d}{2}) / B) + T_{prop}) \tag{11}$$

Where, T_{proc} is the time it takes for a proxy node to complete data fusion, and is a constant; S_{ini} represents the amount of data packets of the Sink node; T_{prop} is the transmission time of the node, mainly based on environmental factors such as the actual transmission distance of the WSN area

4 Simulation Analysis

There are 439 nodes in the sensing area $600 \times 600\, m^2$, the initial node energy is 50J, and 50 bytes per package. The bandwidth is 30Kb/s. It is simulated and analyzed based on D-S theory.

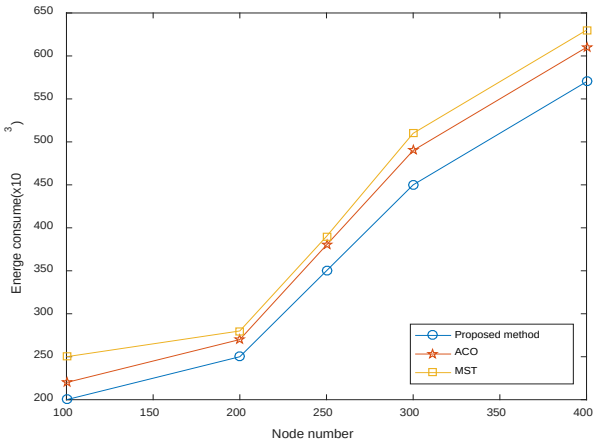

Fig.5 Energy consumption and network nodes

It can be seen from Fig.5 that as the number of network nodes increases, the energy consumption increases gradually. In the case of the same number of nodes, the energy consumption of this method is smaller than the other two traditional methods.

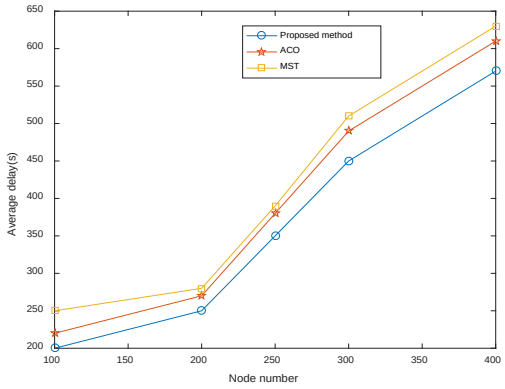

Fig.6 Average delay and node relationship

It can be seen from Fig.6 that as the number of WSN nodes increases, the average delay is on the rise. In the case of the same number of nodes, the average delay of the method in this paper is smaller than ACO and MST.

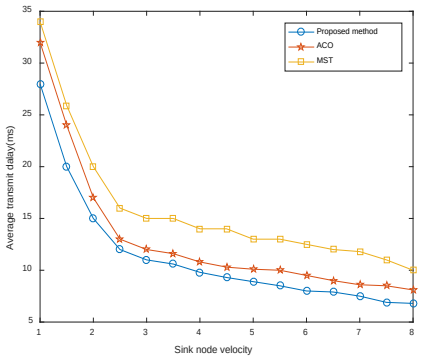

Fig.7 Transmission delay and Sink speed

It can be seen from Fig.7 that as the speed of the Sink node increases, the average transmission delay tends to decrease, and the average transmission delay of the Sink node decreases from 1 to 2.5. But the Sink node speed changes from 2.5 to 8 in the same number of nodes, the average transmission delay is slower, but the transmission delay is still slower. It can be seen that the average delay of the method herein is smaller than ACO and MST.

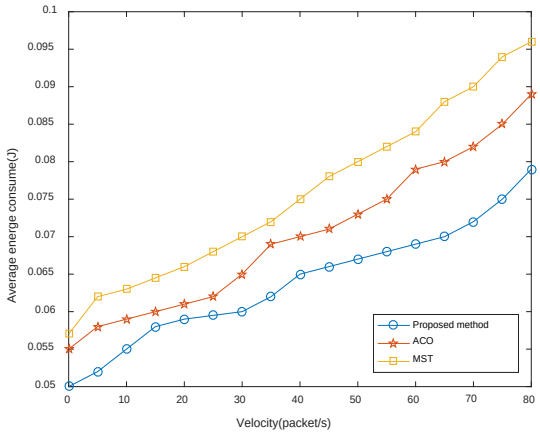

Fig.8 Data rate and energy consumption

It can be seen from Fig.8 that as the data rate increases, the average energy consumption increases gradually. In the case of the same data rate, the energy consumption of this method is smaller than the other two traditional methods.

5 Summary

After analyzing the data fusion mechanism of WSN, the system model of WSN is constructed. A data fusion method based on the theory of D-S argumentation is proposed. Consider the energy consumption and time delay in different node numbers, data rates, and so on. The simulation results show that the larger the number of nodes, the greater the energy consumption and delay. The larger the Sink node's moving rate is, the smaller the delay is. It can be concluded that the performance of this method is better than ACO and MST. The key technical issues to be studied in the next step are: the relationship between the

node energy consumption of WSN and the node density and speed and the node dynamic topology model in the case of a specific total number of nodes.

AUTHOR CONTRIBUTIONS

The authors performed the experiments and analyzed the results together. Introduction, methodology, cosmetic detection algorithms and proposed model have been written by Xiaoyang Liu; while data collection, experimental results and conclusion sections have been written by Ya Luo and Chao Liu.

ACKNOWLEDGMENT

This work was supported in part by Science and Technology Research Program of Chongqing Municipal Education Commission(KJ1709206),National Social Science Fund of China West Project(17XXW004),Young Fund Project of Humanities and Social Sciences Research of Ministry of Education of China(16YJC860010), Social Science of Humanity of Chongqing Municipal Education Commission(17SKG144), 2018 Chongqing Science and Technology Commission Technology Innovation and Application Demonstration (Social Livelihood General) Project(cstc2018jscx-msybX0049),Science and Technology Research Program of Chongqing Municipal Education Commission (Grant No. KJQN201801104), Open Fund Project of Chongqing Technology and Business University, Research Center of Chongqing University Network Public Opinion and Ideological Dynamic (KFJJ2017024).

REFERENCES

[1] Behrouz P, Nima J N.Data aggregation mechanisms in the Internet of things:A systematic review of the literature and recommendations for future research[J].Journal Netw Comput Appl,2017,97:23.

[2] Bo qian,Ting ma,Enbing song. Sensor selection problem for hypothesis testing in wireless sensor networks [J]. Journal of Sichuan University,2018,55:7-12.

[3] Xiong L, Dandan Z, Laurence T Y, et al.A kernel machine-based secure data sensing and fusion scheme in wireless sensor networks for the cyber-physical systems[J].Future Gener Comp Sy,2016, 61:85.

[4] Andrea A, Marco M, Gianluigi F.Information fusion for efficient target detection in large-scale surveillance Wireless Sensor Networks[J].Inform Fusion, 2017, 38:55.

[5] Ricardo S C, Ciaran M G.Decentralised Peer-to-Peer data dissemination in Wireless Sensor Networks[J].Pervasive Mob Comput, 2017,40:242.

[6] Diego S, Gines E A, et al.A hybrid intrusion detection system for virtual jamming attacks on wireless networks[J].Measurement, 2017, 9:79.

[7] Xiaoyu C, Ran J.Statistical modeling for visualization evaluation through data fusion[J].Appl Ergon, 2017,65: 551.

[8] Fatima T Z, Kamalrulnizam A B, Adnan A, Mohsin A T.Routing protocols in wireless body sensor networks: A comprehensive survey[J].Journal Netw and Comput Appl, 2017, 99:73.

[9] Yunfeng H, Jucheng Z, Dajun S.Error control and adjustment method for underwater wireless sensor network localization[J].Appl Acoust, 2018, 130:293.

[10] Mohamed E F, Abderrahim B H, Mostafa S. Mobile Agent Protocol based energy aware data Aggregation for wireless sensor networks[J].Procedia Comput Sci,2017, 113:25.

[11] Li L, Wang Y, Guojun W.Intelligent fusion of information derived from received signal strength and inertial measurements for indoor wireless localization[J].AEU-Int J Electron C, 2016, 70:1105.

[12] Keyur P, Devesh C J.Concealed data aggregation in wireless sensor networks: A comprehensive survey[J].Comput Netw, 2016, 103:207.

[13] Feng G, Zhao H, Gu F, Needham P, Ball A D.Efficient implementation of envelope analysis on resources limited wireless sensor nodes for accurate bearing fault diagnosis[J].Measurement, 2017, 110:307.

[14] Kai K, Vasileios M, Ioannis S, Feng B.Improved distributed particle filters for tracking in a wireless sensor network[J].Comput Stat & Data An, 2018, 117:90.

[15] Diego V Q, Marcelo S A, Ruan D G, et al.Survey and systematic mapping of industrial Wireless Sensor Networks[J].J Netw Comput Appl, 2017, 97:96.

[16] Ioannis K, Sotiris N, Theofanis P R, et al.An algorithmic study in the vector model for Wireless Power Transfer maximization[J].Pervasive Mob Comput, 2017,42:108.

[17] Habib M A.A unified framework for image-coverage and data collection in heterogeneous wireless sensor networks[J].J Parallel Distr Com, 2016, 89:37.

[18 Mohammad M. A, Ali A P, Vahid A. An efficient algorithm for multisensory data fusion under uncertainty condition[J].J Electr Syst Inf Technol, 2017,4: 269.

[19] Taj R S,Huansheng N,Haodi P,Zahid M.DPCA: data prioritization and capacity assignment in wireless sensor networks[J].IEEE Access,2017,5:14991.

[20] Siyao C,Zhipeng C,Jianzhong L,Hong G.Extracting Kernel dataset from big sensory Data in wireless sensor networks[J].IEEE T Knowl Data En,2017,29:813.

[21] Sadia D,Awais A,Anand P,et al.A Cluster-Based Data Fusion Technique to Analyze Big Data in Wireless Multi-Sensor System[J].IEEE Access,2017,5:5069.

[22] Fan W,Sining W, Kunpeng W,Xiaopeng H.Energy-efficient clustering using correlation and random update based on data change rate for wireless sensor networks[J]. IEEE Sens J,2016, 16:5471.

[23] Jonathan C K, Abraham O F. Radio Frequency Energy Harvesting and Data Rate Optimization in Wireless Information and Power Transfer Sensor Networks[J].IEEE Sens J,2017, 17:4862.

[24] Nguyen C L, Dinh T H,Ping W, et al.Data collection and wireless communication in Internet of Things (IoT) using economic analysis and pricing models: a survey[J].IEEE Commun Surv Tut,2016, 18:2546.

[25] Sadia D,Awais A,Anand P.A cluster-based data fusion technique to analyze big data in wireless multi-Sensor system[J].IEEE Access, 2017, 5:5069.

[26] Kevin W,Ashish P.Location data analytics in wireless lighting systems[J].IEEE Sens J,2016, 16:2683.

[27] Luca F,Rebecca M,Azzedine B,Antonio C. Scalable and mobile context data retrieval and distribution for community response heterogeneous wireless networks[J].IEEE Commun Mag,2016, 54:101.

[28] Zaaimia M Z, Touhami R, Talbi L, Nedil M, Yagoub M C.60-GHz statistical channel characterization for wireless data centers[J].IEEE Anten Wirel Pr,2016, 15:976.

[29] Sohail Jabbar Kaleem R. Malik,Mudassar Ahmad,Omar Aldabbas,et al.A Methodology of Real-Time Data Fusion for Localized Big Data Analytics[J]. IEEE Access,2018,6:24510-24520.

[30] Hao Chen,Xinggan Zhang,Qingsi Wang,Yechao Bai. Efficient Data Fusion Using Random Matrix Theory[J].IEEE Signal Processing Letters,2018,25(5):605-609.

[31] Chia-Hsiang Lin, Fei Ma,Chong-Yung Chi, Chih-Hsiang Hsieh. A Convex Optimization-Based Coupled Nonnegative Matrix Factorization Algorithm for Hyperspectral and Multispectral Data Fusion[J]. IEEE Transactions on Geoscience and Remote Sensing, 2018,56(3):1652-1667.

[32] Yan Wang,Shuang Cang,Hongnian Yu. A Data Fusion-Based Hybrid Sensory System for Older People's Daily Activity and Daily Routine Recognition[J]. IEEE Sensors Journal,2018 ,18(16): 6874-6888.

[33] Zhibin Sun, John Davis,Wei Gao. Estimating Error Covariance and Correlation Region in UV Irradiance Data Fusion by Combining TOMS-OMI and UVMRP Ground Observations[J]. IEEE Transactions on Geoscience and Remote Sensing, 2018,56(1): 355-370.

[34] Chaoqun Yang,Li Feng,Heng Zhang, Shibo He,Zhiguo Shi. A Novel Data Fusion Algorithm to Combat False Data Injection Attacks in Networked Radar Systems[J]. IEEE Transactions on Signal and Information Processing over Networks, 2018,4(1):125-136.

[35] Edgar A. Bernal, Xitong Yang,Qun Li,Jayant Kumar,Sriganesh Madhvanath,Palghat Ramesh,Raja Bala. Deep Temporal Multimodal Fusion for Medical Procedure Monitoring Using Wearable Sensors[J]. IEEE Transactions on Multimedia ,2018 ,20(1):107-118.

[36] Changyue Song,Kaibo Liu,Xi Zhang.Integration of Data-Level Fusion Model and Kernel Methods for Degradation Modeling and Prognostic Analysis[J]. IEEE Transactions on Reliability, 2018 ,67(2): 640-650.

[37] Onur Ozdemir,Thomas G. Allen,Sora Choi,Thakshila Wimalajeewa, Pramod K. Varshney. Copula Based Classifier Fusion Under Statistical Dependence[J]. IEEE Transactions on Pattern Analysis and Machine Intelligence, 2018,40(11): 2740-2748.